Practical Algorithms and Analysis for Next-Generation Decentralized Vehicular Networks

Avik Dayal

Dissertation submitted to the Faculty of the
Virginia Polytechnic Institute and State University
in partial fulfillment of the requirements for the degree of

Doctor of Philosophy
in
Electrical Engineering

Jeffrey H. Reed, Chair
Vijay K. Shah
Harpreet S. Dhillon
A. A. (Louis) Beex
Daniel J. Stilwell
Azim Eskandarian

September 23rd, 2021
Blacksburg, Virginia

Keywords: Vehicular Communications, DSRC, C-V2X, NR-V2X, Age-of-Information, Stochastic Geometry
Copyright 2021, Avik Dayal

Practical Algorithms and Analysis for Next-Generation Decentralized Vehicular Networks

Avik Dayal

(ABSTRACT)

The development of autonomous ground and aerial vehicles has driven the requirement for radio access technologies (RATs) to support low latency applications. While onboard sensors such as Light Detection and Ranging (LIDAR), Radio Detection and Ranging (RADAR), and cameras can sense and assess the immediate space around the vehicle, RATs are crucial for the exchange of information on critical events, such as accidents and changes in trajectory, with other vehicles and surrounding infrastructure in a timely manner. Simulations and analytical models are critical in modelling and designing efficient networks.

In this dissertation, we focus on (a) proposing and developing algorithms to improve the performance of decentralized vehicular communications in safety critical situations and (b) supporting these proposals with simulation and analysis of the two most popular RAT standards, the Dedicated Short Range Communications (DSRC) standard, and the Cellular vehicle-to-everything (C-V2X) standard.

In our first contribution, we propose a risk based protocol for vehicles using the DSRC standard. The protocol allows a higher beacon transmission rate for vehicles that are at a higher risk of collision. We verify the benefits of the risk based protocol over conventional DSRC using ns-3 simulations. Two risk based beacon rate protocols are evaluated in our ns-3 simulator, one that adapts the beacon rate between 1 and 10 Hz, and another between 1 and 20 Hz. Our results show that both protocols improve the packet delivery ratio (PDR) performance by up to 45% in congested environments using the 1-10 Hz adaptive beacon rate protocol and by 38% using the 1-20 Hz adaptive scheme. The two adaptive beacon rate protocol simulation results also show that the likelihood of a vehicle collision due to missed packets decreases by up to 41% and 77% respectively, in a three lane dense highway scenario with 160 vehicles operating at different speeds.

In our second contribution, we study the performance of a distance based transmission protocol for vehicular ad hoc network (VANET) using tools from stochastic geometry. We consider

a risk based transmission protocol where vehicles transmit more frequently depending on the distance to adjacent vehicles. We evaluate two transmission policies, a *listen more* policy, in which the transmission rate of vehicles *decreases* as the inter-vehicular distance decreases, and a *talk more* policy, in which the transmission rate of vehicles *increases* as the distance to the vehicle ahead of it decreases. We model the layout of a highway using a 1-D Poisson Point process (PPP) and analyze the performance of a typical receiver in this highway setting. We characterize the success probability of a typical link assuming slotted ALOHA as the channel access scheme. We study the trends in success probability as a function of system parameters.

Our third contribution includes improvements to the 3rd Generation Partnership Project (3GPP) Release 14 C-V2X standard, evaluated using a modified collision framework. In C-V2X basic safety messages (BSMs) are transmitted through Mode-4 communications, introduced in Release 14. Mode-4 communications operate under the principle of sensing-based semi-persistent scheduling (SPS), where vehicles sense and schedule transmissions without a base station present. We propose an improved adaptive semi-persistent scheduling, termed *Ch-RRI* SPS, for Mode-4 C-V2X networks. Specifically, Ch-RRI SPS allows each vehicle to dynamically adjust in real-time the BSM rate, referred to in the LTE standard as the resource reservation interval (RRI). Our study based on system level simulations demonstrates that Ch-RRI SPS greatly outperforms SPS in terms of both on-road safety performance, measured as collision risk, and network performance, measured as packet delivery ratio, in all considered C-V2X scenarios. In high density scenarios, e.g., 80 vehicles/km, Ch-RRI SPS shows a collision risk reduction of 51.27%, 51.20% and 75.41% when compared with SPS with 20 ms, 50 ms, and 100 ms RRI respectively.

In our fourth and final contribution, we look at the tracking error and age-of-information (AoI) of the latest 3GPP Release 16 NR-V2X standard, which includes enhancements to the 3GPP Release 14 C-V2X standard. The successor to Mode-4 C-V2X, known as Mode-2a NR-V2X, makes slight changes to sensing-based semi-persistent scheduling (SPS), though vehicles can still sense and schedule transmissions without a base station present. We use AoI and tracking error, which is the freshness of the information at the receiver and the difference in estimated vs actual location of a transmitting vehicle respectively, to measure the impact of lost and outdated BSMs on a vehicle's ability to *localize* neighboring vehicles. In this work, we again show that such BSM scheduling (with a fixed RRI) suffers from severe under- and over- utilization of radio resources, which severely compromises timely dissemination of BSMs and increases the system AoI and tracking error. To address this, we propose

an RRI selection algorithm that measures the *age* or freshness of messages from neighboring vehicles to select an RRI, termed *Age of Information (AoI)-aware RRI* (AoI-RRI) selection. Specifically, AoI-aware SPS (i) measures the neighborhood AoI (as opposed to channel availability) to select an age-optimal RRI and (ii) uses a modified SPS procedure with the chosen RRI to select BSM transmission opportunities that minimize the overall system AoI. We compare AoI-RRI SPS to Ch-RRI SPS and fixed RRI SPS for NR-V2X. Our experiments based on the Mode-2a NR-V2X standard implemented using system level simulations show both Ch-RRI SPS and AoI-RRI SPS outperform SPS in high density scenarios in terms of tracking error and age-of-information.

Practical Algorithms and Analysis for Next-Generation Decentralized Vehicular Networks

Avik Dayal

(GENERAL AUDIENCE ABSTRACT)

An increasing number of vehicles are equipped with a large set of on-board sensors that enable and support autonomous capabilities. Such sensors, which include Light Detection and Ranging (LIDAR), Radio Detection and Ranging (RADAR), and cameras, are meant to increase passenger and driver safety. However, similar to humans, these sensors are limited to line-of-sight (LOS) visibility, meaning they cannot see beyond other vehicles, corners, and buildings. For this reason, efficient vehicular communications are essential to the next generation of vehicles and could significantly improve road safety. In addition, vehicular communications enable the timely exchange of critical information with other vehicles, cellular and roadside infrastructure, and pedestrians. However, unlike typical wireless and cellular networks, vehicular networks are expected to operate in a distributed manner, as there is no guarantee of the presence of cellular infrastructure.

Accurate simulations and analytical models are critical in improving and guaranteeing the performance of the next generation of vehicular networks. In this dissertation, we propose and develop novel and practical distributed algorithms to enhance the performance of decentralized vehicular communications. We support these algorithms with computer simulations and analytical tools from the field of stochastic geometry.

Dedication

To my parents, Manik, and Rupali.

Acknowledgments

Finally, after many late nights and cups of coffee, my time as a graduate student is coming to an end. Finishing this dissertation marks the end of a long and fulfilling journey that I will remember and cherish forever. Although it is only my name listed as the author, I could not have completed this dissertation without the support of a significant number of friends, family, colleagues, and advisors.

I would like first to thank my advisor and mentor, Dr. Jeffrey H. Reed, for his constant support and feedback throughout all aspects of my academic research. He has always given me the support and freedom to pursue research problems of my own choosing and provided me with numerous professional and academic development opportunities to help my career. His unique skill for identifying essential research areas and problems has helped improve the quality of my research. Thanks for the patience, support, and guidance you have given during my time as a graduate student.

It is necessary to acknowledge the constant support and guidance of my guru, advisor, and teacher, Dr. Vijay K. Shah. He has always been there for moral and intellectual support, from brainstorming at the whiteboard to putting final touches on papers at 1 a.m. Working with him has taught me so much about research and significantly improved my problem-solving and communication skills. Thanks for being patient and correcting the many mistakes I have made over the years. It has been a very memorable and fulfilling experience to have worked with you, and I hope that I can become a guide and researcher like you in the future.

I owe my gratitude to Dr. Harpreet S. Dhillon for being an excellent teacher and mentor. His precious guidance has helped in many of the chapters of this dissertation and, more importantly, has led me to develop critical analytical and writing skills. Thank you for introducing me to stochastic geometry and providing much-needed encouragement during the research process.

I am extremely thankful for the support, encouragement, and insightful comments provided by Dr. A. A. (Louis) Beex, who also served as my advisor during my Masters. Thank you so much for everything you have taught over the years, from signal processing to writing clearly and effectively. Your feedback has made me a better writer and researcher, and I will always be grateful for your teaching.

I would like to thank Dr. Azim Eskandarian and Dr. Daniel Stilwell for taking the time to

be part of my Ph.D. committee and providing valuable feedback on my work. Their review and comments have been essential in shaping the direction of this dissertation. Apart from my academic advisors, I'd like to thank my mentors and collaborators outside of Virginia Tech. I'm especially grateful for the guidance, mentorship, and financial support provided by Dr. Vuk Marojevic from Mississippi State University, Dr. Edward Colbert, Dr. Nandi Leslie, and Dr. Charles Kamhoua from Army Research Lab. Also, a special thanks to Dr. Sandeep Shukla, for initially taking me on as a student and hosting me at IIT Kanpur.

Next, I'd like to thank the friends and colleagues who I've had the pleasure of meeting during my time at Virginia Tech. Thanks to Raghu for making life in lab enjoyable and being a constant source of encouragement and wisdom. I'd also like to thank my fellow co-authors, Biplav and Vishnu. Thank you to Vishnu for your endless patience and effort in explaining stochastic geometry. I'm excited for our work to soon be published. Thanks to Biplav for his work and collaboration on our joint papers. I'm proud of the work we have done together and wish you the best of luck in completing your Ph.D. A special shout-out to all of my Northern Virginia and Blacksburg friends Morteza, Anish, Keerthana, Tarun, Don-Roberts, Charlie, Vireshwar, Dhiraj, Srivats, Mahesh, Prachi, Priyabatra, Tolga, Kartheek, Lakshman, Srikanth, and others forgotten as I write this late at night. My time as a graduate student would not have been the same without you.

I would like to thank my family for all of the support they have shown over the years. My parents, both brilliant immigrant engineers, are responsible for cultivating my interest in math and science. Their sacrifices, love, and hard work gave me the drive and determination to complete this dissertation. Thanks to my brother Manik for always cheering me up and offering advice on any struggles I would face. I would also like to thank Anjana Mausi, Ratna Bhua, and Rohit Chacha for their love and support over the years. I need to give a special thank you to Amit Mausaji for encouraging me to go to graduate school, continuously giving feedback on my work, and being a wonderful role model. And although they are not with us today, I wouldn't be the person I am today without the influence of my late Nanaji, Naniji, Babaji, Dadiji, and Vijay Phupaji. Finally, I would like to thank my best friend and wife, Rupali, for her unwavering support, unconditional love, and endless encouragement.

Contents

List of Figures

List of Tables

Chapter 1

Introduction

Modern vehicles have been equipped with a plethora of sensors to assist with autonomous capabilities [83]. These sensors such as Light Detection and Ranging (LIDAR), Radio Detection and Ranging (RADAR), and cameras assist vehicular control systems in sensing and assessing the status and space around the vehicle. The drawback is that most sensors, including cameras, radars, and LIDAR, are limited to line of sight (LOS) visibility and are constrained in their scope [73]. This LOS constraint is a major motivation for the development of radio access technologies (RATs), and specifically, Vehicle-to-Everything (V2X) communications. V2X communications enables both LOS and NLOS exchange of sensor data with neighboring vehicles, thereby increasing the range of a vehicle's *awareness* of surrounding vehicles and infrastructure [74].

With the development and interest in autonomous ground and aerial vehicles, RATs are being developed to support low latency applications. These RATs are expected to play a role in intelligent transportation systems (ITSs) to increase the safety and transportation efficiency on the highways and roads of the future. V2X communications, which is considered to consist of vehicle-to-infrastructure (V2I), vehicle-to-vehicle (V2V), and vehicle-to-pedestrian (V2P) communications, is a promising technology for next generation intelligent transportation systems, mainly due to its potential of improving the safety of vehicles [74].

These V2X services are designed with strict quality of service (QoS) requirements to guarantee traffic safety and improve traffic efficiency, among others. There are two competing technologies that enable V2X communications, Dedicated Short Range Communications (DSRC) and Cellular-V2X (C-V2X) [64]. DSRC is a decentralized wireless communications protocol based on the 802.11 standard designed for short to medium ranges [10]. It is standardized by IEEE as 802.11p in the US and its European equivalent by the European Telecommunications Standards Institute (ETSI). Alternatively, Cellular-based V2X (C-V2X) is standardized by the Third Generation Partnership Project (3GPP), which defines two new modes of operation for LTE that are specifically designed for V2X communications.

1.1 Motivation and Contributions

Various studies, such as [43] [14], have shown that the performances of DSRC and C-V2X suffer at high traffic densities, offering inadequate support in congested vehicular environments. Whereas congestion control on top of a given message delivery protocol is expected to improve the low packet delivery ratio (PDR) at high congestion, such schemes do not necessarily address the quality of service (QoS) requirements for vehicles at risk of collision.

1.2 Risk Controlled Beacon Transmission in DSRC Communications

Chapter 3 proposes a variable beacon transmission rate protocol for each vehicle communicating via DSRC. The chosen transmission rate depends on the risk of collision each vehicle poses to the surrounding vehicles. This risk is computed using vehicular kinematics and is a function of the time and probability that a vehicle has of colliding with nearby vehicles. It is important to note that the proposed method is agnostic to the V2X protocol and allows applying congestion control mechanisms on top of it.

The specific contributions of this work are:

- Introduction of a metric for assigning priorities based on collision risk to vehicles sharing a road.
- Design of an adaptive beaconing protocol at the MAC layer that allows for a higher beacon rate for high risk vehicles.
- Implementation of the adaptive beaconing protocol in ns-3 and comparison of the PDR of the proposed scheme with that of the traditional fixed beacon rate based on comprehensive numerical results. These results show significant improvement in PDR at low, medium and high vehicle densities.

Publications

The work presented in this chapter is part of the following peer reviewed publications:

- A. Dayal, E. Colbert, V. Marojevic, and J. Reed. Risk Controlled Beacon Transmission in V2V Communications. In *2019 IEEE 89th Vehicular Technology Conference (VTC2019-Spring)*, pages 1–6, 2019.

- B. Choudhury, V. K. Shah, A. Dayal, and J. H. Reed. Experimental Analysis of Safety Application Reliability in V2V Networks. In *2020 IEEE 91st Vehicular Technology Conference (VTC2020-Spring)*, pages 1–5, 2020.

1.3 Stochastic Analysis of Beacon Transmission in V2V Communications

Although system level simulations can be used to evaluate the performance of a risk based scheme, analytical models are also critical to the analysis of vehicular networks. In this chapter, we study the performance of two distance-based transmission protocols for vehicular ad hoc networks (VANET) using tools from stochastic geometry. We consider a risk-based protocol, where the distance to adjacent vehicles determines the *riskiness* of a vehicle and thus how frequently a vehicle transmits. Assuming slotted ALOHA as the channel access scheme and Nakagami-m fading, we evaluate two transmission policies, a *listen more* policy, in which the transmission rate of vehicles *decreases* as the inter-vehicular distance decreases, and a *talk more* policy, in which the transmission rate of vehicles *increases* as the inter-vehicular distance decreases. We model the layout of a highway using a 1-D Poisson Point process (PPP) and characterize the success probability of the typical link under the two transmission policies. Finally, we study the trends in success probability as a function of system parameters. The risk based policy is modeled by assigning a Bernoulli random variable to each vehicle, and the resulting coverage probability is derived and analyzed.

The specific contributions of this work are:

- Introduction of a marked point process for assigning probabilities of interference based on distances to adjacent vehicles sharing a road.

- Derivation of success probability of a typical link in a VANET with vehicles' probabilities of transmission modeled as a 1-D marked point process.

- Computation of the coverage probability for a risk-based protocol for two transmission policies.

Publications

The work presented in this chapter is intended to be submitted as a Transactions on Vehicular Technology Correspondence letter.

1.4 Ch-RRI SPS: Adaptive Semi-Persistent Scheduling for C-V2X Networks

The Third Generation Partnership Project (3GPP) has recently standardized two modes (Mode-3 and Mode-4) of operation that are specifically designed for V2X communications in the Long Term Evolution (LTE) standard. The LTE standard built these two modes on top of proximity services (ProSe) for Device to Device (D2D) communications (referred to as ProSe Mode-1 and Mode-2).

The mechanism driving C-V2X and Mode-4 communications is semi-persistent scheduling (SPS), which allows vehicles to self select resources from a pool of resource blocks for the transmission of BSMs. The time in between transmissions is tied to a fixed periodicity known as the resource reservation interval (RRI). Though the standard allows for different RRIs such as 20, 50, and 100 ms, they are fixed and remain the same for a given C-V2X network. This fixed periodicity of BSMs means that the channel resources could be perpetually underutilized or overly congested, depending on the sparse or dense C-V2X scenarios and RRI prespecified at each vehicle by the SPS protocol. For instance, if a larger value of RRI is chosen (say 100 ms) then it would lead to under-utilization of channel resources in case of sparse C-V2X scenarios. Whereas if a lower value of RRI is selected, say 20 ms, then it will result in overly congested channel resources, and many dropped BSMs in case of denser C-V2X scenarios. Both under- and over-utilization of channel resources negatively impact the up-to-date sharing of BSMs, which in turn, severely compromises the road safety of C-V2X.

To address these shortcoming of SPS and improve the road safety of C-V2X, in this chapter we propose an *channel-aware* RRI selection algorithm for semi-persistent scheduling, termed

1.4. Ch-RRI SPS: Adaptive Semi-Persistent Scheduling for C-V2X Networks

Ch-RRI SPS. Ch-RRI SPS allows each vehicle to adapt to the considered time-varying C-V2X scenarios (i.e., sparse or dense C-V2X and correspondingly, the availability of channel resources over time), and dynamically adjust RRI (or BSM rate) for each vehicle in the network. This enables each vehicle to judiciously utilize all the available channel resources, and broadcast the most recent BSMs, which in turn, enhances the tracking error – which is critical for the road safety of C-V2X networks. See Section 5.2 for details.

This work makes the following key contributions:

- Development of an adaptive semi-persistent scheduling, termed Ch-RRI SPS, algorithm for C-V2X networks, that allows each vehicle to dynamically adjust in real-time the RRI depending upon the considered C-V2X scenario.

- Presentation of asystem model and a collision model, which is based on the concept of tracking error, for the considered C-V2X networks.

- Extensive experiments based on system level simulations that show that Ch-RRI SPS outperforms the baseline SPS in terms of road safety performance, measured as collision risk, across all considered C-V2X setting. When compared to SPS with 20 ms, 50 ms, and 100 ms RRI, the results show a significant improvement in the reduction of collision risks respectively by 51.27%, 51.20%, and 75.41% for 80 vehicles/km. The results are consistent for other considered C-V2X scenarios. Furthermore, Ch-RRI SPS performs well in terms of packet delivery ratio in all considered scenarios.

Publications

The work presented in this chapter is part of the following peer reviewed publications:

- Avik Dayal, Vijay K. Shah, Biplav Choudhury, Vuk Marojevic, Carl Dietrich, and Jeffrey H. Reed. Adaptive Semi-Persistent Scheduling for Enhanced On-road Safety in Decentralized V2X Networks. In *2021 IFIP Networking Conference (IFIP Networking)*, pages 1–9, 2021.

1.5 Adaptive RRI Selection Algorithms for Improved Cooperative Awareness in Decentralized NR-V2X

In this final contribution, we investigate and propose improvements for the newest 3GPP Release 16 V2X communications technology that uses the 5G New Radio (NR) air interface, referred to as 5G NR-V2X. NR-V2X includes enhancements to the 3GPP's previous (C-V2X) based on the Long-Term Evolution (LTE) standard. NR-V2X offers two modes of operation, termed Mode-1 and Mode-2, that use sidelink communications, which is direct communication between users or vehicles without data passing through the gNodeB [67]. NR-V2X Mode-1, analogous to C-V2X Mode-3, employs a centralized scheduling approach, where a gNodeB schedules and assigns sidelink radio resources for two or more vehicles to communicate and exchange data directly. NR-V2X Mode-2, the successor to the C-V2X Mode-4 standard, assumes communications to occur outside the coverage of an gNodeB; therefore, every vehicle uses a sensing-based semi-persistent scheduling (SPS) protocol to sense and reserve sidelink radio resources. As mentioned previously, SPS was introduced as part of the Release 14 C-V2X Mode-4 standard, the predecessor to NR-V2X Mode-2 [77]. Since cellular connectivity can not be assumed ubiquitous, NR-V2X Mode-2 is considered as the baseline mode for NR-V2X.

In this work, we focus on improving the NR-V2X performance for *cooperative awareness*, the localization and trajectory prediction of neighboring vehicles and infrastructure. One metric that can quantify cooperative awareness performance is tracking error, the difference between a vehicle's actual and perceived location (via most recent BSM) by its neighboring vehicles. Tracking error, as opposed to conventional communication metrics such as packet delivery ratio (PDR) and throughput, captures the impact of multiple lost or outdated BSMs on a vehicle's awareness.

Since BSMs carry time-sensitive information, outdated BSMs (due to large RRIs) and/or lost BSMs (due to channel congestion) negatively impact the performance of cooperative awareness applications, mainly due to wrong localization of neighboring vehicles. Therefore, it is critical that the state information in each vehicles transmission be *fresh*, as stale information can compromise the aggregate awareness of the vehicular network. The freshness of information at receiving vehicles can be measured using Age-of-Information (AoI). AoI is the time elapsed since new state information has been generated and is a promising metric to measure the freshness of system state information. Results in [29] have found that AoI

has a strong correlation with tracking error in vehicular networks, which motivates further study of AoI.

In this final chapter, we introduce a new adaptive RRI algorithm, termed AoI-aware RRI (AoI-RRI) selection. Motivated by the benefits of reducing AoI, we propose AoI-RRI, an AoI-aware RRI selection algorithm for NR-V2X Mode-2 SPS that uses the average AoI observed by neighboring vehicles to select an optimal RRI. We compare AoI-RRI SPS to Ch-RRI (introduced in the previous contribution) and NR-V2X Mode-2 with static RRIs.

In this work, we make following key contributions:

- We again show for NR-V2X Mode-2 SPS that static RRIs suffer severely from under- and over-provisioning of radio resources (depending upon the vehicle densities). This in turn negatively impacts the timely successful delivery of BSMs and compromises the cooperative awareness of NR-V2X Mode-2 SPS.

- In a similar vein to Ch-RRI SPS, we develop AoI-RRI SPS, SPS powered by a *AoI aware* RRI selection algorithm. The AoI-RRI algorithm uses neighborhood age and channel resource measurements to choose an age optimal RRI iteratively.

- Experiments developed on our NR-V2X simulator show that when compared to NR-V2X Mode-2 SPS with 20 ms, 50 ms, and 100 ms RRI, the proposed Ch-RRI and AoI-RRI SPS demonstrate a substantial reduction of tracking error. Ch-RRI as compared to AoI-RRI shows a lower AoI and tracking error in low density highway scenarios, and is faster in converging to a local minimum AoI. However, the average AoI and tracking error of AoI-RRI is lower at higher densities.

Publications

The work presented in this chapter is part of the following peer reviewed publications:

- A. Dayal, V. K. Shah, H. Dhillon, and J. Reed. Adaptive RRI Selection Algorithms for Improved Cooperative Awareness in Decentralized NR-V2X. *Submitted to IEEE Transactions on Intelligent Transportation Systems (Under Review)*, pages 1–12.

1.6 Other Publications

The following peer reviewed publications pertaining to cyber physical systems have inspired some of the research presented in this dissertation, but are not a part of this dissertation.

- A. Dayal, Yi Deng, A. Tbaileh, and S. Shukla. VSCADA: A reconfigurable virtual SCADA test-bed for simulating power utility control center operations. In *2015 IEEE Power Energy Society General Meeting*, pages 1–5.
- A. Dayal, A. Tbaileh, Y. Deng, and S. Shukla. Distributed VSCADA: An integrated heterogeneous framework for power system utility security modeling and simulation. In *2015 Workshop on Modeling and Simulation of Cyber-Physical Energy Systems (MSCPES)*, pages 1–6.
- Biplav Choudhury, Vijay K Shah, Avik Dayal, and Jeffrey H Reed. Joint age of information and self risk assessment for safer 802.11 p based V2V networks. In *IEEE INFOCOM 2021-IEEE Conference on Computer Communications*, pages 1–10. IEEE, 2021.

Chapter 2

Technical Background

In 1999, the US Federal Communications Commission (FCC) reserved 75 MHz of spectrum (spanning 5.85-5.925 GHz) in the 5.9 GHz band for Intelligent Transportation Services (ITS) [52]. The European Communication Commission soon followed, allocating three 10 MHz channels. The allocation has led to significant research activity and the development of Vehicle-to-everything (V2X) communications. Vehicle-to-everything (V2X) [1] communications has potential of improving on-road safety, leading to the prevention/reduction of road accidents and more efficient traffic management [74]. There are two competing technologies that enable V2X communications, Dedicated Short Range Communications (DSRC) and Cellular-V2X (C-V2X) [64]. DSRC was the first set of radio standards to be completed in 2010 and was based on the 802.11p standard [10].

The ITS band is divided into seven 10 MHz channels. The DSRC spectrum at 5.9 GHz consists of seven 10 MHz channels. The U.S. channels are numbered 172 through 184, with Ch. 178 as the Control Channel (CCH), and Chs. 172, 174, 176, 180, 182, and 184 as Service Channels (SCHs) [55]. The Physical (PHY) and Medium Access Control (MAC) layer protocols for DSRC are defined in the 801.11p amendment of the IEEE 802.11p standards, known as the Wireless Access in Vehicular Environments (WAVE) amendment. The counterpart European DSRC standard is known as European Telecommunications Standards Institute (ETSI) Technical Specification 101 [1].

There are two major V2X use cases: basic safety and cooperative traffic efficiency messages. Basic safety messages (BSMs) are periodic messages that contain information about vehicle position and speed. They are expected to have a latency of less than 100 ms, a transmission rate of 10 Hz, and transmission range from 100 m to 1 km [15]. Cooperative traffic efficiency messages are event triggered messages that are intended to help vehicular flow. These messages are required to have a latency of less than 200 ms over a distance of 300 m to 5 km

[1] V2X refers to vehicle-to-infrastructure (V2I), vehicle-to-vehicle (V2V), and vehicle-to-pedestrian (V2P) communications.

and a transmission frequency of 10 Hz. The focus of this dissertation is primarily focused on the use and dissemination of basic safety messages (BSMs), though many of the ideas developed in this dissertation can be adapted for cooperative traffic efficiency messages.

Table 2.1: Requirement ranges for 3GPP use cases

Use Case	Payload (Bytes)	Transmit Rate (Messages/sec)	Reliability (%)	Range (m)
Vehicular Platooning	50-6000	2-50	90-99.99%	80-350
Advanced Driving	300-12000	10-100	90-99.99%	360-700
Extended Sensors	1600	10	90-99.99%	50-1000
Remote Driving	16000-41700	33-200	99.99%	1000

2.1 Dedicated Short Range Communications

DSRC is a 802.11-based communications standard created to support vehicular communications. The PHY and MAC protocols for DSRC are defined in the 802.11p amendment to the IEEE 802.11 standard, known as the Wireless Access in Vehicular Environments (WAVE) [48]. The 802.11p modulation uses orthogonal frequency division multiplexing and the waveform is considered a variation of the IEEE 802.11a standard, with changes designed for vehicles travelling at high speeds [56]. The 802.11p packet is made up of a preamble, signal field, and data field. Each OFDM symbol consists of 64 subcarriers, of which 48 are data subcarriers, 4 are pilot subcarriers, and the remaining 12 are null subcarriers [53]. The channel bandwidth is 10 MHz, and the subcarrier spacing is 312 kHz. The 802.11p standard uses a block-comb-type pilot pattern for channel estimation. The two symbols at the beginning of the IEEE 802.11p packet are the block pilot, and each OFDM symbol then uses the pilot as the comb type.

At the MAC layer, DSRC employs Carrier Sense Multiple Access [44]. However, DSRC CSMA has no exponential back-off, meaning the contention window size remains fixed in DSRC. The removal of the exponential back-off is in part because DSRC is *broadcast based*, with no acknowledgment message sent back to the transmitter. Using exponential back-off

causes large contention window sizes, leading to increased latency. The DSRC protocol also allows for packet expiration at the transmitter. Packet expiration means that packets are discarded at the transmitter if the transmitting vehicle cannot gain access to the channel within the broadcast interval. The reasoning behind packet expiration is due to the delay-sensitive nature of vehicular networks; since the packet information for the vehicle has *aged* and is no longer valid, the vehicle should generate a new packet in the next broadcast interval. Another notable design aspect of the DSRC standard is that vehicles do not use the request-to-send (RTS)/ clear-to-send (CTS) handshake mechanism present in traditional 802.11 networks. The RTS/CTS handshake mechanism was removed to reduce the significant overhead in transmissions. For a more in-depth discussion on the DSRC standard, please refer to [79].

2.2 C-V2X and NR-V2X Sidelink

In this section we discuss the cellular based competitor to DSRC, the Release 14 C-V2X Mode-4 and Release 16 NR-V2X Mode-2 standards. We start with the physical layer for both standards and then detail the inner workings of sensing-based semi-persistent scheduling (SPS) that allows vehicles to find and reserve suitable transmission opportunities.
Under Release 12 for public safety, the Third Generation Partnership Project (3GPP) introduced the concept of device-to-device (D2D) communications. D2D communications allow for the quick exchange of data over short distances with a direct link between nodes. These D2D communications (also referred to as sidelink communications) can also enable user equipments (UEs) to bypass the central LTE base station. In 2016, 3GPP Release 14 introduced four communication modes for device-to-device (D2D) communications [58]. Modes 1 and 2 were designed to extend the battery life for mobile devices while increasing end-to-end latency. Modes 3 and 4, referred to as C-V2X Mode-3 and Mode-4, were specifically designed for V2V communications [24]. In Mode-3, the eNodeB is responsible for scheduling and allocating resources for vehicles, and there is assumed network coverage. In Mode-4, partial/no network coverage is assumed, and resource allocation occurs in a distributed manner, with no eNodeB. This Mode-4 standard is used for V2X communications, and is the baseline for the C-V2X standard. In Release 16, 3GPP has introduced a new V2X communications technology that uses the 5G New Radio (NR) air interface, referred to as 5G NR-V2X. NR-V2X includes enhancements to the 3GPP's previous cellular V2X communications technology (C-V2X) based on the Long-Term Evolution (LTE) standard. NR-V2X offers two modes of

operation, termed NR-V2X Mode-1 and Mode-2, that use sidelink communications with no data passing through the gNodeB [67].

Similar to C-V2X Mode-3, NR-V2X Mode-1 employs a centralized scheduling approach, where a gNodeB schedules and assigns sidelink radio resources for two or more vehicles to communicate and exchange data directly. NR-V2X Mode-2, the successor to C-V2X Mode-4, assumes communications to occur outside the coverage of a gNodeB; therefore, every vehicle uses a sensing-based semi-persistent scheduling (SPS) protocol to sense and reserve sidelink radio resources. SPS was introduced as part of the Release 14 C-V2X Mode-4 standard, the predecessor to NR-V2X Mode-2 [77]. Since cellular connectivity can not be assumed ubiquitous, NR-V2X Mode-2 is considered as the baseline mode for NR-V2X. Fig. 2.1 illustrates the modes of C-V2X and NR-V2X. For the purposes of this dissertation, we focus on the two decentralized vehicular communication protocols: C-V2X Mode-4 and NR-V2X Mode-2.

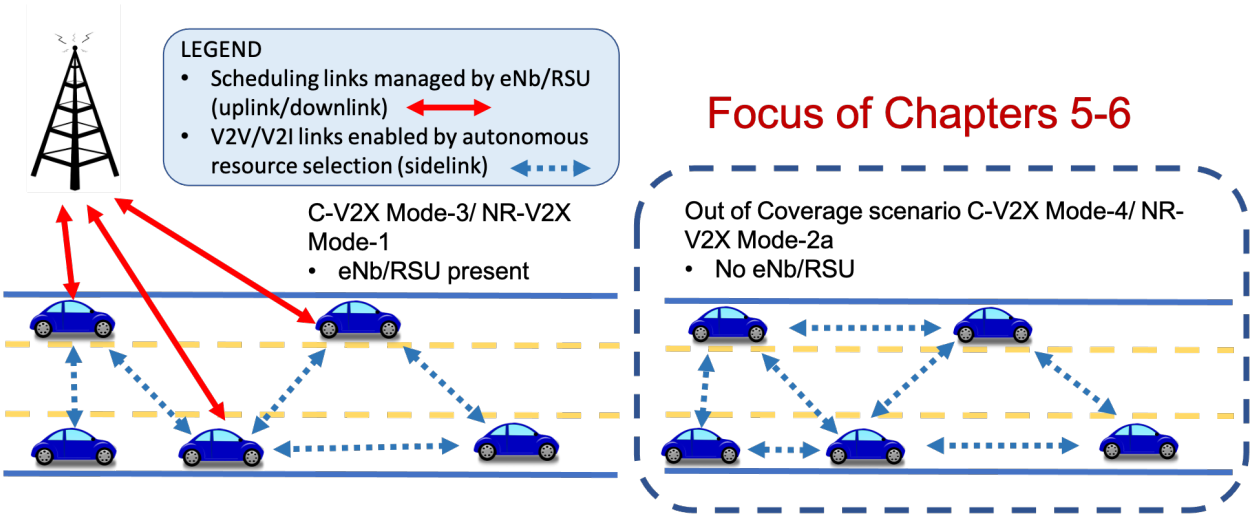

Figure 2.1: Illustration of C-V2X Mode-3 (NR-V2X Mode 1) and Mode-4 (NR-V2X Mode 2).

2.2.1 Release 14 C-V2X and Release 16 NR-V2X Sidelink Physical Layer Structure

At the physical layer, C-V2X is similar to the LTE uplink and uses single-carrier frequency division multiple access (SC-FDMA) [5]. C-V2X supports 10 and 20 MHz channels at 5.9 GHz.

In Mode-4, the time-frequency resources are divided into resource blocks (RBs), subframes (sf), and subchannels. Frames are 10 ms in length, and are comprised of 10 subframes. Subframes are typically comprised of 2 resource blocks in time [14]. A resource block is the smallest schedulable unit of time and frequency that can be allocated to users. Each RB is made up of 7 SC-FDMA symbols and is 180 kHz wide in frequency with 12 equally spaced subcarriers. Each RB occupies 0.5 ms in time, with a minimum allocation time interval of 1 ms, also referred to as the transmission time interval (TTI). Subchannels are composed of resource blocks contiguously located in frequency. In C-V2X, the data packet to be transmitted, called the Transport Block (TB), typically takes up one or more subchannels. Each TB is transmitted in the same subframe along a sidelink control information (SCI), that contains the modulation and coding scheme (MCS) [77].

The Rel. 16 NR-V2X sidelink is similar in principle to the C-V2X sidelink, with some notable differences. The NR-V2X sidelink is designed to operate in two different frequency ranges, from 410 MHz - 7.125 GHz (FR1) and 24.25 GHz - 52.5 GHz (FR2) [38]. Though both frequency ranges are supported in Rel. 16, NR-V2X is expected to operate in the FR1. Resources in the NR-V2X time domain are made up of frames, subframes, and slots. Similar to Release 14 C-V2X, each frame is made up of 10 subframes, and each frame time length is typically 10 ms. Subframes are typically 1 ms in length, and are further broken down into slots. A slot consists of 4 OFDM symbols, which means that the length of each slot depends on the chosen subcarrier spacing. The NR V2X sidelink uses cylic prefix orthogonal frequency modulation (CP-OFDM), as opposed to C-V2X SC-FDMA, and supports multiple subcarrier spacings of 15, 30, and 60 kHz.

2.2.2 Semi-Persistent Scheduling (SPS)

At the MAC layer, both C-V2X Mode-4 and NR-V2X Mode-2 utilize SPS that uses sensing to determine suitable semi-persistent transmission opportunities, i.e., set of subframes, for BSM transmission. Fig. 2.2 depicts the SPS algorithm[2] for the C-V2X Mode-4 and NR-V2X Mode-2, with the steps that are changed for NR-V2X Mode-2 highlighted with dotted boxes. We use sf_i^j to refer to a single-subframe resource where i is the subframe index and j is the subchannel index of J total subchannels. See Fig. 2.3 for the illustration of subframe and other key terminologies (e.g., sensing window) related to SPS.

[2]Please refer to [64], [14], [38], and [67] for a detailed discussion on SPS.

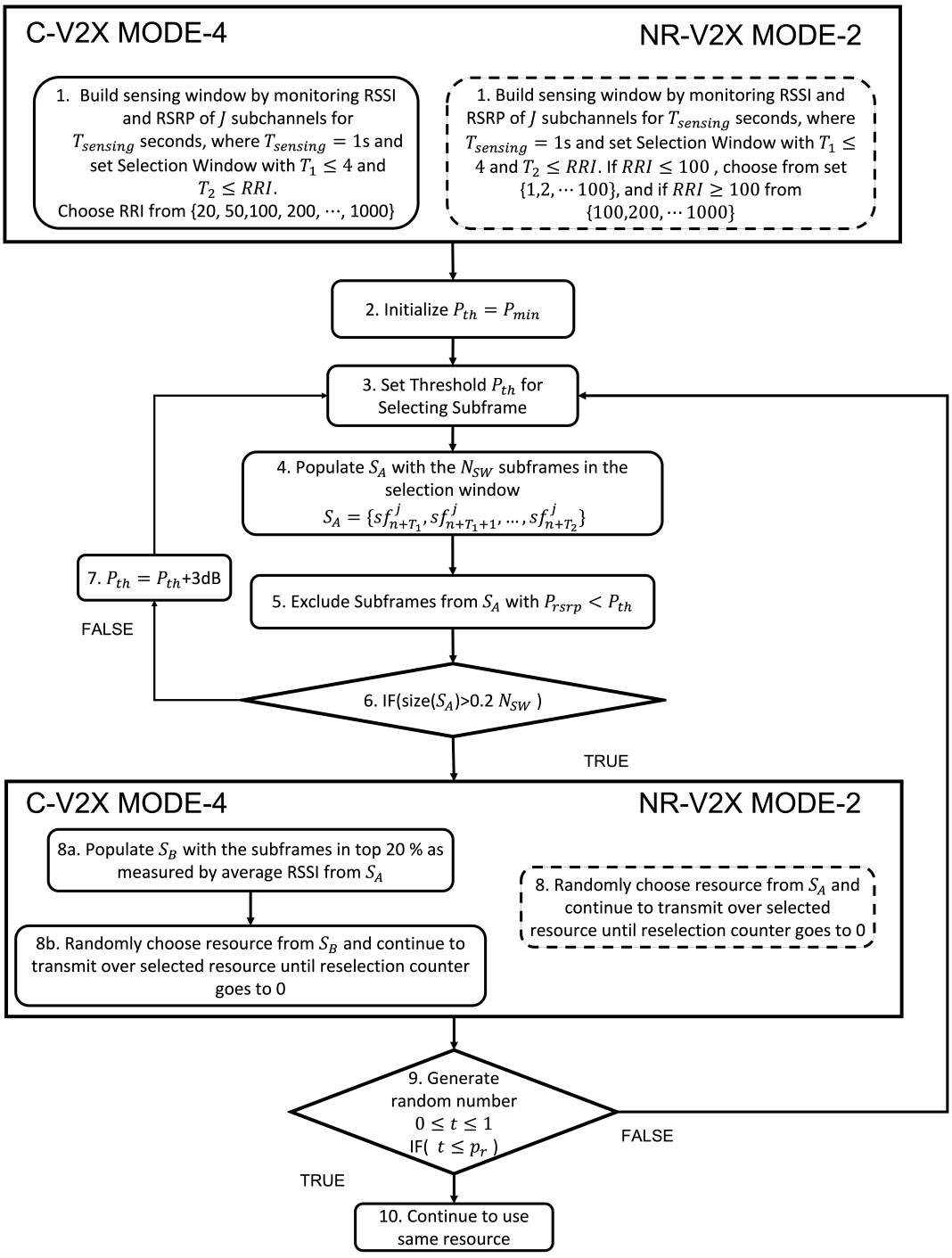

Figure 2.2: Flowchart of SPS algorithm for C-V2X Mode-4 and NR-V2X Mode-2.

- **Sensing (Step 1):** Each vehicle continuously monitors the subframes by measuring the reference signal received power (RSRP) and the sidelink received signal strength

indicator (S-RSSI) across all J subchannels; and stores sensing measurements for a prespecified $T_{sensing}$ time, known as the *sensing window*. $T_{sensing}$ is set to 1 s for C-V2X Mode-4 and 100 ms for NR-V2X Mode-2. Let subframe sf_n denote the first subframe after the sensing window. Then we can write the sensing window at sf_n as the following set of single-subframe resources for the j^{th} subchannel: $\left[sf^j_{n-N_{sensing}}, \ldots, sf^j_{n-1}\right]$.

- **Identifying available resources (Steps 2-8):** Each vehicle initializes a *selection window* with a set of consecutive candidate subframes (See Step 2). $T_1 \leq 4$ and $T_2 \leq RRI$ are the start and end subframes for the selection window. The **RRI** refers to the time interval between two consecutive BSM transmissions (See Fig. 2.3 for illustration). Each vehicle utilizes $N_{sensing}$ subframes (obtained in Step 1) to identify and subsequently select the available subframe within the selection window for BSM transmission as follows.

  1. The vehicle sets (i) the RSRP threshold, P_{th}, to a minimum RSRP value, P_{min} (Step 3) and (ii) initializes set S_A as all subframes in the selection window, i.e., $S_A = [sf_{n+T_1}, sf_{n+T_1+1}, \cdots, sf_{n+T_2}]$, and S_B as an empty set (See Step 5).
  2. As shown in Step 6, the vehicle excludes all candidate subframes from set S_A if one of the following conditions are met (i) the vehicle has not monitored the corresponding candidate subframe in the sensing window (i.e., $N_{sensing}$) and (ii) the linear average RSRP measurement for corresponding candidate subframe is higher than P_{th}. The RSRP exclusion criteria for the i^{th} subframe (for jth subchannel) in the selection window can be written as

$$\frac{1}{\mathcal{K}} \sum_{k=0}^{\mathcal{K}} RSRP\left(sf^j_{n+T_1+i-N_{sensing}+k\cdot RRI}\right) \geq P_{th} \tag{2.1}$$

     where $\mathcal{K} = \frac{N_{sensing}}{RRI}$. If $RRI = 100$ ms and $N_{sensing} = 1000$ ms and $i = 4$, then, we look at RSRP value across following 10 subframes – $\{4, 104, 204, \ldots, 904\}$ and divide it by $\mathcal{K} = \frac{1000}{100} = 10$ to find the average RSRP.
  3. If the remaining subframes in S_A is less than 20% of total available subframes (Step 7), then P_{th} is increased by 3 dB (Step 8), and Steps 4 to 7 are repeated.

- **Resource Selection (Steps 8-10):** If more than 20% of available channel resources are identified, then, as shown in Step 8a, the vehicle populates S_B with the first 20% of candidate subframes which have the lowest average S-RSSI in set R_A. The vehicle

then randomly selects a candidate subframe from set S_B as the selected resource for the first BSM transmission (See Step 8b).

$$RSSI\left(\sum_{k=0}^{\mathcal{K}} sf^{j}_{n+T_1+i-N_{sensing}+k\cdot RRI}\right) \tag{2.2}$$

Note that in NR-V2X Mode-2, step 8a is removed, and the vehicle randomly selects a candidate subframe from set S_A.

- **Resource Reselection (Steps 9-10):** Each vehicle can reserve the same subframe (selected in Step 8b) for the next *Resource Counter (RC)* [3] number of subsequent transmissions with the same transmission interval, i.e., *RRI*. The RC varies with the RRI to ensure that the selected subframe/resource is in use for at least 0.5 s and at most 1.5 s. This means that for a 20 ms RRI, $25 \leq$ RC ≤ 75, for 50 ms RRI, $10 \leq$ RC ≤ 30, and for a 100 ms RRI, $5 \leq$ RC ≤ 15. After RC reaches 0, the vehicle can either continue utilizing the preselected resources with a probability p_r or reselect new resources for BSM transmissions with a probability $(1 - p_r)$ (See Steps 11-13).

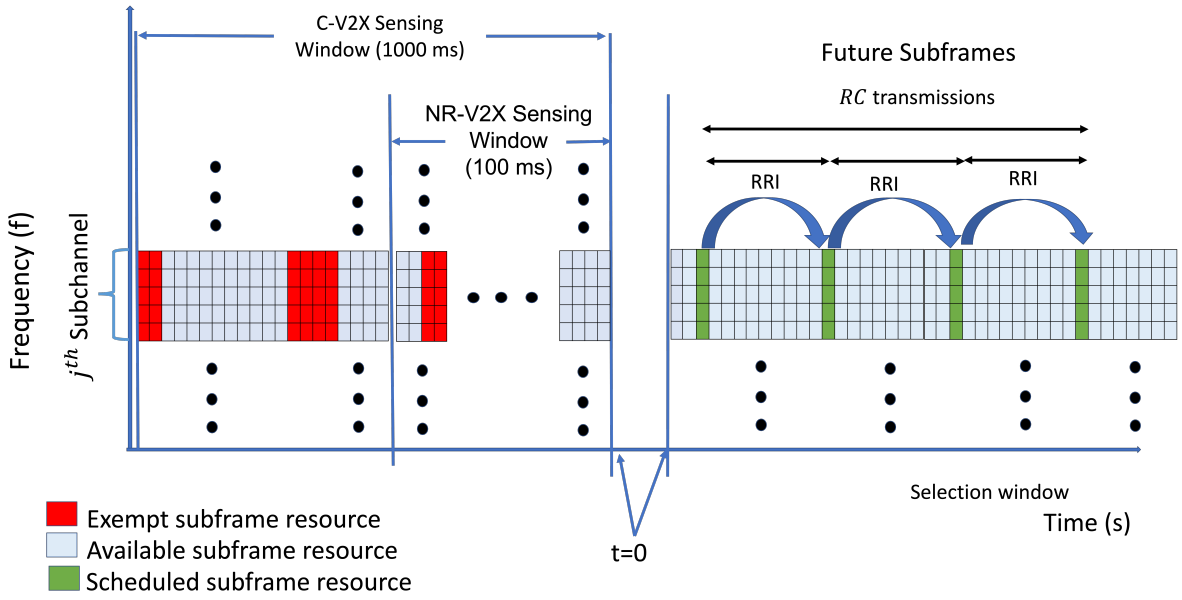

Figure 2.3: Illustration of semi-persistent scheduling for C-V2X Mode-4 and NR-V2X Mode-2.

[3] Resource Counter (RC) is the maximum number of transmissions a certain vehicle is allowed (by utilizing the selected subframe/resource in the current selection window) before having to reselect a new set of resources.

Differences between C-V2X and NR-V2X SPS

Figure 2.2 shows a few differences between C-V2X Mode-4 and NR-V2X SPS that are worth mentioning, which the changes in the NR-V2X SPS standard presented in dotted boxes. Release 14 SPS has an additional selection criteria that selects subframe resources with the lowest sidelink received strength indicator (S-RSSI) measurement. This was removed in Release 16 to accommodate smaller RRIs [9]. In the Release 14 C-V2X standard, RRIs equal to or below 100 ms were restricted to 20 ms, 50 ms, or 100 ms [64]. Release 16 NR-V2X Mode-2 provides more flexibility by allowing any integer RRI between 1 and 99 ms for any RRIs below 100 ms [38]. In NR-V2X Mode-2 SPS, each vehicle selects an RRI at the time of resource selection, although the standard leaves the selection of RRI up to the user [38].

2.3 3GPP Evaluation Methodology

Before proposing improvements to SPS in Chapters 5 and 6, we briefly discuss the recommended 3GPP simulation guidelines and topologies for the performance evaluation of C-V2X and NR-V2X. We use these topologies to verify the performance of our SPS simulations. The 3GPP Release 14 and Release 16 consider two evaluation environments for both C-V2X and NR-V2X: the urban grid and highway environments [7].

2.3.1 WINNER + B1 Channel Model

Both the urban grid and highway environments use the 3GPP WINNER+B1 channel models for evaluating C-V2X Mode-4 [7]. The LOS and NLOS path losses for the WINNER B1 channel model in the 5.9 GHz band are computed as

$$PL_{LOS}(dB) = \begin{cases} 22.7 \cdot \log_{10}(d) + 27.0 + 20.0 \cdot \log_{10}(f_c) & 30 \text{ m} < d < d_{BP} \\ 40.0 \cdot \log_{10}(d) + 9 - 16.2 \cdot \log_{10}(h_{BS}) & \\ -16.2 \cdot \log_{10}(h_{MS} + 3.8 \cdot \log_{10}(f_c)\,. & d_{BP} < d < 5 \text{ km} \end{cases} \tag{2.3}$$

$$\begin{aligned} PL_{NLOS}(dB) = (44.9 - 6.55 \cdot \log_{10}(h_{BS})) \cdot \log_{10}(d) \\ +5.83 \cdot \log_{10}(h_{BS}) + 15.38 + 23 \cdot \log_{10}(f_c)\,, \end{aligned} \tag{2.4}$$

where f_c is the carrier frequency, d is the distance between the transmitter and receiver, h and d_{BP} is the breakpoint distance. For the purposes of vehicular communications, the antenna heights h_{MS} and h_{BS} are set to 1.5 m [7]. d_{BP} is computed as

$$d_{BP} = 4 \cdot (h_{BS} - 1) \cdot (h_{MS} - 1) \cdot f_c/c, \tag{2.5}$$

where $c = 3 \cdot 10^8$ m/s. The 3GPP highway scenario only uses the LOS path loss. In the urban scenario, if there is no building present between the two vehicles, the LOS path loss is used. Otherwise, if there is a building present between two vehicles, the NLOS path loss model is assumed.

2.3.2 3GPP Highway Scenario

The 3GPP highway scenario is illustrated in Fig. 2.4. In the highway scenario, vehicles move along a 2 km, six lane highway, with three lanes dedicated to each direction. The highway model assumes each vehicle moves with a constant velocity and the vehicles in the top three lanes to move in the positive x direction (from left to right) and the vehicles in the bottom three lanes to move in the negative x direction (from right to left). For each density, the inter-vehicle distance in each lane is computed as the distance traveled by a vehicle in 2.5 seconds. There are two standard 3GPP highway scenarios: the highway fast and highway slow scenarios. The highway fast scenario is 120 vehicles traveling at 140 km/hr in the highway scenario, which is used extensively in Chapter 5. The highway slow scenario consists of 240 vehicles traveling at 70 km/hr in the same highway scenario.

We validate our SPS simulator by comparing the simulator highway fast and slow packet delivery ratio (PDR) of SPS with a 100 ms RRI to the highway fast and slow scenarios referenced in [4] and [64]. Unlike the simulation settings described in Chapters 5 and 6, all vehicles travel at a constant velocity. Additionally, only PDR is used to evaluate the performance of our SPS simulator, and compare directly to the results of [64]. Figures. 2.5(a) and 2.5(b) compare the PDR performance of our SPS implementation averaged across 5 trials to the PDR performance in [64], with the error bars indicating the standard deviation across trials. Notice from Figs. 2.5(a) and 2.5(b) that the performance of our SPS implementation matches closely to [64], and most of the PDR results fall within the margin of error. However there are a few discrepancies, most notably with the 150 m range in Fig. 2.5(a). This could be attributed to different values used from the block error rate (BLER) curves in

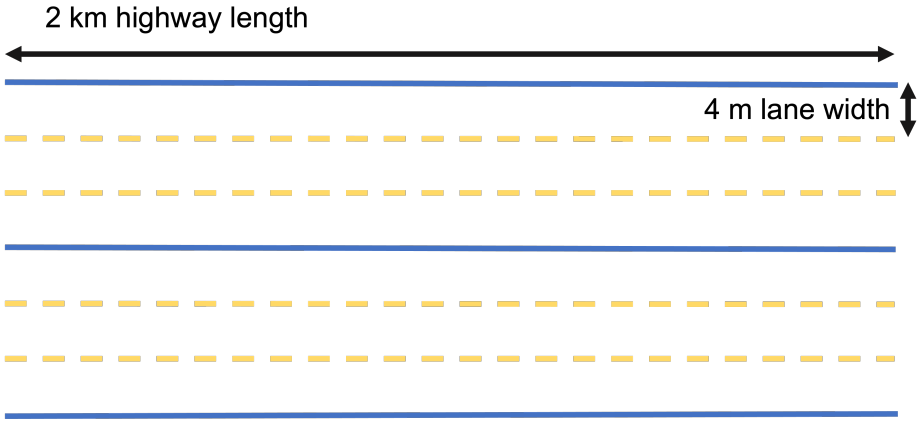

Figure 2.4: 3GPP highway scenario.

[6]. Figures. 2.6(a) and 2.6(b) compare the PDR performance of our SPS implementation averaged across 5 trials with a 20 ms, 50 ms, and 100 ms RRI. Note from Figs. 2.6(a) and 2.6(b) that the PDR performance drops as the RRI decreases. A smaller RRI implies an increase in congestion, leading to more packet collisions.

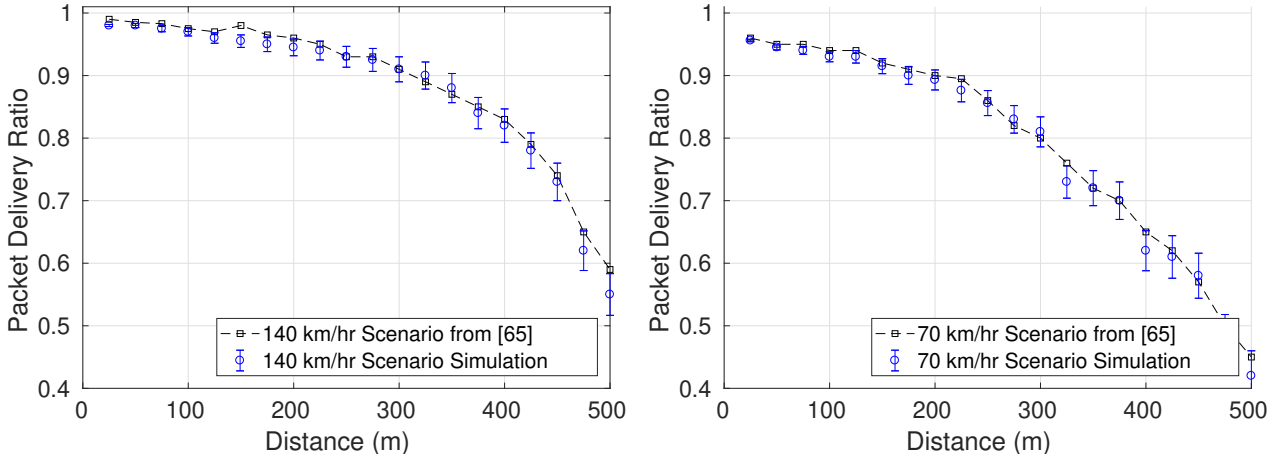

(a) 120 vehicles traveling at 140 km/hr

(b) 240 vehicles traveling at 70 km/hr

Figure 2.5: 100 ms RRI PDR across highway fast and slow scenarios.

2.3.3 3GPP Urban Scenario

The 3GPP urban scenario is illustrated in Fig. 2.7. The urban scenario requires vehicles be spread out over 3 × 3 blocks, and each block size is 250 × 433 m. Vehicles are dropped

Table 2.2: 3GPP SPS highway simulation parameters

Parameter	Value
Vehicle density	{60, 120} veh
Length of road	2000 m
Number of lanes	6
Lane width	4 m
PDR distance bins	25-500 m
Simulation time	8 seconds
Transmission Power	23 dBm
Transmission Range	300 m
Sensing Range	300 m
P_{th}	-110 dBm
Vehicle speeds	140 km/hr, 70 km/hr
Packet Size	190, 300 Bytes
MCS Index	7
Propagation Model	Winner+ B1 LOS Model
Number of trials	5

according a Poisson distribution, and as in the highway scenario, the inter-vehicle distance in each lane is computed as the distance traveled by a vehicle in 2.5 seconds. Each vehicle moves with a constant velocity of 60 km/hr. As in the highway scenario, each lane has two lanes in each direction. The width of each lane is 3.5 m and each street has a 3 m sidewalk on each side. Once a vehicle is dropped in the simulation and reaches a intersection, the vehicle goes straight, turns left, and turns right with the probability of 0.5, 0.25, and 0.25, respectively. The urban scenario is simulated with 200 and 600 vehicles.

Figures. 2.8(a) and 2.8(b) compare the PDR performance of our SPS implementation averaged across 5 trials with a 20 ms, 50 ms, and 100 ms RRI. Note from Figs. 2.8(a) and 2.8(b) that similar to the highway scenarios, the PDR performance drops as the RRI decreases. This implies that a smaller RRI leads to an increase in packet collisions. However, the baseline PDR performance of the urban scenario is considerably worse than the PDR of the highway scenario. This is an impact from the combination of the more severe LOS path loss and the NLOS path loss.

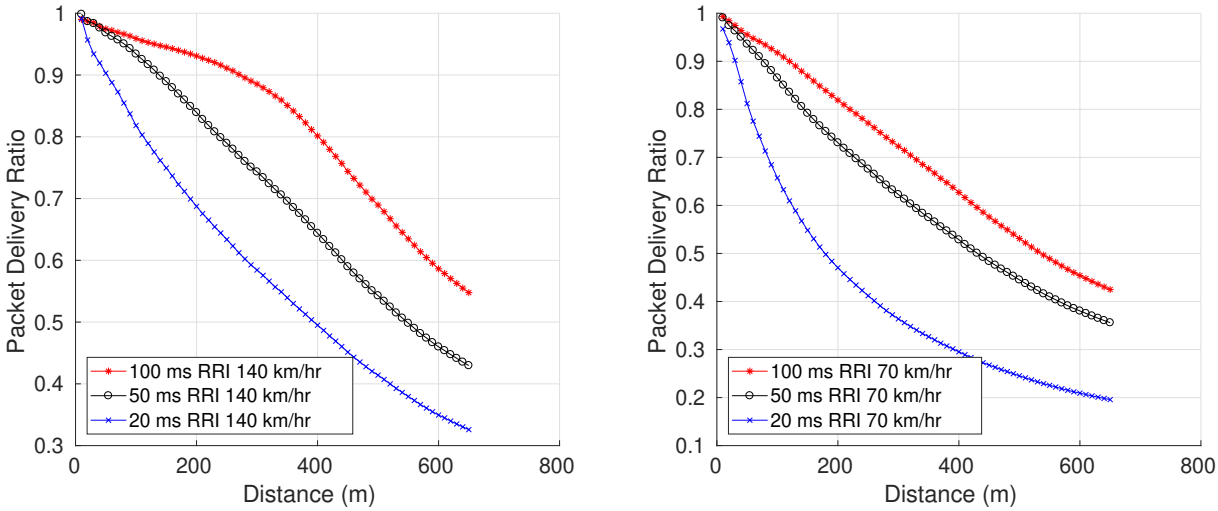

(a) 120 vehicles traveling at 140 km/hr

(b) 240 vehicles traveling at 70 km/hr

Figure 2.6: 20 ms, 50 ms, and 100 ms RRI PDR across highway fast and slow scenarios.

Table 2.3: 3GPP SPS urban simulation parameters

Parameter	Value
Number of Vehicles	{200, 600} veh
PDR distance bins	10-450 m
Simulation time	20 seconds
Transmission Power	23 dBm
Transmission Range	300 m
Sensing Range	300 m
P_{th}	-110 dBm
Vehicle speeds	60 km/hr
Packet Size	190, 300 Bytes
MCS Index	7
Propagation Model	Winner+ B1 Model
Number of trials	5

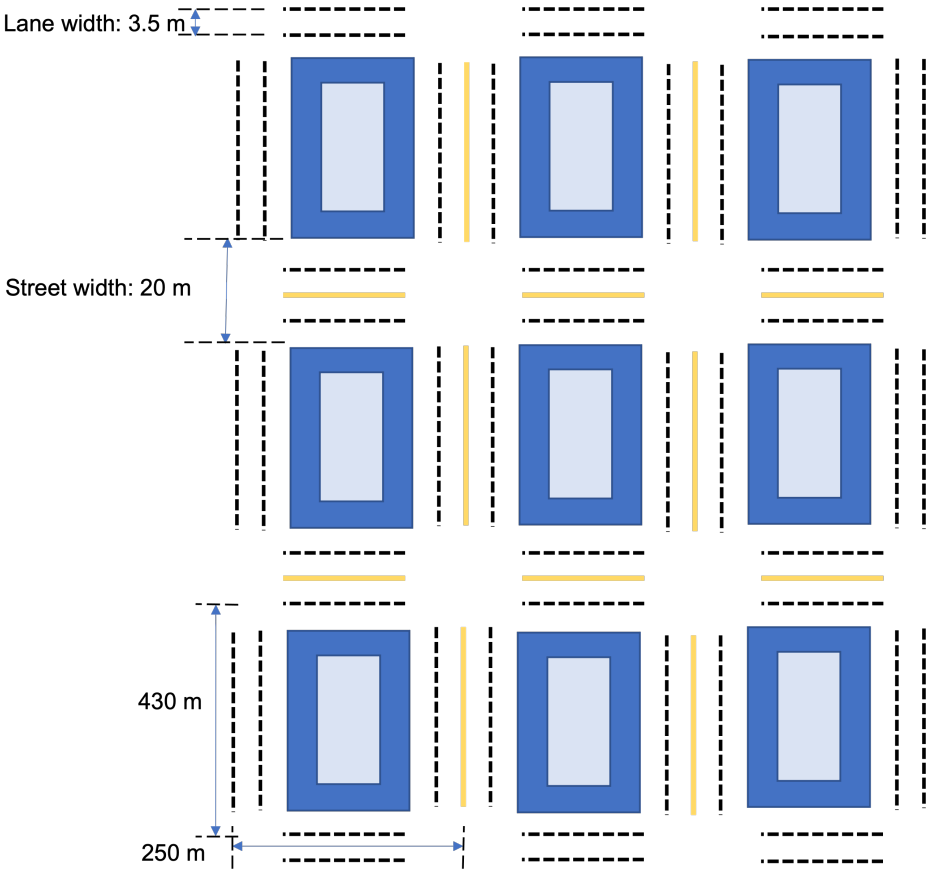

Figure 2.7: 3GPP Manhattan grid scenario

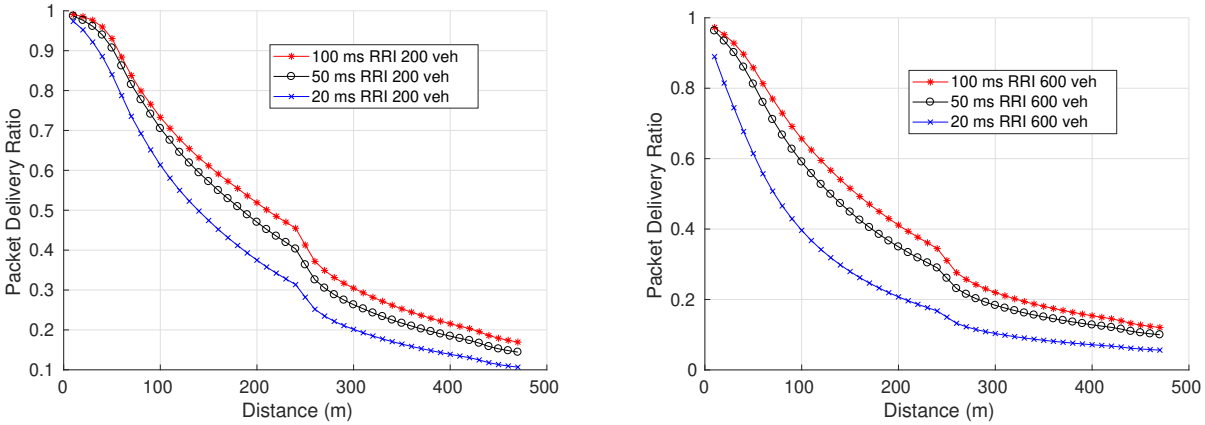

(a) 200 vehicles traveling at 60 km/hr

(b) 600 vehicles traveling at 60 km/hr

Figure 2.8: 20 ms, 50 ms, and 100 ms RRI PDR across 200 and 600 vehicle urban scenarios.

Chapter 3

Risk Controlled Beacon Transmission in V2V Communications

Spectrum regulators and stakeholders from the wireless industry and intelligent transportation system (ITS) communities are exploring the use of the 5.9 GHz band for the dissemination of safety messages, also referred to as safety beacons or basic safety messages (BSMs) that are broadcast by the vehicles. Dedicated short range communications (DSRC) sends out these messages at a constant rate of 10 Hz and packet collisions occur in dense vehicular environments. In this chapter, we propose a dynamic beaconing protocol, where the priorities are established as a function of the risk of collision. The protocol determines a higher beacon transmission rate for vehicles that are at a higher risk of collision than for vehicles that are at a lower risk. Two risk based beacon rate protocols are evaluated in our ns-3 simulator, one that adapts the beacon rate between 1 and 10 Hz, and another between 1 and 20 Hz. The packet delivery ratio (PDR) performance is improved by up to 45% in congested environments using the 1 - 10 Hz adaptive beacon rate protocol and by 38% using the 1 - 20 Hz adaptive protocol. The simulation results also show that the likelihood of a vehicle collision due to a missed packet decreases by up to 41 % and 77% in a three lane dense highway scenario with 160 vehicles operating at different speeds by using 1-10 Hz and 1-20 Hz adaptive rate protocol, respectively. Note that while the 1-10 Hz adaptive rate protocol shows a better PDR performance, this does not necessarily translate to a lower collision rate, due to the benefits of lower inter-packet transmission time. These results advocate for an adaptive beacon rate protocol, but with a higher beacon safety rate of 20 Hz.

3.1 Literature Review

There has been extensive work on controlling channel congestion of DSRC safety beacons. While the current WAVE standard calls for a 100 ms interval (corresponding to a beacon rate of 10 Hz) between road safety messages, many papers ([13], [75] [10], and [59]) have been published on more optimal beacon rates and adaptive beacon rate control algorithms. The comparison of these various protocols can be difficult because of the variety of different performance metrics that are used to judge the effectiveness of vehicular ad hoc networks. Most of these works focus on reducing the congestion of the control channel, and as far as we know, none consider the dynamic location and velocity of the neighbors to determine the beacon rate. This section concentrates on some of the most popular works being considered in the ETSI and WAVE standard. Recent work on beacon rate optimization [75] analyze the effectiveness of the 100 ms delay between messages and use an optimization algorithm to improve network performance by selecting the most optimal beacon rate. The authors of [60] use vehicle densities and hidden terminals in their analysis.

One of the most popular rate congestion techniques, Linear Message Rate Integrated Control (LIMERIC) [13], provides a method for controlling the beacon rate to minimize channel congestion but without knowledge of nearby neighbors. The jth vehicle adjusts its rate according to:

$$r_j(t) = (1 - \alpha)r_j(t - 1) + \beta(r_g - r(t - 1)) \tag{3.1}$$

where α and β are system parameters, r_g is the overall target packet frequency and $r(t-1)$ represents the measured overall packet frequency by the vehicle in the previous time window. LIMERIC ensures that the transmission rate for a vehicle is chosen such that the total channel load remains below a specific threshold. In [75], the Periodically Updated Load Sensitive Adaptive Rate (PULSAR) mechanism shares information such that all vehicles within the interference range of the most congested node converge to the same message rate limit cycle. Tielert et al. [76] adapt both the power and beacon rate to prioritize safety and the congestion of the control channel, but do not use the information of surrounding traffic conditions to adjust the rate.

This work differentiates from previous studies by considering the risk based on distance, velocity, and acceleration of each individual vehicle with respect to the nearby vehicles

around it, and modifying the interval rate accordingly.

3.2 Problem Formulation

The general problem with vehicular communications in highway and general road scenarios is illustrated in Fig. 3.1. With two vehicles approaching each other along a road, each vehicle's position and critical information must be transmitted to the other vehicles before a vehicular collision occurs. The total time for a vehicle to collide with another is denoted as t_{coll}. As shown in Fig. 3.1, t_{coll} can be broken into three parts, the communications system time (t_s) required for a car to communicate with surrounding vehicles, the reaction time (t_{react}) required for a car to make a decision on future actions, and the braking interval (t_{brake}), the amount of time that the vehicle requires to slow down or take evasive action.

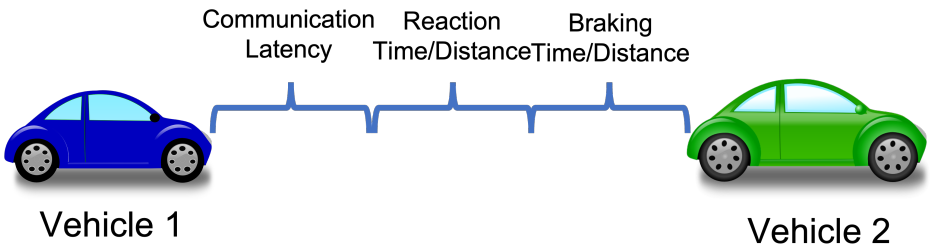

Figure 3.1: Time to collision between two vehicles on the highway

Though there are many complex models for the collision time of each vehicle, a simplified model based on vehicle kinematics is used initially. The formula below is used to determine the t_{coll}.

$$t_{coll} = \frac{d_{coll}}{\Delta v} = \frac{\frac{\Delta v^2}{a} + (t_r + t_s)\Delta v}{\Delta v} = \frac{\Delta v}{a} + (t_{react} + t_s) \tag{3.2}$$

where Δv is the relative velocity between two vehicles, and a is the maximum deceleration assumed by each vehicle. t_{brake} corresponds to $\frac{\Delta v}{a}$, and t_r and t_s are the vehicle reaction time and system delay, respectively. These three terms correspond to the three time intervals illustrated in Fig. 3.1. The purpose of this work is to minimize the number of dropped packets which brings down the average communication system delay t_s. Since 802.11p is an ad-hoc network protocol where each vehicle transmits at a fixed interval, the most effective

method to ensure this is by minimizing the probability of a packet being dropped.

3.3 Risk Model Description and Methodology

In order to reduce the probability of a dropped packet, the proposed risk based beacon control protocol adjusts the beacon rate depending on the vehicle collision risk seen by each vehicle. Vehicles that have a larger t_{coll} to the surrounding vehicles transmit at a lower beacon interval rate as compared to the vehicles at a lower risk for an accident or vehicular collision around it. This reduces the likelihood of channel congestion for high priority vehicles - those judged to be more likely at risk.

A vehicle message priority is allocated dependent on their t_{coll} to nearby vehicles. Since the t_{react} time is assumed to be constant across all vehicles in the simulation, the t_{coll} time is primarily dependent on the vehicle's t_{brake}, or the relative velocity and distance it has with respect to the vehicles around it. For the purposes of this chapter, a vehicle priority status is 5 (the highest priority) if they have a t_{coll} of below 5 sec. This value was chosen based on t_{coll} value chosen in Section 3.2, and t_s value of 1 s. Fig. 3.2 shows the priority designation of the vehicles dependent on the t_{coll} and illustrates the concept of a vehicular collision. A vehicle is considered to have collided in the simulation when the t_{coll} is below $t_{brake}+t_{react}$ time for each vehicle. Typically, this time threshold is below 4 s, though it varies depending on the relative speed of the vehicle to the vehicles around it. Once designated as a high priority vehicle, the vehicle has around 1 s to receive a message before a collision will become unavoidable.

The risk based adaptive beaconing protocol prioritizes transmissions as a function of the collision risk that each vehicle observes. The adaptive rate algorithm considers a DSRC broadcast network where each vehicle is continuously broadcasting safety beacons. Each vehicle decides to change the beacon depending on the t_{coll} it calculates with respect to the other vehicles. The first protocol, described by Algorithm 1, allows the highest priority messages to transmit at a beacon rate of 10 Hz, the maximum beacon rate allowed in the IEEE WAVE standard, while the lower priority messages are broadcast at a varying beacon rate from 1 Hz up to 10 Hz. The second adaptive rate protocol allows the highest priority messages to transmit at a beacon rate of 20 Hz, while the lower priority messages are broadcast at a varying beacon rate from 1 Hz up to 20 Hz. The broadcast rate for each

message is determined by Algorithm 2.

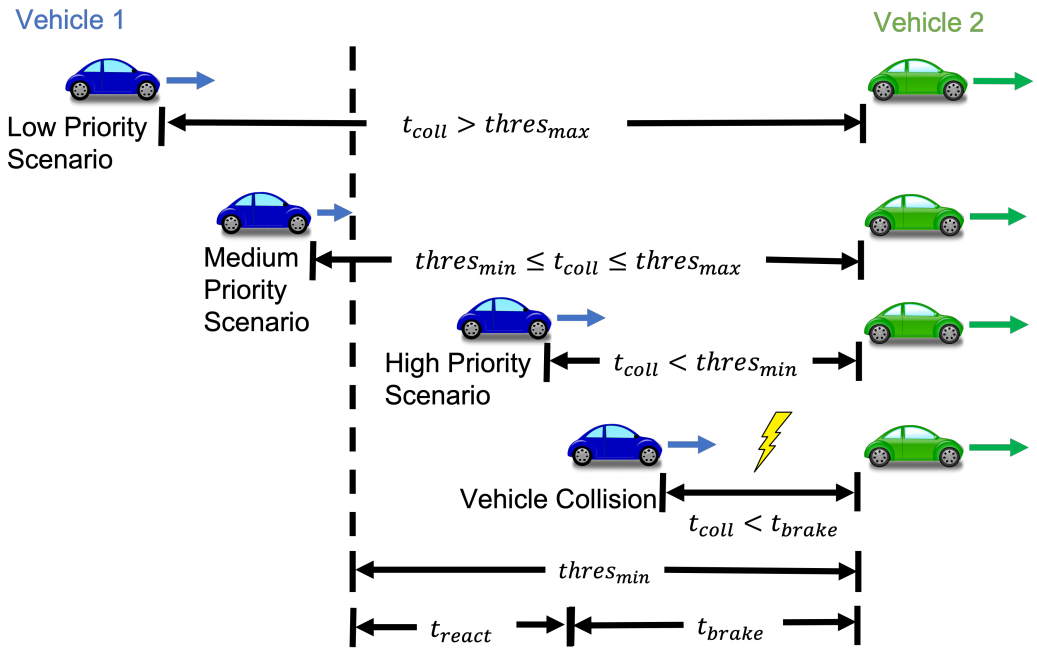

Figure 3.2: Illustration of priority designation in context of simulation, where different t_{coll} correspond to different priorities.

Algorithm 1 10 Hz Risk Based Rate Determination Algorithm

procedure Rate determination($a, v, d, a_i, v_i, d_i, thres_{coll}, thres_{max}$)
  $r \leftarrow 10Hz$ ▷ Set default Rate r to 10 Hz
  $r_{max} \leftarrow 10Hz$
  $r_{min} \leftarrow 1Hz$
  while $i < N$ **do** ▷ For every i out of N vehicles received
    $t_{coll} \leftarrow \max(\frac{(v-v_i)}{a}, \frac{v}{a})$ ▷ Calculate time to collision
    if $(t_{coll} \leq thres_{coll})$
    $r \leftarrow r_{max}$
    else if $(t_{coll} \geq thres_{max})$
    $r \leftarrow r_{min}$
    else
    $r \leftarrow c + \frac{r_{max}-r_{min}}{thres_{max}-thres_{min}} t_{coll}$ ▷ c is a calculated constant that helps map t_{coll} to the interbroadcast rate
  return r ▷ Output of rate algorithm

Algorithm 2 20 Hz Risk Based Rate Determination Algorithm

procedure Rate determination($a, v, d, a_i, v_i, d_i, thres_{coll}, thres_{max}$)
  $r \leftarrow 20Hz$ ▷ Set default Rate r to 20 Hz
  $r_{max} \leftarrow 20Hz$
  $r_{min} \leftarrow 1Hz$
  while $i < N$ **do** ▷ For every i out of N vehicles received
    $t_{coll} \leftarrow \max(\frac{(v-v_i)}{a}, \frac{v}{a})$ ▷ Calculate time to collision
    if $(t_{coll} \leq thres_{coll})$
    $r \leftarrow r_{max}$
    else if $(t_{coll} \geq thres_{max})$
    $r \leftarrow r_{min}$
    else
    $r \leftarrow c + \frac{r_{max}-r_{min}}{thres_{max}-thres_{min}} t_{coll}$ ▷ c is a calculated constant that helps map t_{coll} to the interbroadcast rate
  return r ▷ Output of rate algorithm

The overall beacon rate selection is illustrated in Fig. 3.3. Depending on t_{coll} that each vehicle anticipates, the rate at which it transmits beacons varies. A linear slope was chosen between t_{coll} of 5 and 15, as abrupt changes in the vehicle beacon rate were observed to have a negative impact on the collision avoidance. An upper t_{coll} rate, designated $thres_{max}$ in Algorithms 1 and 2, is chosen as 15 s in this analysis. The lower limit for t_{coll}, designated $thres_{coll}$ in Algorithms 1 and 2, is chosen to be 5 s. The reasoning behind this is to be roughly 1 s greater than $t_{brake} + t_{react}$ time. In this simulation, each vehicle has approximately 1 s after being designated high priority to send messages before getting into a simulated collision. Ideally, most vehicles will be able to adapt well before becoming high risk. The performance of this adaptive beacon rate adjustment is compared to the 10 Hz constant beacon rate standard.

3.4 Simulation Description and Results

The three simulations ran with densities ranging from 20 to 160 vehicles along a 1 km stretch of highway. Each simulation had a duration of 5000 seconds. For the simulations with a higher density of vehicles, it was observed that a significant number of vehicle collisions

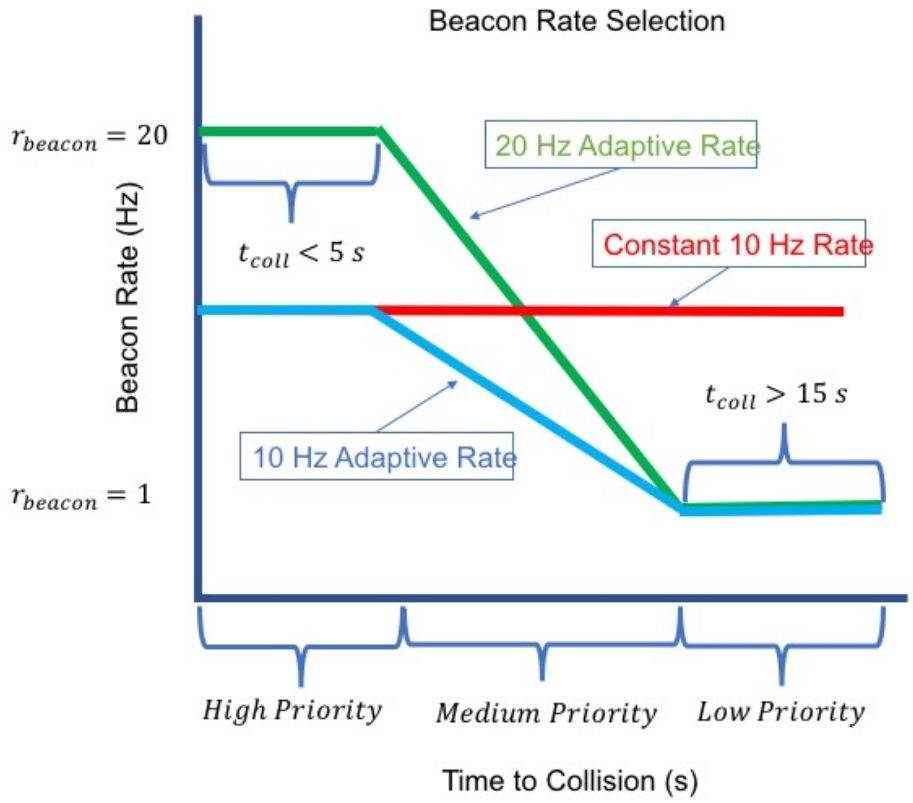

Figure 3.3: Illustration of 10 and 20 Hz adaptive beacon rate selection compared with constant 10 Hz beacon rate.

occurred at the start of the simulation because of the initial placement and velocities of the vehicles. These collisions were excluded from the results since dropped safety packets did not cause these collisions.

In order to measure the performance of the priority protocol against the WAVE standard, simulations with various densities of vehicles traveling along a highway were created. Packet delivery ratios (PDRs) and simulated vehicular collisions were used to judge the performance of the adaptive rate algorithm as compared to the IEEE WAVE standard. The first simulation, designated the control simulation, uses the WAVE standard beacon frequency of 10 Hz for every vehicle, regardless of risk. The second simulation dynamically adapts the beacon rate based on the perceived risk (described below and in Algorithm 1 [see Section 3.3]).

3.4.1 Vehicle Behavior

In the simulations, each vehicle travels in the same direction, and has the same maximum deceleration of 4.572 m/s^2. At every time instant, each vehicle used the messages from nearby vehicles to calculate its t_{coll}, which in turn is used to compute its priority. The priority algorithm, discussed in Section 3.3 as part of the adaptive-rate protocol, gives each vehicle a priority anywhere from 1 to 5. In this simulation, a priority level of 5 indicates the vehicle is at high risk of colliding with a vehicle around it, while a priority level of 1 indicates a low risk of collision. For the adaptive rate approach, each vehicle adjusts its beacon rate based on its calculated priority. Upon receiving a high priority message, if the faster vehicle receiving the message is behind the slower vehicle, the faster vehicle at risk adjusts its speed to that of the vehicle in front. The formerly at-risk vehicle then continues to trail the slower vehicle in front.

The simulation is configured with N different vehicles randomly placed with varying velocities and positions along a three lane highway with a length of 1 km. Each vehicle is positioned in one of the three lanes along the highway. At the beginning of the simulation, each vehicle is spaced equally. Thus, each vehicle starts the simulation the same distance away from the vehicle immediately in front of it. The initial configuration of the simulation is illustrated in Fig. 3.4. The velocity of each vehicle was determined by a Gaussian random variable centered around 26.8224 m/s, with a standard deviation of 2 m/s. The 26.8224 m/s average velocity corresponds to a vehicle traveling at 60 mph, which is reasonable for US highway speeds. A study by [36] has shown Gaussian random variables to be a reliably predictable indicator of vehicular traffic speeds. A 2 m/s standard deviation was chosen to minimize the number of immediate collisions found in higher vehicular density simulations. Upon starting the simulation every vehicle followed the same behavior.

In order to verify the effectiveness of this proposed protocol, realistic values for t_{react} and t_{brake} must be used for the simulation. Since this contribution primarily targets vehicles that are traveling along a highway, a few assumptions are made about the nature of the vehicles and their behavior, taken from studies about vehicular behavior. A study by [40] gives reaction times of 0.75 s (best case) and 1.25 s for vehicles traveling along a highway with an average speed of 60 mph, or 96.6 km/s. For the purposes of this simulation, an average of those two reaction times is used, giving a t_{react} value of 1.0 s. Finally, a value for t_{brake} is computed by assuming a uniform maximum deceleration for all vehicles. [40] gives

a common maximum deceleration of 4.572 m/s. A car traveling at the speed of 96.6 km/s has a t_{brake} of 2.93 s to come to a complete halt. For the purposes of this chapter, a uniform maximum deceleration of 4.572 m/s is used to calculate the t_{brake} value. The combination of t_{brake} (3 s) and t_{react} (1 s) times gives an overall minimum braking time of 4 s for a vehicle to come to a complete stop from first observing the vehicle directly in front of it.

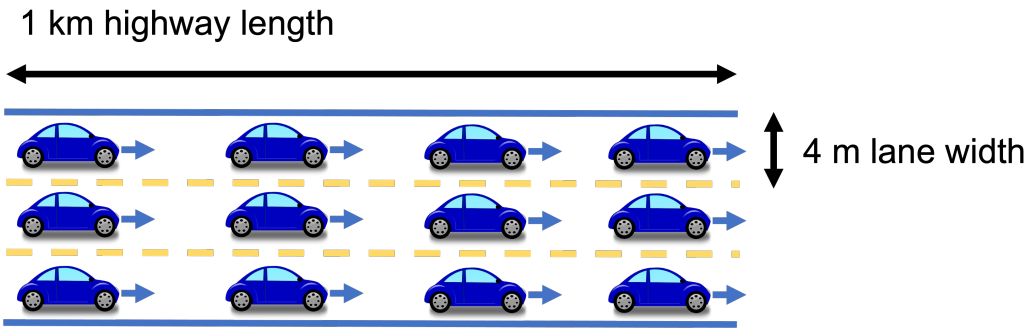

Figure 3.4: Initial configuration of vehicles (blue) with different velocities equally spaced along a three lane highway.

3.4.2 Simulation Metrics

To judge the effectiveness of this protocol, it is necessary to define some common terms used in evaluating vehicular ad hoc network (VANET) communications. A common method of evaluating the network and communication performance in the WAVE and ETSI standards is by the PDR [41]. The PDR is the probability that all vehicles within the range of the transmitting vehicle, receives the transmitted packet. Formally, the PDR is defined as $PDR_i = \frac{PR_i}{PD_i}$. PD_i is the number of packets sent by vehicle i and PR_i is the number of packets send by vehicle i received by neighboring vehicles. The PDR is measured by varying distance bins around the transmitting vehicle, and calculated every simulated second of the simulation. For example, a PDR measurement for 50 m will count the number of vehicles that have received packets from the transmitting vehicle within a range of 50 m.

The other major metric that is used in this simulation is a collision metric, described in Section 3.3. The collision metric was defined as the number of situations that a high priority vehicle did not receive a message by the time it passed the minimum braking time required to stop to avoid a collision.

Table 3.1: Risk aware DSRC simulation parameters.

Parameter	Value
Vehicle density	{20,40,60,70,80,90,120,160} veh/km
Length of road	1000 meters
Number of lanes	3
Lane width	4 meters
PDR distance bins	{50, 100, 250, 350} meters
Safety beacon rate	1.0- 10.0 Hz
Simulation time	5000 seconds
Gain (Tx and Rx)	7.5 dBm
Transmission Range	300 meters
Sensing Range	300 meters
Data Rate	6 Mbps
Packet Length	1000 bytes
Distribution of vehicle speeds	N(26.8 m/s,$\sqrt[2]{2}$ m/s)
t_{brake}	3 seconds
t_{react}	1 second
Maximum Beacon Rate	10 Hz, 20 Hz
Minimum Beacon Rate	1 Hz
$thres_{coll}$	5 s
$thres_{max}$	15 s

The distances and vehicle densities used to evaluate the simulation are summarized in Table 3.1. Different densities of vehicles are used to highlight the effectiveness of the protocol under high and low traffic conditions. As explained in Section 3.2, the average vehicle velocity was at 26.8 m/s, while the positions of the vehicles were uniformly distributed between 0 and 1000 m. The PDR and the simulated collision metric (discussed above) are both used to evaluate the effectiveness of the rate adaptive method. Table 3.1 also summarizes the values used select the beacon rate in the adaptive beacon rate simulation.

3.4.3 Simulation Results

The PDR of high priority (HP) and low priority (LP) messages are used to evaluate the 10 Hz adaptive beacon rate and 20 Hz adaptive beacon rate protocols. Figure 3.5 shows the PDR of HP messages for the constant 10 Hz beacon rate, the 10 Hz adaptive beacon rate, and the 20 Hz adaptive beacon rate simulations across the different vehicular densities. The PDR

drops significantly with higher vehicle densities for both HP and LP messages. Figure 3.6 shows the PDR for all messages (both HP and LP messages) for the constant 10 Hz beacon rate, the 10 Hz adaptive beacon rate, and the 20 Hz adaptive beacon rate simulations. The adaptive beacon rate has a much better PDR across densities and remains above 90 % for all vehicular densities simulated. The PDR performance is slightly better for the combined HP and LP messages as compared to HP messages under the adaptive rate simulation, though this difference is slight. Additionally, the PDR performance for both the constant 10 Hz beacon rate and for the adaptive beacon rate gets worse depending on the distance range that the PDR is being measured. Note from Figs. 3.5 and 3.6 that the increase in density does not necessarily correspond to a drop in PDR performance, particularly between 60 and 100 veh/km. This is due to a combination of the changing spatiotemporal characteristics of the moving vehicles and the randomness of the channel. Notice even from Figs. 2.5(a) and 2.5(b) that the packet loss of increased congestion does not drop dramatically at smaller distances, even with twice as many vehicles in Fig. 2.5(b) as Fig. 2.5(a). However, dramatic increases in densities (such as 80 veh/km as compared to 160 veh/km) over larger distances (200 m), cause dramatic changes in performance.

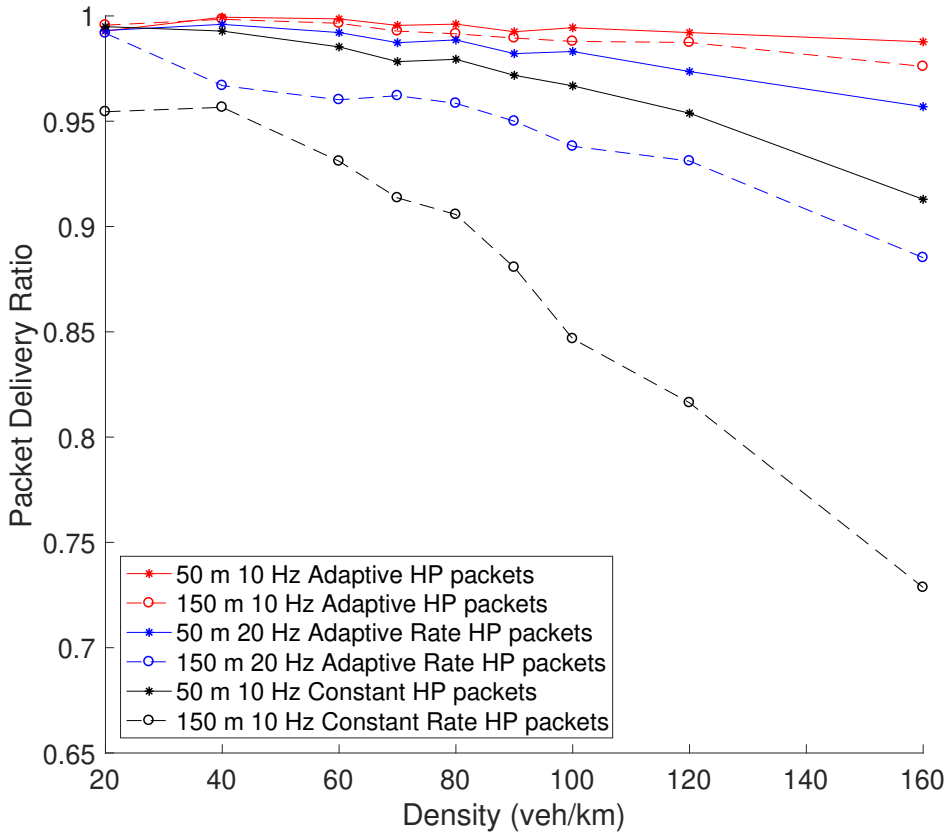

Figure 3.5: Comparison between constant 10 Hz beacon rate, 10 Hz risk based adaptive beacon rate, and 20 Hz risk based adaptive beacon rate for HP messages across vehicular densities

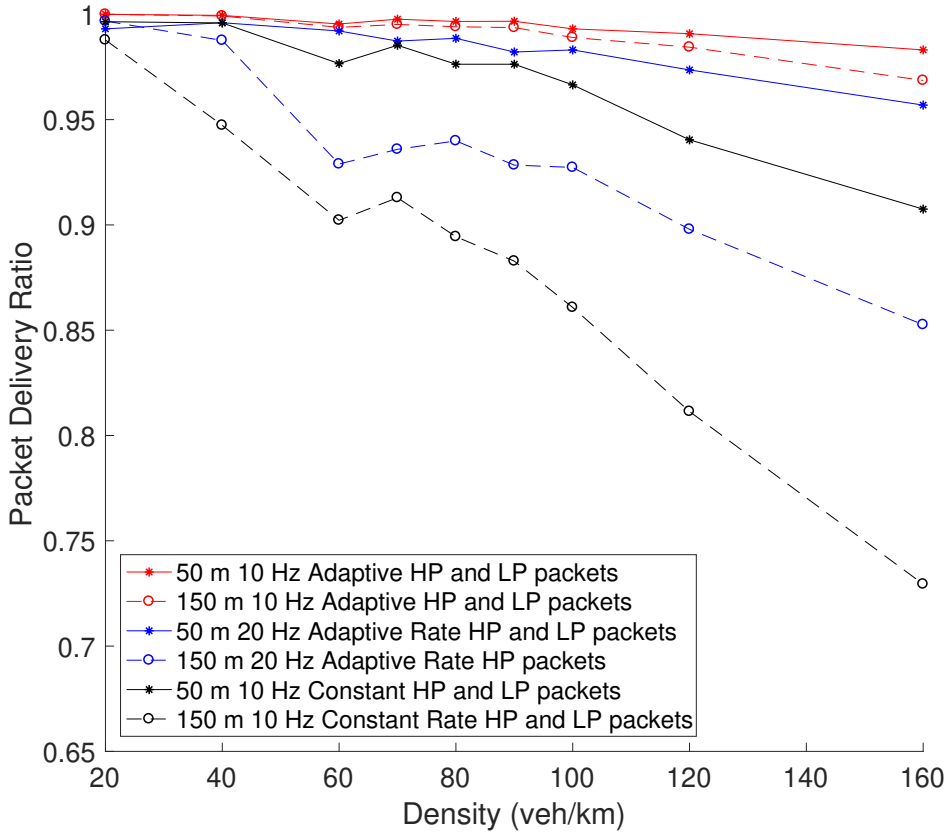

Figure 3.6: Comparison between constant 10 Hz beacon rate, 10 Hz risk based adaptive beacon rate, and 20 Hz risk based adaptive beacon rate for all (HP and LP) messages across vehicular densities

Figure 3.7 shows the results of simulated collisions vs the vehicle density for all three protocols. As with the PDR, both the 10 and 20 Hz adaptive rate protocols show a significant decrease in simulated vehicular collisions compared to the constant 10 Hz protocol. In terms of vehicular collisions, the 20 Hz adaptive case provides significant improvement over both protocols. For 160 nodes, the 20 Hz adaptive beacon rate results in a 77% reduction in collisions as compared to the constant 10 Hz beacon rate, and 62% reduction in collisions compared to the 10 Hz adaptive beacon rate. These results advocate for a higher beacon safety rate of 20 Hz as part of the standard. For 160 nodes, the 10 Hz adaptive beacon rate also provided a 41% reduction in collisions over the constant 10 Hz beacon rate. This result shows that a risk based adaptive beacon rate, even without a higher beacon safety rate, can decrease vehicular collisions. Note that the lower vehicle densities of 20, 40, and 60 veh/km resulted in 0 collisions for the 10 Hz adaptive and 10 Hz constant rate case and for 20, 40,

60, 80, 90, and 100 veh/km for the 20 Hz adaptive rate. Since each simulation was run for 5000 seconds, it means there were no simulated collisions for the lower vehicle densities during the time interval the simulation was run for. The simulation would need to be run for significantly more time to observe collisions for these vehicle densities. It is important to realize that these simulated collisions make certain assumptions about the vehicle behavior, discussed in Section 3.3. Also, it was observed that the distribution of vehicle velocities played a large part in the vehicular collisions. Different velocity distributions resulted in varying numbers of collisions.

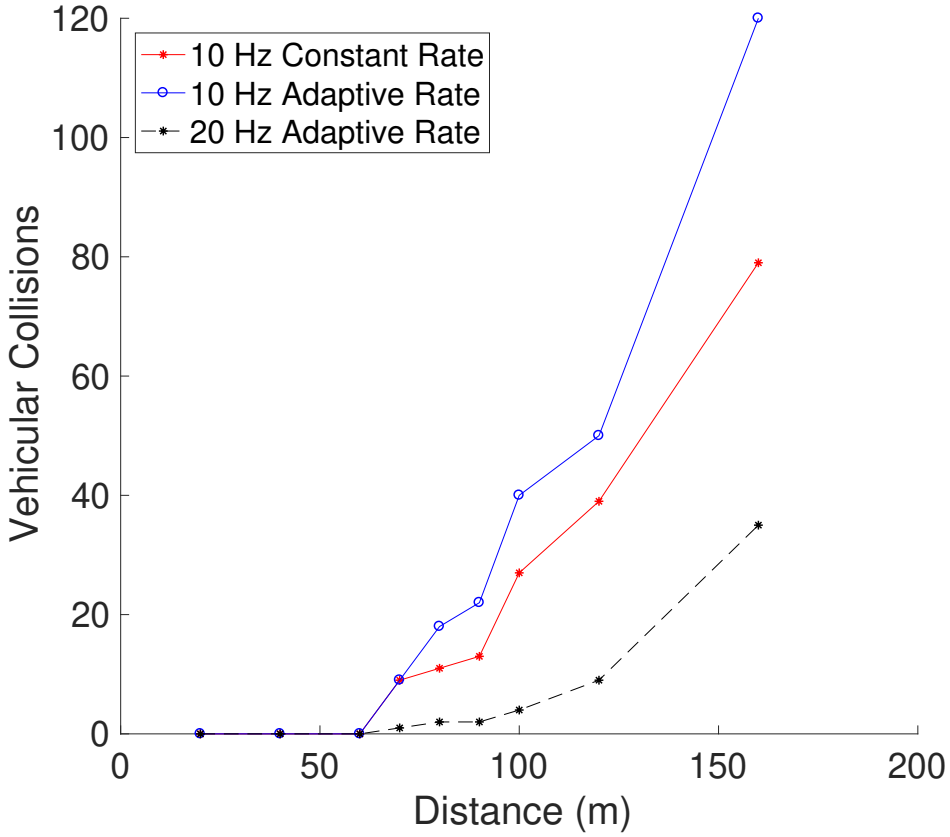

Figure 3.7: Average number of simulated vehicular collisions during the total simulation time for 10 Hz constant rate, 10 Hz adaptive rate, and 20 Hz adaptive rate across vehicular densities.

Continued research in this area is needed and includes exploring an optimization based approach to decide on the upper limits of the beacon rate protocols. Additional research needs to investigate how the distribution of vehicle velocities can affect the performance of the adaptive beacon rate protocol. Future work can also test these adaptive rate protocols

on actual vehicular traces to observe the benefits of the adaptive beacon rate selection. Further investigation is needed to see if both adaptive beacon rate protocols continue to show impressive gains over the constant 10 Hz standard for higher densities and across different vehicle speed distributions.

Chapter 4

Stochastic Analysis of Beacon Transmission in V2V Communications

In this chapter, we study the performance of a distance based transmission protocol for vehicular ad hoc networks (VANET) using tools from stochastic geometry. We consider a variant of the risk based protocol from Chapter 3, where the distance to adjacent vehicles (instead of the TTC) determines the *riskiness* of a vehicle and thus how frequently a vehicle transmits. Assuming slotted ALOHA as the channel access scheme, we evaluate two transmission policies, a *listen more* policy, in which the transmission rate of vehicles *decreases* as the inter-vehicular distance decreases, and a *talk more* policy, in which the transmission rate of vehicles *increases* as the inter-vehicular distance decreases. We model the layout of a highway using a 1-D Poisson Point process (PPP) and characterize the success probability of the typical link under the two transmission policies. Finally, we analyze the trends in success probability as a function of system parameters.

4.1 Introduction

Vehicular ad hoc networks (VANETs) allow vehicles and surrounding infrastructure to share critical information such as up-to-date location information, road conditions, and accident locations through the periodic transmission of *safety messages*. Since this information is considered time-critical, such networks are under strict latency and coverage constraints. However, it has been found in [8, 63] that the performance of VANETs suffers in congested environments. For that reason, congestion control protocols that control the transmission of such beacons are popular, and aim to improve probabilities of success at high densities, primarily through adjusting the rate at which beacons are transmitted. Recently, congestion control protocols specific to vehicular networks have proposed using contextual information

to prioritize transmissions [11, 31, 82]. In these works, the relative distance to neighboring vehicles plays a large role in the collision risk of the vehicle. However, the majority of these protocols and studies are based on system level simulations. While such computer simulations are an important part of verifying the performance of vehicular networks, it is equally important to develop complementary analytical approaches for a holistic performance analysis.

4.1.1 Related Works

There have been several works that have used spatial models such as 1D and 2D PPPs to model the locations of vehicles and RSUs [78]. Most of the works so far have focused on vehicular ad hoc networks (VANETs) using the dedicated short range communication standard (DSRC) such as [18, 19, 78], though recently there has been work on extending analysis to C-V2X [25]. The works that concentrate on the DSRC standard can further be classified into two major approaches: those works that use transmit via slotted ALOHA such as [18, 19, 26], where nodes transmit independently of other nodes in the network with a probability and those that consider transmission via CSMA [37], [78]. Typically the analysis of CSMA networks requires using Matérn hard core point process of type II (MHCPP-II). The work in [26], [18] and [19] analyze the performance of a vehicular adhoc network (VANET), where vehicles transmit via ALOHA. For the purpose of this work, we consider a vehicular ad hoc network (VANET), where vehicles are transmitting via slotted ALOHA, though in future work we could expand our analysis to a CSMA network.

4.1.2 Contributions

In this chapter, we analyze the success probability of the typical link under two possible priority transmission policies. The first is a *listen more* policy, in which the transmission rate of vehicles *decreases* as the inter-vehicular distance decreases. The second policy is a *talk more* policy, in which the transmission rate of vehicles *increases* as the distance to the vehicle ahead of it decreases. Assuming a vehicular ad hoc network where the spatial layout of vehicles is modeled by a 1-D Poisson point process, we characterize the success probability of the typical link assuming the transmission rate of each vehicle is adjusted based on the spacing between adjacent nodes. We derive an simple yet accurate approximation

for success probability of the reference receiver for both policies using a dominant interferer-based approach. The dominant interferer approach accurately captures the effect of dominant interferer and approximates the aggregate interference from the rest of the interferers.

4.2 System Model

4.2.1 Spatial Model

We analyze the performance of an adaptive transmission rate algorithm where the locations of the vehicular nodes along the road systems are modeled by a 1D PPP Φ with density λ. Without loss of generality, we assume that the typical receiver or the receiver node of the typical link is located at the origin o. In wireless networks, the severity and effect of fading can vary significantly. In order to capture the performance a wide range of fading environments, we choose Nakagami-m fading with the parameter m.

4.2.2 Transmission Policy and Channel Model

In our risk based approach, the transmission rate of each vehicle is adjusted based on the distance between adjacent nodes. We consider two different policies in this work where each of them would be beneficial over the other under different operational regimes. In the first policy, we consider that the transmission rate of vehicles decreases as its distance to the vehicle ahead of it decreases. The rationale behind this policy is that a vehicle that approaches another vehicle from behind should *listen more* so that it can take the necessary actions such as sudden braking or slowing down when the vehicle ahead stops or slows down. We model this assigning a Bernoulli random variable θ_i to each node at x_i. Under this policy, the probability that node at x_i is transmitting ($\theta_i = 1$) is modeled as follows

$$P[\theta_i = 1] = 1 - \exp(-c(x_{i+1} - x_i)), \tag{4.1}$$

where c is a constant scaling parameter.

In the second policy, we consider that the transmission rate of vehicles increases as its distance to the vehicle ahead of it decreases. The rationale behind this policy is that a vehicle that approaches another vehicle from behind should *talk more* so that the vehicles

that are following this vehicle can take the necessary actions to prevent a rear-end collision. In this case, we model the transmission policy as Bernoulli random variable such that

$$P[\theta_i = 1] = \exp(-c(x_{i+1} - x_i)). \tag{4.2}$$

4.2.3 Success Probability

Our goal is to characterize the signal-to-interference ratio (SIR) based success probability for the typical link. We assume that the system is interference limited and thus, thermal noise is neglected in our coverage analysis. We assume that all the nodes transmit at the same power P_t and consider a power-law path-loss model with a path-loss exponent $\alpha > 2$. The SIR at the receiver node of the typical link is given by

$$\text{SIR} = \frac{P_t h_0 |d|^{-\alpha}}{\sum_{x_i \epsilon \Phi} P_t \theta_i h_{x_i} |x_i|^{-\alpha}} \tag{4.3}$$

where h_0 is the channel fading gain of the typical link, h_{x_i} is the channel fading gain between the receiver node of the typical link and the interfering node at the location x_i, and d is the link distance. We compute the success probability of the link, with a receiver node located a distance d from the respective transmitting node on the line. With the assumption of Nakagami-m fading, the channel fading gains h_0, h_{x_i} follow a gamma distribution with a probability distribution function (PDF),

$$f_H(h) = \frac{m^m h^{m-1}}{\Gamma(m)} \exp(-mh).$$

4.3 Success Probability of Listen More Policy

This is the main technical section of this chapter where we compute the SIR-based success probability of the typical link for the *listen more* policy. In this section, we use a dominant interferer-based approach in which the effect of the dominant interferer is exactly captured and the residual interference from the other interferers is approximated.

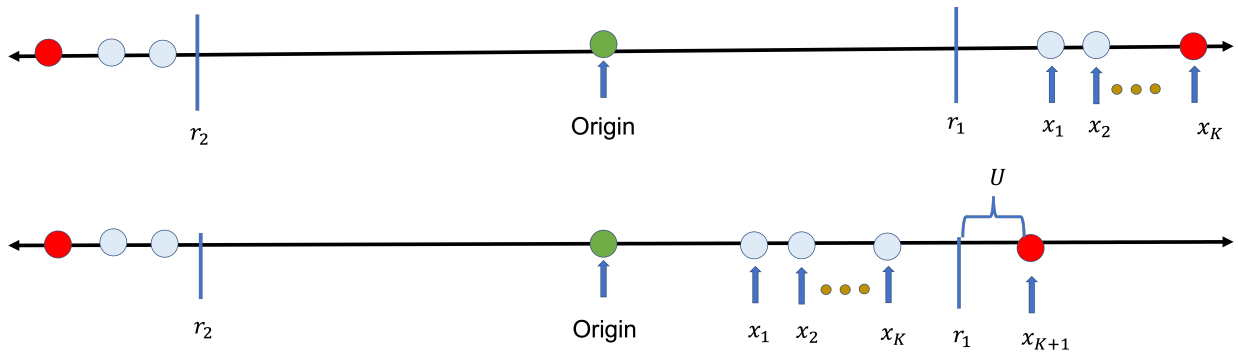

Figure 4.1: Illustration of Event 1 (top), where no interfering nodes are in the range $[0, r_1]$, and Event 2 (bottom), where at least one interfering node is in the range $[0, r_1]$. The blue and red circles represent inactive and active transmitters in the network, respectively.

4.3.1 Dominant Interferer Distance Distribution

We begin by finding the cumulative distribution function (CDF) of the dominant interferer distance. We denote the dominant interferer distance as $R = \min\{R_1, R_2\}$, where R_1 and R_2 denote the distances to the closest interfering node from the origin to the right and left of the origin, respectively. We first derive the CDF of R_1.

Lemma 4.1. *The CDF of the distance from the receiver to the closest transmitting node to the right of the origin, R_1, is given by*

$$F_{R_1}(r_1) = 1 - e^{-\lambda r_1} + \left(1 - e^{-\lambda r_1}\right) \times \left(\int_{r_1}^{\infty} \int_{0}^{r_1} e^{-c(x_{k+1} - x_1)} \cdot \frac{\lambda e^{-\lambda x_1}}{1 - e^{-\lambda r_1}} \cdot \lambda e^{-\lambda(x_{k+1} - r_1)} \mathrm{d}x_1 \mathrm{d}x_{k+1} \right) \tag{4.4}$$

Proof. The CDF of R_1 can be computed as

$$F_{R_1}(r_1) = 1 - \mathbb{P}(R_1 > r_1). \tag{4.5}$$

To compute $\mathbb{P}(R_1 > r_1)$, we consider two possibilities, the event in which there are no nodes in the range $[o, r_1]$, denoted as E_1, and the event in which there exists at least one node in

$[o, r_1]$, denoted as E_2. Now, we write

$$\begin{aligned}\mathbb{P}(R_1 > r_1) =& \mathbb{P}(R_1 > r_1|E_1)\mathbb{P}(E_1) \\ &+ \mathbb{P}(R_1 > r_1|E_2)\mathbb{P}(E_2).\end{aligned} \tag{4.6}$$

We will determine each term in 4.6. Let $N(\Phi \cap [o, r_1])$ denote the number of nodes in the range $[o, r_1]$.

$$\mathbb{P}(E_1) = \mathbb{P}(N(\Phi \cap [o, r_1]) = 0) = e^{-\lambda r_1} \tag{4.7}$$

$$\mathbb{P}(R_1 > r_1|E_1) = 1. \tag{4.8}$$

$$\mathbb{P}(E_2) = 1 - \mathbb{P}(E_1) = 1 - e^{-\lambda r_1}. \tag{4.9}$$

Assuming there to be $k > 0$ nodes in the nodes in the range $[o, r_1]$ and letting $N_{Tx}([o, r_1])$ denote the number of active transmitters in the range $[o, r_1]$, $\mathbb{P}(R_1 > r_1|E_2)$ can be computed as

$$\begin{aligned}\mathbb{P}(R_1 > r_1|E_2) =& \mathbb{P}(N_{Tx}([o, r_1]) = 0|E_2) \\ =& \mathbb{E}_\Phi\left[e^{-c(x_2-x_1)} \dots e^{-c(x_{k+1}-x_k)}|E_2\right] \\ =& \mathbb{E}_\Phi\left[e^{-c(x_{k+1}-x_1)}|E_2\right] \\ =& \int_{r_1}^{\infty}\int_{0}^{r_1} e^{-c(x_{k+1}-x_1)} f_{X_1}(x_1|E_2) \\ & f_{X_{k+1}}(x_{k+1}|E_2)\mathrm{d}x_1\mathrm{d}x_{k+1}.\end{aligned} \tag{4.10}$$

We will now derive the conditional PDFs of X_1 and X_{k+1}. Now computing $F_{X_1}(x_1|E_2)$,

$$\begin{aligned} F_{X_1}(x_1|E_2) &= 1 - P(X_1 > x_1|E_2) \\ &= 1 - \frac{P(X_1 > x_1, E_2)}{P(E_2)} \\ &= 1 - \frac{P(x_1 < X_1, X_1 < r_1)}{1 - e^{-\lambda r_1}} \\ &= 1 - \frac{F_{X_1}(r_1) - F_{X_1}(x_1)}{1 - e^{-\lambda r_1}} \\ &= 1 - \frac{e^{-\lambda x_1} - e^{-\lambda r_1}}{1 - e^{-\lambda r_1}} \\ &= \frac{1 - e^{-\lambda x_1}}{1 - e^{-\lambda r_1}} \end{aligned} \tag{4.11}$$

The conditional PDF of X_1 can be derived by taking the derivative of $F_{X_1}(x_1|E_2)$ with respect to x_1

$$f_{X_1}(x_1|E_2) = \frac{\lambda e^{-\lambda x_1}}{1 - e^{-\lambda r_1}}, \quad 0 \leq x_1 \leq r_1. \tag{4.12}$$

We can compute $F_{x_{k+1}}(x_{k+1}|E_2)$ by using an intermediary random variable, U, where U is the distance from r_1. U and its relation to r_1 is illustrated in Fig. 4.1

$$\begin{aligned} F_{X_{k+1}}(x_{k+1}|E_2) &= 1 - P(X_{k+1} > x_{k+1}|E_2) \\ &= 1 - P(r_1 + U > x_{k+1}|E_2) \\ &= 1 - P(U > x_{k+1} - r_1|E_2) \\ &= 1 - P(N[(x_{k+1}, r_1) = 0]) \\ &= 1 - e^{-\lambda(x_{k+1} - r_1)} \end{aligned} \tag{4.13}$$

Taking the derivative of $F_{x_{k+1}}(x_{k+1}|E_2)$, we obtain

$$f_{X_{k+1}}(x_{k+1}|E_2) = \lambda e^{-\lambda(x_{k+1} - r_1)}, \quad r_1 \leq x_{k+1} < \infty. \tag{4.14}$$

Substituting (4.12) and (4.14) in (4.10), we obtain the CDF of R_1. □

We can obtain the CDF of R_2 by following the same procedure.

Lemma 4.2. *The CDF of the distance from the receiver to the closest transmitting node to*

the left of the origin, R_2, is given by

$$\begin{aligned} F_{R_2}(r_2) =& 1 - e^{-\lambda r_2} + \left(1 - e^{-\lambda r_2}\right) \\ & \times \left(\int_0^{r_2} e^{-c(x_k)} f_{X_k}\left(x_k | E_2\right) \mathrm{d}x_k\right) \end{aligned} \tag{4.15}$$

where

$$f_{X_k}(x_k|E_4) = \frac{\lambda e^{-\lambda(r_2 - x_k)}}{1 - e^{-\lambda r_2}}, \quad r_2 \leq x_k < \infty. \tag{4.16}$$

Proof. The CDF of R_2 can be computed in the same manner as R_1, where we need to find

$$F_{R_2}(r_2) = 1 - \mathbb{P}(R_2 > r_2). \tag{4.17}$$

where

$$\begin{aligned} \mathbb{P}(R_2 > r_2) =& \mathbb{P}(R_2 > r_2|E_3)\mathbb{P}(E_3) \\ & + \mathbb{P}(R_2 > r_2|E_4)\mathbb{P}(E_4). \end{aligned} \tag{4.18}$$

To compute $\mathbb{P}(R_2 > r_2)$, we denote E_3 as the event in which there are no nodes in the range $[r_2, o]$ and E_4 as the event in which there exists at least one node in $[r_2, o]$. Computing $\mathbb{P}(R_2 > r_2|E_3)$, $\mathbb{P}(E_3)$, and $\mathbb{P}(E_4)$ is done in a similar manner to 4.7, 4.8, and 4.9. We will now focus on the term $\mathbb{P}(R_2 > r_2|E_4)$. Let us say that there are k nodes in the nodes in the range $[r_2, o]$. Now, this term can be computed as

$$\begin{aligned} \mathbb{P}(R_1 > r_1|E_4) =& \mathbb{P}\left(N_{Tx}([r_2, o]) = 0|E_4\right) \\ =& \mathbb{E}_\Phi\left[e^{-c(x_k - x_{k-1})} \ldots e^{-c(x_1)})|E_4\right] \\ =& \mathbb{E}_\Phi\left[e^{-c(x_k)}|E_4\right] \\ =& \int_0^r e^{-c(x_k)} f_{X_k}(x_k|E_4) \mathrm{d}x_k. \end{aligned} \tag{4.19}$$

The CDF $F_{X_1}(x_1|E_4)$ is given by

$$\begin{aligned} F_{X_k}(x_k|E_4) &= 1 - P(X_k > x_k|E_4) \\ &= 1 - P(r_2 > x_k + U|E_4) \\ &= 1 - P(U > x_{k+1} - r_2|E_4) \\ &= 1 - \frac{e^{-\lambda(r_2 - x_k)}}{1 - e^{-\lambda r_2}}, \quad r_2 \leq x_k < \infty \end{aligned} \tag{4.20}$$

□

Lemma 4.3. *The PDF of R is*

$$f_R(r) = f_{R_1}(r)\left(1 - F_{R_2}(r)\right) + f_{R_2}(r)\left(1 - F_{R_1}(r)\right). \tag{4.21}$$

Proof. As R_1 and R_2 are independent random variables, the CDF of R can be obtained as

$$F_R(r) = 1 - (1 - F_{R_1}(r))(1 - F_{R_2}(r)). \tag{4.22}$$

We then obtain the PDF of the dominant interferer distance by computing the derivative of $F_R(r)$ w.r.t. r. □

4.3.2 Laplace Transform of Interference Distribution

In this subsection, we derive the Laplace transform of the distribution of the dominant interferer and approximate the remaining interference power at the receiver node of the typical link for the *listen more* policy. The Laplace transform of the overall interference can be decomposed into two components as

$$\mathcal{L}_I(s) \approx \mathcal{L}_{I_{Dom}}(s)\mathcal{L}_{I_{Rem}}(s) \tag{4.23}$$

where $\mathcal{L}_{I_{Dom}}(s)$ is the Laplace transform of the distribution of the dominant (closest interferer), and is independent of the remaining interference (I_{Rem}).

Lemma 4.4. *The Laplace transform of the interference is approximated by*

$$\mathcal{L}_I(s) \approx \int_0^\infty \left(1+\frac{sr^{-\alpha}}{m_1}\right)^{-m_1} f_R(r)\mathrm{d}r \times \int_0^\infty e^{\left(-2\lambda\int_r^\infty\left[1-e^{-cz_i}-\left(1-e^{-cz_i}\right)\left(1+\frac{sx_i^{-\alpha}}{m_1}\right)^{-m_1}\right]dx_i\right)}\lambda e^{-\lambda z_i}dz_i \tag{4.24}$$

Proof. The Laplace Transform of the interference of the dominant interferer is given by

$$\mathcal{L}_{I_{Dom}}(s) \overset{(a)}{=} \int_0^\infty \left(1+\frac{sr^{-\alpha}}{m_1}\right)^{-m_1} f_R(r)\mathrm{d}r.$$

where (a) follows from the Nakagami-m fading assumption. The Laplace transform of the interference power from the rest of the interfering nodes can be approximated as

$$\begin{aligned}
\mathcal{L}_{I_{Rem}}(s|R) &\approx \mathbb{E}_{\Phi HZ\theta}\left[\prod_{x_i\epsilon\Phi,\|x_i\|>R} e^{-s\theta h_x|x_i|^{-\alpha}}\right] \\
&\overset{(a)}{\approx}\mathbb{E}_{\Phi HZ}\left[\prod_{x_i\epsilon\Phi,\|x_i\|>R} e^{-sh_x|x_i|^{-\alpha}}(1-e^{-cz_i})+e^{-cz_i}\right] \\
&\overset{(b)}{\approx}\mathbb{E}_{\Phi Z}\left[\prod_{x_i\epsilon\Phi,\|x_i\|>R}\left[e^{-cz_i}+\left(1-e^{-cz_i}\right)\left(1+\frac{sx_i^{-\alpha}}{m_1}\right)^{-m_1}\right]\right] \\
&\overset{(c)}{\approx}\mathbb{E}_Z\left[e^{\left(-2\lambda\int_r^\infty\left[1-e^{-cz_i}-\left(1-e^{-cz_i}\right)\left(1+\frac{sx_i^{-\alpha}}{m_1}\right)^{-m_1}\right]dx_i\right)}\right] \\
&\overset{(d)}{\approx}\int_0^\infty e^{\left(-2\lambda\int_r^\infty\left[1-e^{-cz_i}-\left(1-e^{-cz_i}\right)\left(1+\frac{sx_i^{-\alpha}}{m_1}\right)^{-m_1}\right]dx_i\right)}\lambda e^{-\lambda z_i}dz_i
\end{aligned} \tag{4.25}$$

where z_i comes from a change in variables with $z_i = x_{i+1} - x_i$. (a) comes from taking the expectation of the Bernoulli random variable θ_i, (b) comes from taking the expectation with respect to H. (c) comes from applying the PGFL. In (d) we take the expectation with respect to z_i, which we treat as an exponential random variable. □

4.3.3 Success Probability

The success probability is formally defined as the probability with which the SIR measured at the receiver exceeds a predetermined threshold β.

Theorem 4.1. *Using the Laplace transform of the interference power distribution, the success probability is computed as the following*

$$\mathrm{P_c} = \sum_{k=0}^{m_0-1} \frac{(-m_0\beta r^\alpha)^k}{k!} \left[\frac{\partial^k}{\partial s^k} L_I(s)\right]_{s=m_0\beta d^\alpha}. \tag{4.26}$$

where $L_I(s)$ is the Laplace transform of the distribution of interference power, given by Eq. 4.24

Proof.

$$\begin{aligned}
\mathrm{P_c} &= \mathbb{P}(\mathrm{SIR} > \beta) \\
&= \mathbb{E}_I\left[\left(H_0 > \beta d^\alpha I \middle| I\right)\right] \\
&\overset{(a)}{=} \mathbb{E}_I\left[\frac{\Gamma(m_0, m_0\beta d^\alpha I)}{\Gamma(m_0)}\right] \\
&\overset{(b)}{=} \mathbb{E}_I\left[\sum_{k=0}^{m_0-1} \frac{(m_0\beta r^\alpha I)^k}{k!} e^{-m_0\beta r^\alpha I}\right] \\
&= \sum_{k=0}^{m_0-1} \frac{(-m_0\beta r^\alpha)^k}{k!} \left[\frac{\partial^k}{\partial s^k} L_I(s)\right]_{s=m_0\beta d^\alpha}
\end{aligned} \tag{4.27}$$

Following the approach presented in [27] and [72], we can express the conditional success probability in terms of the derivative of the Laplace transform of the distribution of interference power using the properties of the Gamma function. (a) comes from the CCDF of the gamma random variable H_0, and (b) follows from the definition of the incomplete gamma function for integer values of m_0. □

4.4 Success Probability of Talk More Policy

In this section, we compute the SIR success probability of the typical link for the *talk more* policy. Following the same procedure as in the previous section, we have the probability that $P(R_1 > r_1)$ is

$$\begin{aligned} P(R_1 > r_1) =& P(E_1)P(R_1 > r_1|E_1) \\ &+ P(E_2)P(R_1 > r_1|E_2) \end{aligned} \tag{4.28}$$

where

$$\mathbb{P}(E_1) = e^{-\lambda r_1}, \tag{4.29}$$

$$\mathbb{P}(R_1 > r_1|E_1) = 1, \tag{4.30}$$

$$\mathbb{P}(E_2) = 1 - e^{-\lambda r_1}. \tag{4.31}$$

Upon conditioning on Φ, we obtain

$$\begin{aligned} &\mathbb{P}(R_1 > r_1|E_2) = \mathbb{P}\left(N_{Tx}([o, r_1]) = 0|E_2\right) \\ &= \mathbb{E}_\Phi\left[\left(1 - e^{-c(x_2 - x_1)}\right) \dots \left(1 - e^{-c(x_{k+1} - x_k)}\right)|E_2\right] \\ &= \int_{r_1}^{\infty} \int_0^{r_1} \left(\left(1 - e^{-c(x_{k+1} - x_k)}\right) \dots \left(1 - e^{-c(x_2 - x_1)}\right)\right) \\ &\quad f_{X_{k+1}}(x_{k+1}|E_2) \dots f_{X_1}(x_1|E_2) \mathrm{d}x_{k+1} \dots \mathrm{d}x_1. \end{aligned} \tag{4.32}$$

4.4.1 Laplace Transform of Interference Distribution and Success Probability

In this subsection, we derive the Laplace transform of the distribution of the dominant interferer and approximate the remaining interference power at the receiver node of the typical link for the *talk more* policy. We then compute the SIR success probability of the typical link for the *talk more* policy.

Lemma 4.5. *The Laplace transform of the interference for the talk more policy is approxi-*

mated by

$$\mathcal{L}_I(s) \approx \int_0^\infty \left(1+\frac{sr^{-\alpha}}{m_1}\right)^{-m_1} f_R(r)\mathrm{d}r \times \int_0^\infty e^{\left(-2\lambda\int_r^\infty\left[e^{-cz_i}-e^{-cz_i}\left(1+\frac{sx_i^{-\alpha}}{m_1}\right)^{-m_1}\right]dx_i\right)}\lambda e^{-\lambda z_i}dz_i. \tag{4.33}$$

Proof. The Laplace Transform of the interference of the dominant interferer is given by

$$\mathcal{L}_{I_{Dom}}(s) \overset{(a)}{=} \int_0^\infty \left(1+\frac{sr^{-\alpha}}{m_1}\right)^{-m_1} f_R(r)\mathrm{d}r.$$

where (a) comes from the definition of the Laplace transform. The Laplace transform of the interference power from the rest of the interfering nodes for the talk more policy can be approximated as

$$\begin{aligned}
\mathcal{L}_{I_{Rem}}(s|R) &\approx \mathbb{E}_{\Phi HZ\theta}\left[\prod_{x_i\epsilon\Phi,\|x_i\|>R} e^{-s\theta h_x|x_i|^{-\alpha}}\right] \\
&\overset{(a)}{\approx}\mathbb{E}_{\Phi HZ}\left[\prod_{x_i\epsilon\Phi,\|x_i\|>R} e^{-cz_i}e^{-sh_x|x_i|^{-\alpha}}+(1-e^{-cz_i})\right] \\
&\overset{(b)}{\approx}\mathbb{E}_{\Phi Z}\left[\prod_{x_i\epsilon\Phi,\|x_i\|>R}\left[e^{-cz_i}\left(1+\frac{sx_i^{-\alpha}}{m_1}\right)^{-m_1}+\left(1-e^{-cz_i}\right)\right]\right] \\
&\overset{(c)}{\approx}\mathbb{E}_Z\left[e^{\left(-2\lambda\int_r^\infty\left[e^{-cz_i}-e^{-cz_i}\left(1+\frac{sx_i^{-\alpha}}{m_1}\right)^{-m_1}\right]dx_i\right)}\right] \\
&\overset{(d)}{\approx}\int_0^\infty e^{\left(-2\lambda\int_r^\infty\left[e^{-cz_i}-e^{-cz_i}\left(1+\frac{sx_i^{-\alpha}}{m_1}\right)^{-m_1}\right]dx_i\right)}\lambda e^{-\lambda z_i}dz_i
\end{aligned} \tag{4.34}$$

where z_i comes from a change in variables with $z_i = x_{i+1} - x_i$. (a) comes from taking the expectation of the Bernoulli random variable θ_i, (b) comes from taking the expectation with respect to H. (c) comes from applying the PGFL. In (d) we take the expectation with respect to z_i, which we treat as an exponential random variable. □

Theorem 4.2. *Using the Laplace transform of the interference power distribution, the*

success probability for the talk more policy is computed as the following

$$\mathrm{P_c} = \sum_{k=0}^{m_0-1} \frac{(-m_0\beta r^\alpha)^k}{k!} \left[\frac{\partial^k}{\partial s^k} L_I(s)\right]_{s=m_0\beta d^\alpha}. \tag{4.35}$$

where $L_I(s)$ is the Laplace transform of the distribution of interference power, given by Eq. 4.33.

Proof. The proof follows along the same lines as that of Theorem 4.2. □

4.5 Results and Discussion

In this section, we verify the accuracy of our analytical results by comparing them to results from Monte-Carlo simulations. We also analyze the impact of vehicle density and c on the success probability for the two transmission policies in Figs. 4.3 and 4.2.

Notice from Fig. 4.2, that an increase in density yields an increase and decrease in the success probability for the *listen more* and *talk more* policies, respectively. Figure 4.3 shows that an increase in the velocity constant c yields a decrease in the success probability for the *listen more* policy. Likewise, an increase in the velocity constant c for the *talk more* policy yields an increase in success probability. Through this analysis, we can suggest an optimal value of c that depends on density of vehicles that are observed on a highway.

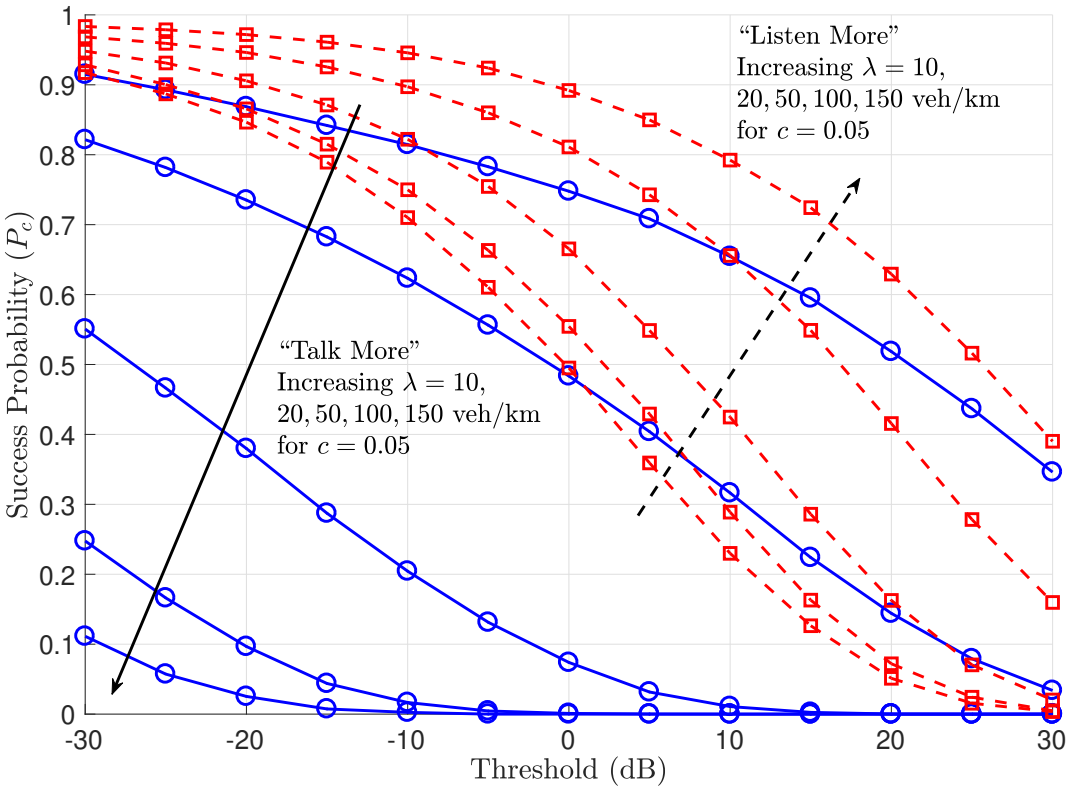

Figure 4.2: "Talk more" and "Listen more" success probability as function of SIR threshold as λ increases.

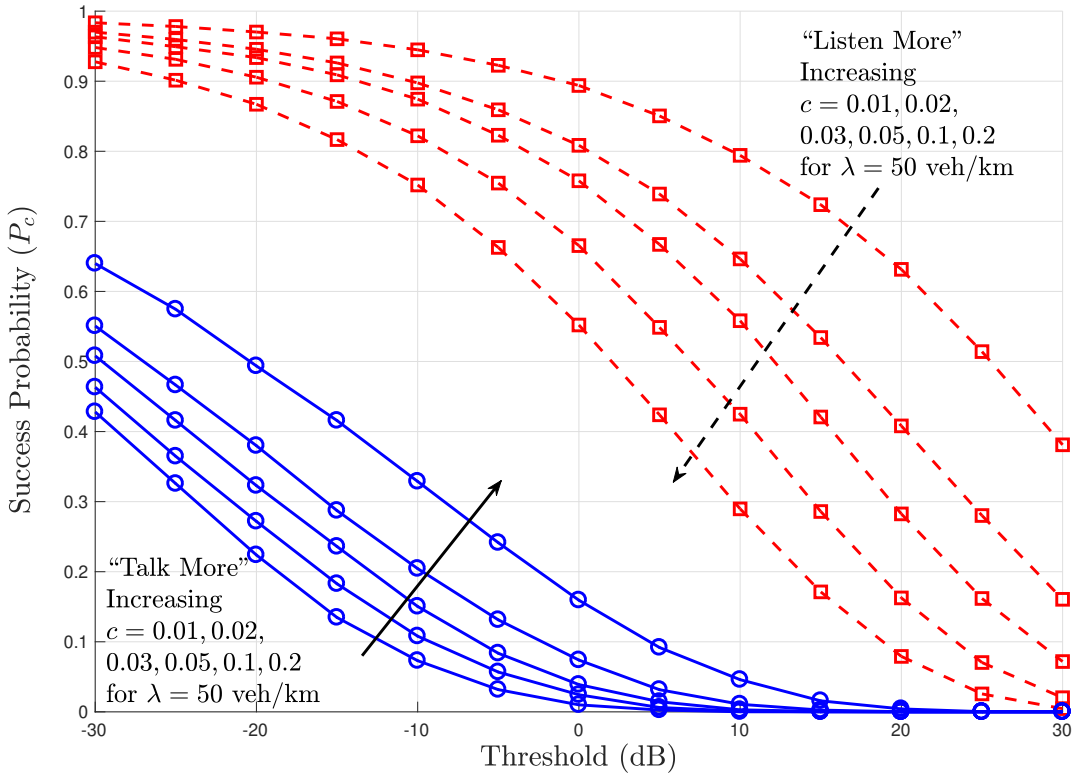

Figure 4.3: "Talk more" and "Listen more" success probability as function of SIR threshold as c increases.

Chapter 5

Ch-RRI SPS: Channel-aware Semi-Persistent Scheduling for C-V2X Networks

Decentralized vehicle-to-everything (V2X) networks (i.e., C-V2X Mode-4 and Mode 2a NR-V2X), rely on periodic Basic Safety Messages (BSMs) to disseminate time-sensitive information (e.g., vehicle position). These messages have the potential to increase each vehicles awareness and improve on-road safety. Decentralized V2X networks utilize sensing-based semi-persistent scheduling (SPS), where vehicles sense radio resources and select suitable resources for BSM transmissions at prespecified periodic intervals termed the Resource Reservation Interval (RRI). In this chapter, we show that such a BSM scheduling (with a fixed RRI) suffers from severe under- and over- utilization of radio resources under varying vehicle traffic scenarios; that behavior severely compromises timely dissemination of BSMs, which in turn leads to increased collision risks. To address this, we extend SPS to accommodate an adaptive RRI, termed Ch-RRI SPS. Specifically, Ch-RRI SPS allows each vehicle (i) to dynamically adjust RRI based on the channel resource availability (by accounting for various vehicle traffic scenarios), and then, (ii) select suitable transmission opportunities for timely BSM transmissions at the chosen RRI. Our experiments based on the C-V2X Mode-4 standard implemented using the ns-3 simulator show that Ch-RRI SPS outperforms SPS by at least 50% in terms of improved on-road safety performance, in all considered simulation scenarios.

5.1 Related Work

Recent works have simulated and proposed resource allocation improvements to C-V2X Mode-4. Molina-Masegos et al. [64] and Chen et al. [23] develop and use simulations to assess the performance of the SPS algorithm in highway and city scenarios, and showed the improved performance of C-V2X over DSRC. Research in [66], [14], and [77] investigates the performance of parameters used in SPS such as RRI, probability of reselection, and selection window on the packet delivery ratio (PDR). Gonzalez-Martin et al. [39] build the first known analytical model of SPS based C-V2X. Recently, [45] proposed short term sensing before resource selection to help reduce packet collisions and improve SPS performance. Halder et al. [42] suggest adjusting the transmission power to improve the overall performance of SPS, but only focus on improving the PDR performance of C-V2X.

As opposed to prior works, which focus on communication-centric metrics such as throughput and PDR, we focus on on-road safety performance of decentralized V2X networks, such as, tracking error and collision risks. It is worth mentioning that designing an optimal beacon rate in the case of DSRC for improved safety performance of DSRC based V2X networks has been explored fairly well [10, 28, 31, 49]. However, note that designing rate control algorithms for DSRC is fundamentally different from designing scheduling protocols for decentralized C-V2X Mode-4 networks, and existing rate control protocols can not be directly applied to improving on-road safety performance in our context of C-V2X Mode-4 networks. *To the best of our understanding, this is the first work which investigates designing a BSM scheduling protocol for improved on-road safety performance of C-V2X Mode-4.*

5.2 On-Road Safety Performance

In this section, we propose a collision risk model, which measures the on-road safety performance of C-V2X Mode-4 networks. Our proposed collision risk model is inspired by a risk model presented in the literature [28], and is based on tracking error and time-to-collision (TTC) as discussed below.

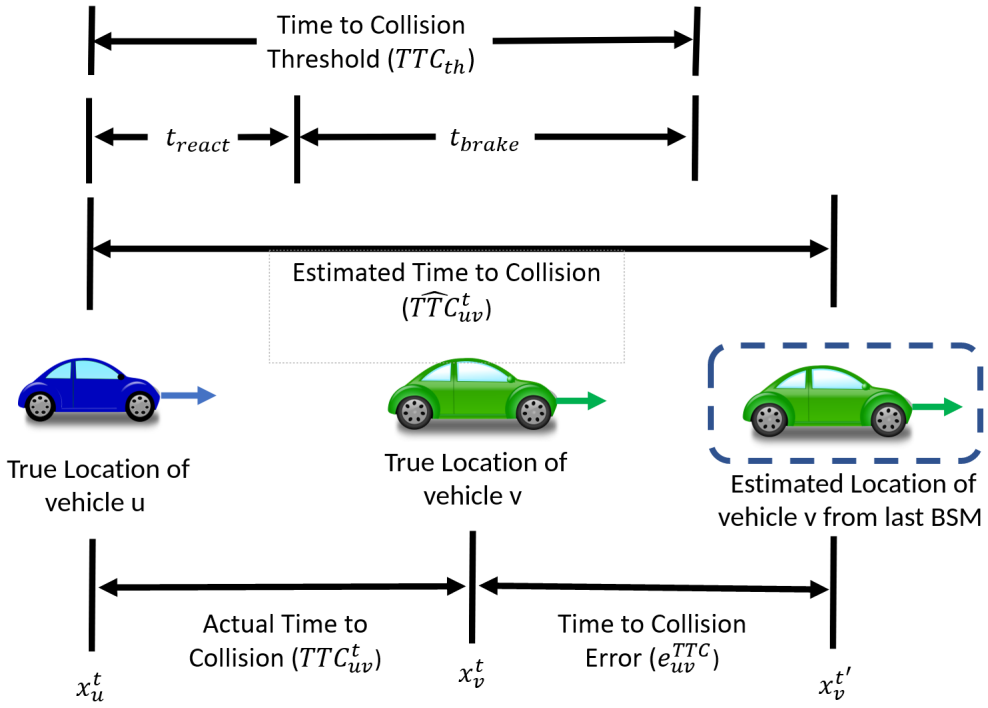

Figure 5.1: Illustration of Collision Risky scenario caused by a large tracking error.

5.2.1 Tracking Error (TE)

Tracking error (TE), e^{track}_{uv}, is defined as the difference between the ground truth location of the sender vehicle u and u's location as estimated by the neighboring receiver vehicle v. Let the most recent BSM received at v from u have been generated at time t'. At time $t > t'$, the tracking error (TE) that v has in tracking u can be calculated as follows:

$$e^{track}_{uv} = |x^t_u - x^{t'}_u| \tag{5.1}$$

x^t_u is the actual location of u at time t and $x^{t'}_u$ is the u's location information contained in the most recent BSM received from u. We consider x-coordinate to calculate the tracking error as the vehicle moves in x-direction only [1]. The TE is usually significant because

1. Each BSM takes non-zero channel delay (e.g., propagation delay) to be successfully delivered to the receiver after being generated, and the sender would have moved a

[1]For the ease of presentation, we consider a simple tracking error (TE) model with no lateral movements across lane.

non-zero distance during the time period.

2. The RRI (or in other words, inter-BSM transmission interval) is significant. For example, if RRI is 100 ms, it means there is at least 100 ms inter-reception delay between two consecutive BSM from sender vehicle u at the receiver v even if the channel delay is zero. Thus, TE at vehicle v would be significant as vehicle u would have moved to a different location during this time interval.

3. Lost or delayed BSM, mainly due to channel congestion, will further deteriorate TE.

Note that a lower TE value at the receiver vehicle v means that v is able to track u well (i.e., accurately position vehicle u). Thus, TE across all vehicles is used to measure TTC and Collision risk as discussed in the next subsection.

5.2.2 Time-to-Collision (TTC) and Collision Risk

TTC for a pair of vehicles is defined as the time needed for the distance between the two vehicles to become zero, which denotes a potential collision between them. We relate the collision risk (or on-road safety performance) to the TTC, which in turn, utilizes tracking error.

At any time t, the receiver v can estimate TTC with respect to its neighboring vehicle u based on the BSM sent by u as:

$$\text{Estimated TTC,} \quad \widehat{TTC}_{uv}^{t} = \frac{|\widehat{x}_u^{t'} - x_v^t|}{s_{u,v}} \tag{5.2}$$

where $\widehat{x}_u^t$ is u's location as per the last received BSM at v from u with generation time t' and x_v^t is the v's actual location at time t. $s_{u,v}$ is the relative velocity between them.

However, since sender u is currently at location x_u^t at time t (and not $x_u^{t'}$), the true TTC at time t is:

$$\text{True TTC,} \quad TTC_{uv}^{t} = \frac{|x_u^t - x_v^t|}{s_{u,v}} \tag{5.3}$$

Using Equations 5.1, 5.2, and 5.3, we get

$$\widehat{TTC}^{t}_{uv} = TTC^{t}_{uv} + \frac{|e^{track}_{uv}|}{s_{uv}} \tag{5.4}$$

We designate $\frac{|e^{track}_{uv}|}{s_{uv}}$ as the TTC error, e^{TTC}_{uv}. From Eq. 5.4, it is clear that the tracking error affects the TTC calculation. This estimated TTC, $\widehat{TTC}^{t}_{uv}$ can lead to collision risky situations, and its significance in collision warning was studied in [71]. For example, consider that v overestimated/underestimated [2] the TTC to u and is about to take a route/maneuver based on this errorneous value of $\widehat{TTC}^{t}_{uv}$. Such a situation can be safely avoided by manual intervention if the time taken by the driver to react and apply the brakes to make the vehicle stop, defined as, TTC threshold (TTC_{th}), is less than the true TTC (i.e., TTC^{t}_{uv}) at any given time t. Mathematically, TTC threshold, TTC_{th} is given by:

$$TTC_{th} = t_{brake} + t_{react} \tag{5.5}$$

where t_{react} is 1 second and represents the time taken by the driver to respond to the situation and apply the brakes [40]. t_{brake} is the time taken by the vehicle to come to a complete stop after the brakes have been applied. Assuming vehicle u has velocity s_u and every vehicle has a maximum deceleration a as 4.6 m/s^2 (from [40]) makes $t_{brake} = s_u/a$. If the true TTC, i.e., TTC^{t}_{uv}, between a pair of vehicles exceeds the TTC_{th} (i.e., driver's controllability), it results in a collision risky scenario.

It means, given TTC_{th}, and TTC^{t}_{uv}, the collision risk, CR^{t}_{uv}, for a given vehicle pair u and v at any given time t, can be computed as follows:

$$CR^{t}_{uv} = \begin{cases} 1 & TTC^{t}_{uv} \leq TTC_{th} \\ 0 & otherwise \end{cases} \tag{5.6}$$

Using Eq. 5.4, Eq. 5.6 can be rewritten as:

$$CR^{t}_{uv} = \begin{cases} 1 & (\widehat{TTC}^{t}_{uv} - e^{TTC}_{uv}) \leq TTC_{th} \\ 0 & otherwise \end{cases} \tag{5.7}$$

[2] Both overestimating and underestimating TTC are hazardous as overestimating means the vehicle gets too close, and decision based on understimated values will impact the other vehicles.

From Eq. 5.7, it is evident that improving on-road safety performance of C-V2X, i.e., reducing collision risky scenarios, is directly proportional to minimizing TE, e_{uv}^{track}, between each pair of vehicles in the C-V2X networks.

Figure 5.1 illustrates how the TTC error causes a collision risky scenario. In Fig. 5.1, vehicle u estimates vehicle v to have a TTC, $\widehat{TTC}_{uv}^{t}$ beyond TTC_{th}, i.e., in a "safe" position. However in reality, vehicle u is close to vehicle v and the true TTC TTC_{uv} is within the TTC_{th}^{t}, and causes collision risky scenario. Thus, ideally TTC error should be non-existent (or zero) in order to prevent such a collision risky scenario. However, as discussed earlier, TTC error exists as the TE is significant (mainly, due to scheduling, transmission and communication delays). As per the recommendations by SAE-J2945 [3], there exists a TE threshold $e_{th}^{track} = 0.5$m which does not lead to a collision risky situation. We use this TE threshold to rewrite Collision risk in Eq 5.7 as follows.

$$CR_{uv}^{t} = \begin{cases} 1 & (e_{uv}^{TTC} > \frac{|e_{th}^{track}|}{s_{uv}}) \textbf{ and } (TTC_{uv}^{t} < TTC_{th}) \\ 0 & otherwise \end{cases} \tag{5.8}$$

$s_{u,v}$ is set to be the average relative velocity between a pair of vehicles u and v.

Using Eq. 5.7, we count the number of instances between each pair of vehicles in which TTC error exceeds the ratio $\frac{|e_{th}^{track}|}{s_{uv}}$ and true TTC, TTC_{uv}^{t}, is within TTC threshold, TTC_{th}, as the measure of collision risks.

5.3 Ch-RRI SPS: Semi-persistent Scheduling using Channel Aware RRI Selection

In this section, we present the limitations of the conventional SPS protocol in terms of improving cooperative awareness performance of NR-V2X Mode-2, followed by detailed discussion on SPS powered by a channel aware channel aware RRI selection algorithm (Ch-RRI SPS). The Ch-RRI SPS discussion first formulates the channel aware RRI selection problem as an Integer Linear Programming (ILP) problem and then goes into the algorithmic details of the proposed Ch-RRI SPS protocol.

5.3.1 Limitations of SPS on Cooperative Awareness

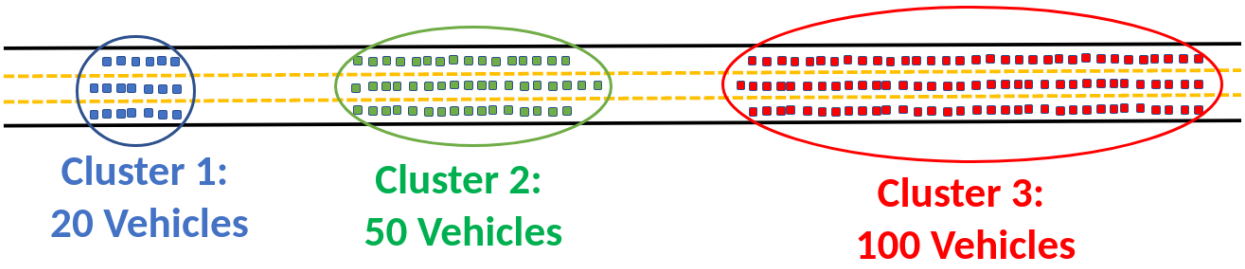

Figure 5.2: NR-V2X example network with three clusters of vehicles.

We present the limitations of SPS through a simple NR-V2X example (See Fig. 5.2). The example NR-V2X network consists of three clusters [3], of vehicles, where cluster 1, 2, and 3 respectively have 20, 50, and 100 vehicles. We make the following **assumptions** for all example NR-V2X scenarios.

- We assume $T_1 = 0$ and $T_2 = \text{RRI}$, which means, the size of selection window is equal to the RRI.
- The NR-V2X physical layer consists of 2 subchannels only. Each BSM transmission uses both subchannels and takes 1 ms to transmit. This means if the selection window is 100 ms (i.e., RRI = 100 ms), then at most 100 distinct vehicles have unique BSM transmission opportunities (assuming no collision in resource selection).
- Each cluster of vehicles is sufficiently spaced apart from each other so that there is no inter-cluster interference. This means, for example, no transmissions from cluster 2 interfere with any transmissions from cluster 1, and vice-versa.

Under the above assumptions, let us look at the (i) *Channel Occupancy Percentage* C_{occup}, defined as the percentage of the number of vehicles transmitting to the total number of available subframes transmission opportunities, and (ii) *Probability of Successful Reception* (P_{suc}). For simplicity, let P_{suc} be given by $\frac{1}{N}$ where N is the number of vehicles using the same subframe for BSM transmissions. (In reality, P_s gets worse as the N, the number of vehicles, increases.)

[3]Each vehicle is at 1-hop (i.e., within the transmission range) of every other vehicles belonging to a certain cluster of vehicle

5.3. Ch-RRI SPS: Semi-persistent Scheduling using Channel Aware RRI Selection

Table 5.1: Conventional SPS with static RRIs vs Ch-RRI scheduling with adaptive RRI

Metrics	Conventional SPS			**Ch-RRI**
	20 ms	50 ms	100 ms	**Adaptive RRI**
Channel Occupancy Percentage	379.4%	152.94%	75.88%	100%
Probability of Successful Reception	0.35	0.7058	1	1

Table 5.1 depicts the average C_{occup} and P_{suc} observed in the example NR-V2X network under conventional SPS with three different values of RRI, i.e., 20 ms, 50 ms, and 100 ms. For instance, the average C_{occup} for SPS with low RRI = 20 ms is given by $\frac{\sum RRI \times (C_{occup} \text{in each cluster i})}{\text{total number of vehicles}}$. C_{occup} for each cluster can be computed as follows: Since RRI is 20 ms, there are 20 transmission opportunities (or subframes), (i) in cluster 1, 20 vehicles attempt to transmit, it means $C^1_{occup} = \frac{20}{20} \times 100 = 100\%$, (ii) in cluster 2, 50 vehicles attempt to transmit, which results in $C^2_{occup} = \frac{50}{20} \times 100 = 250\%$, and (iii) in cluster 3, 100 vehicles attempt to transmit, resulting in $C^3_{occup} = 500\%$. Thus, the average C_{occup} is $\frac{20 \times C^1_{occup} + 50 \times C^2_{occup} + C^3_{occup}}{20+50+100} \times 100 = 379.4\%$. The average P_s can be computed in similar fashion, and it turns out to be 0.35 in case of SPS with RRI as 20 ms. On contrary for SPS with high RRI = 100 ms the average C_{occup} and P_s are 75.88% and 1 respectively.

Note that SPS with low RRI, such as 20 ms, leads to *overly congested radio channels* (379.4%), and thus a large number of dropped BSM packets (0.35), particularly in clusters 2 and 3 with $>$ 20 vehicles). The lost packets result in high tracking error, which compromises the awareness of considered NR-V2X network. Whereas, in the case of SPS with high RRI of 100 ms, the radio resources are under-utilized (75%), particularly in cluster 1 and 2 with $<$ 100 vehicles. Tracking error performance can be significantly improved by choosing a lower value of RRI as a lower value of RRIs will improve timely delivery of BSMs. From the above discussion, it is evident that SPS with fixed RRI (irrespective of the chosen value of RRI) is limited in the context of improving overall cooperative awareness of NR-V2X networks.

To address the limitations of conventional SPS (and as detailed in the next section), we propose Ch-RRI, which allows each vehicle to adapt its RRI, based on its neighboring vehicle density at any given time. In case of the example NR-V2X network, under such Ch-RRI strategy, each vehicle in cluster 1 (with 20 vehicles) will choose RRI = 20 ms. Similarly,

Ch-RRI will choose RRI = 50 ms for cluster 2 (with 50 vehicles) and RRI = 100 ms for cluster 3 (with 100 vehicles) – which will result in $C_{occup} = 100\%$ and $P_s = 1$ (See Table 5.1). It means that the proposed Ch-RRI strategy with adaptive RRI enables judicious utilization of the radio resources. This in turn reduces the tracking error and enhances the cooperative awareness of NR-V2X networks.

5.3.2 Problem Formulation

Notations. At each time instant $t \in T$, let $sf(t, P_{th})$ denote the set of available subframes (subframes with observed power less than P_{th}) in the neighborhood of any vehicle v. RRI_v is the v^{th} vehicle's RRI and $\mathcal{N}$ is the set of all vehicles in the environment.

Objective function. As shown in Eq. 5.9, the objective function is to minimize the resource reservation interval (RRI) (or maximize BSM rate) at each vehicle v (where $v \in \mathcal{N}$) over the entire time duration T.

$$\min \sum_{t \in T} \frac{1}{|\mathcal{N}|} \sum_{v \in \mathcal{N}} \text{RRI}_v(t) \tag{5.9}$$

$$\text{subject to} \sum_{v \in \mathcal{N}} \text{RRI}_v(t) \leq sf(t, P_{th}), \forall v \in \mathcal{N}, t \in T \tag{5.10}$$

$$\text{RRI}_{min} \leq \text{RRI}_v(t) \leq \text{RRI}_{max}, \forall v \in \mathcal{N}, t \in T \tag{5.11}$$

Constraints. Equation 5.10 constrains the sum total of the RRI interval to be less than the number of subframes available to each vehicle v at time instant t. This constraint ensures that the channel congestion or the outage probability across all vehicles not compromised. Equation 5.11 restricts the RRI for each vehicle to be within the range [RRI_{min},RRI_{max}].

Note that solving the afore-stated ILP formulation would provide the optimal solution to Ch-RRI. However, this is impractical in a real-world NR-V2X setting because of changing mobility of vehicles and lack of global knowledge. Additionally, in order to solve the ILP problem, we would require knowledge of the available subframes at future time instants, which is impractical to obtain in time varying NR-V2X networks. Ch-RRI SPS is based on decentralized SPS and estimates the latest channel occupancy (via sensing window), selecting the suitable value of RRI at each vehicle in the NR-V2X network based on its local

knowledge.

Figure 5.3: Flowchart of Ch-RRI SPS

5.3.3 Ch-RRI SPS Description

This subsection discusses in detail the proposed Ch-RRI SPS protocol. As shown in Fig. 5.3, Ch-RRI SPS makes significant enhancements to the conventional SPS algorithm. The green boxes represent the steps of the Ch-RRI algorithm and all other steps are borrowed from conventional SPS.

- **RRI Initialization and Sensing (Steps 1-2):** Similar to SPS, Ch-RRI SPS continuously monitors the previous N_{sensing} subframes by measuring RSRP and S-RSSI and

stores the sensing measurements for the sensing window, i.e., N_{sensing} subframes (Step 1). In Step 2, Ch-RRI initializes the estimated $\widehat{\text{RRI}}$ to RRI_{min}. Ch-RRI also initializes the RSRP threshold (P_{th}) to a minimum value P_{min}. Unlike SPS, the selection window is not initialized before starting the resource selection (see Step 2 of Mode-4 SPS in Fig. 2.2), and is varied as available resources are identified and the estimated $\widehat{\text{RRI}}$ is updated. Like SPS, Ch-RRI SPS sets and updates the P_{th}(See Step 3).

- **Ch-RRI: Channel-aware RRI selection (Steps 4-10):** Each vehicle utilizes N_{sensing} subframes (obtained in Step 2) for identifying the available subframes and subsequently, selecting the minimum RRI possible in between transmission while ensuring that there remain resources (or subframes) for other vehicles.

  1. In Step 4, Ch-RRI updates the estimated $\widehat{\text{RRI}}$ and initializes the selection window with $T_1 = 1$ and $T_2 = \widehat{\text{RRI}}$. T_1 is fixed to 1 to maximize subframe resources.

  2. Each vehicle populates set S_A with all subframes in the selection window and S_B as a empty set (See Step 5). The candidate subframe exclusion criteria is also borrowed from SPS, except that, $\widehat{RRI}$ is an adjustable parameter in Ch-RRI.

  3. If the remaining subframes in S_A is less than 20% of total available subframes (Step 7), then, Ch-RRI, unlike SPS, first checks whether the $\widehat{\text{RRI}} < \text{RRI}_{max}$ (Step 8). If yes, $\widehat{\text{RRI}}$ is increased by Δ as shown in Step 9, and Steps 4 - 7 are repeated. Once $\widehat{\text{RRI}}$ has reached RRI_{max}, then P_{th} is increased by 3 dB in Step 10, and Steps 3 - 7 are repeated.

- **Resource Selection** (Step 11) and **Resource Reselection** (Step 12) are similar to SPS. As in SPS, a reselection counter (RC) value is chosen such that the resource reservation is restricted to between 0.5 and 1.5 s, irrespective of chosen $\widehat{\text{RRI}}$. However, in the chase of Ch-RRI SPS, since RC is zero, unlike SPS (see Steps 8-9 in SPS flowchart), Ch-RRI SPS does not allow re-reservation of subframe resources. Both these modifications are to ensure that Ch-RRI allows each vehicle to adjust its RRI at the time of resource reselection and account for changing vehicle traffic conditions.

5.4 Simulation Description and Results

This section describes the simulation setting, followed by experimental results for the proposed Ch-RRI SPS compared against conventional SPS protocol.

5.4.1 Simulation Setting

Both SPS and Ch-RRI SPS protocols are implemented on top of a modified system-level network simulator (ns-3) which supports C-V2X Mode-4 communications. NIST originally implemented Mode 1 and 2 of the LTE sidelink in network simulator (ns-3) [69], which was extended to support Mode-3 and C-V2X Mode-4 Communication by Nabil et al. [66].

The highway mobility model assumes vehicles to be moving in a six lane highway road, with three lanes in each direction. While existing works [64], [66] and [4] largely assume a constant velocity model, we consider a more realistic vehicle velocity model where the velocity of a certain vehicle follows a Gaussian distribution centered around v_{avg} (in forward direction, i.e., lane 1, 2 and 3) and $-v_{avg}$ (in reverse direction, i.e., lane 4, 5, and 6). In our experiments, the mean v_{avg} is set to 19.44 m/s (70 km/hr) and the variance is set to 3.0 m/s. [20] supports the assumption of Gaussian random variables as reliable for modelling highway traffic speeds. When each vehicle reaches the end of the highway segment, a warp is applied that moves the vehicle immediately to the other end of the road segment, and the vehicle is kept in the same lane. Vehicles with velocities normally distributed around v_{avg} are assigned to lanes 1, 2, and 3 (the 3 bottom most lanes in Fig.1), while vehicles normally distributed around $-v_{avg}$ are assigned to lanes 4, 5, and 6. Each vehicle in the same lane travelled in the same direction and had a maximum deceleration of 4.6 m/s^2. A Poisson distribution was used for the initial placement of vehicles along the highway.

For extensive analysis, we compare the performance of Ch-RRI SPS against the conventional SPS protocol with three different fixed RRIs: 20 ms RRI, 50 ms RRI, and 100 ms RRI. The simulations were run with varying vehicle densities, ranging from 40 to 160 vehicles. For the purposes of our simulations we assume a 10 MHz channel, though this can be easily adjusted. The initial positions and velocities were kept the same for the same considered vehicle density scenario across the Ch-RRI SPS and conventional SPS simulations. Each scenario had a simulation time of 8 seconds, and results were averaged across 10 trials. Table 5.2 summarizes the key simulation parameters for both Ch-RRI SPS and conventional

Table 5.2: Ch-RRI simulation Parameters

Parameter	Value
Vehicle density	{20-80} veh/km
Road Length/Number of lanes/Lane width	2000 m/ 6 lanes/ 4 m
Simulation time	8 seconds
Transmission Power	23 dBm
Transmission and Sensing Range	300 meters
Distribution of vehicle speeds	N(19.44 m/s, 3 m/s)
Deceleration a	4.6 m/s^2
t_{react}	1 second
Ch-RRI SPS RRI_{max}	100 ms
Ch-RRI SPS RRI_{min}	20 ms
Packet Size	190 B
MCS Index	7
Propagation Model	Winner+ B1 Model
Number of trials	10
RSRP threshold, P_{th}	-110 dBm

SPS with fixed RRIs.

5.4.2 Performance Metrics

We use the following two performance metrics for the evaluation of Ch-RRI SPS against conventional SPS.

- **Tracking error ($\mathbf{e_{track}}$)** is the difference between transmitting vehicle u's actual location and u's location obtained from the most recent BSM received from u at receiver vehicle v. (see Section 5.2.1).

- **Collision Risk Ratio** measures the overall on-road safety performance of C-V2X Mode-4 networks, and is defined as the ratio of number of collision risky instances (computed using Eq. 5.7) to that of both non-risky and risky instances between each pair of vehicles.

- **Packet Delivery Ratio (PDR)** is the probability that all vehicles within the range of the transmitting vehicle receives the transmitted packet. The PDR is calculated as

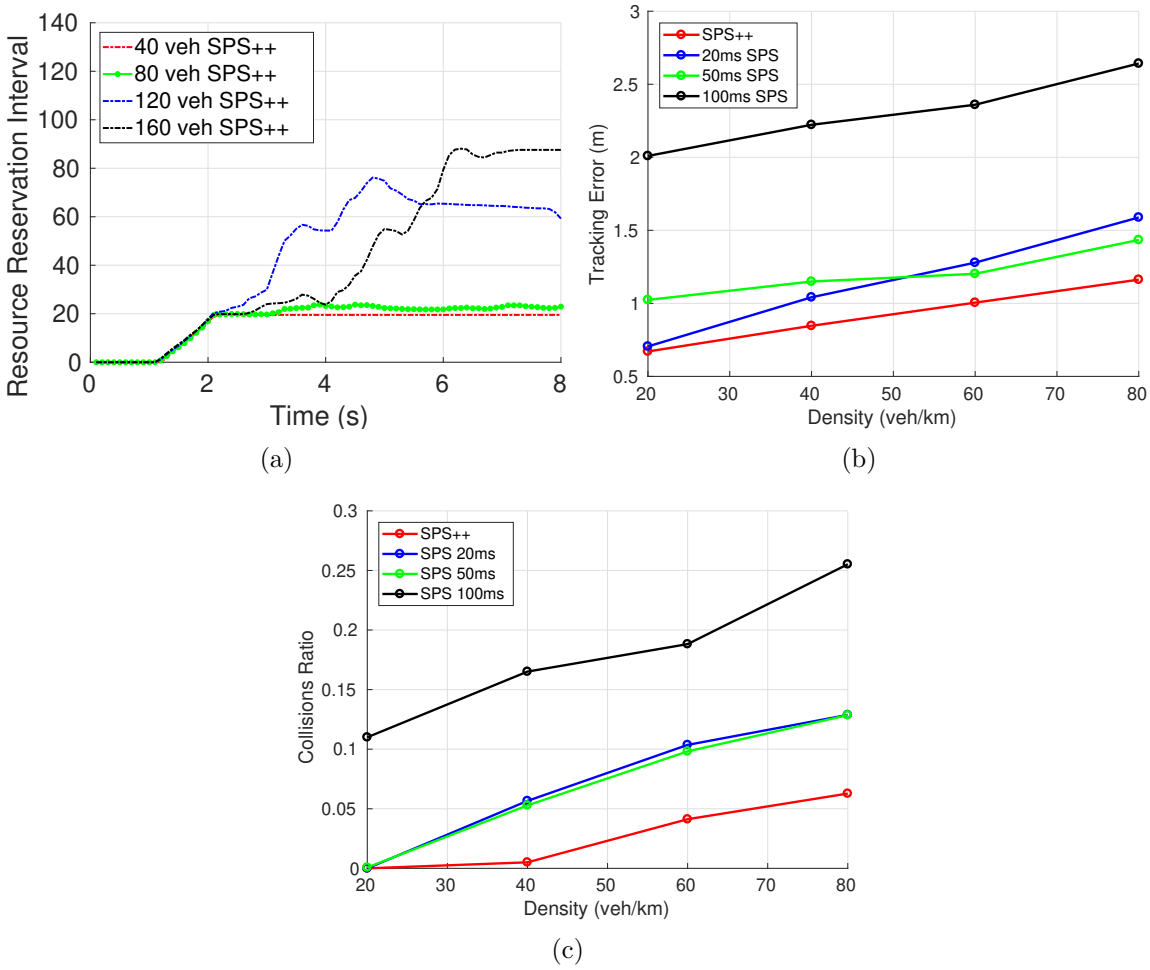

Figure 5.4: (a) RRI chosen by Ch-RRI SPS over time and varying vehicle densities: (b) Average high risk tracking error, and (c) Collision Risk.

$\text{PDR}_u = \frac{PR_u}{PD_u}$, where PD_u is the number of BSMs transmitted by vehicle u and PR_u is the number of BSMs sent by vehicle u received by neighboring vehicles.

5.4.3 Experimental Results

Before we discuss the comparative analysis of Ch-RRI SPS and SPS in terms of aforestated performance metrics, we first briefly discuss how Ch-RRI SPS is able to adjust the RRI at each vehicle given varying vehicle densities and over time.

Figure 5.4(a) shows how Ch-RRI SPS chooses, on average, the RRI across all vehicles for

each considered vehicle density scenario (i.e., 40, 80, 120 and 160) under varying simulation time. We observe over 10 trials that the average chosen RRI increases over simulation time as vehicles enter the simulation for each considered vehicle density. After 2 seconds, the RRI chosen for each vehicle setting converges to a certain unique RRI value. The chosen RRI in the cases of 40 and 80 vehicle density (i.e., sparse) is almost four to five times that of the 120 or 160 (i.e., dense) vehicle setting, thanks to the ability of Ch-RRI SPS to adjust RRI in real-time and adapt to the varying C-V2X environment. Vehicles also take a longer time in dense vehicle settings (5 and 6 seconds for 120 and 160 vehicles respectively) to converge to a chosen RRI value, likely because it takes longer for all vehicles to enter the simulation.

Figures 6.4(b)-6.4(f) show average Ch-RRI SPS RRI distributions over the last second of the simulation and show a large RRI variance in the 80, 120 and 160 vehicle density simulations. This is likely due to the large spatio-temporal dynamics at play, and vehicles choosing different RRIs depending on the number of vehicles in their vicinity. The average RRI of 40 vehicles, on the other hand, converges to the RRI_{min} of 20 ms. This will be because there are sufficient channel resources to support 20 ms RRI for each vehicle in case of 40 vehicles, irrespective of varying neighborhood sizes. Notice from Figs. 6.4(e) and 6.4(f) that while the RRI distribution is skewed to RRI_{max}, there are a number of vehicles still transmitting at lower RRIs.

Tracking Error and Collision Risk Analysis. The tracking error (Fig. 5.4(b)) and the collision risk (Fig. 5.4(c)) are both used to compare the effectiveness of Ch-RRI SPS to 20 ms, 50 ms, and 100 ms fixed RRI SPS, in terms of improved road safety performance of C-V2X networks. Fig. 5.4(b) shows that the tracking error increases as the vehicle density increases, and 20 ms RRI SPS and 50 ms RRI SPS tracking error alternate as the best performing fixed RRI SPS. At higher vehicle density scenarios, 50 ms RRI performs better in terms of tracking error, likely because the 20 ms RRI leads to increased packet losses at higher densities. Notice that the tracking error for Ch-RRI SPS is significantly lower than the tracking error associated with SPS (either with RRI 20 ms, 50 ms or 100 ms) across all vehicle densities. On average, Ch-RRI SPS outperforms 50 ms RRI SPS (the best performing fixed RRI) by almost 17% and 23% repectively at 60 and 80 veh/km. This indicates that the Ch-RRI SPS protocol is able to choose a suitable RRI at each vehicle that minimizes packet losses and enables up-to-date BSM sharing between a certain vehicle and its neighboring nodes. The tracking error improvements found with Ch-RRI SPS expectedly extend to the collision risk. Fig. 5.4(c) shows a significant decrease in high risk scenarios at 60 and 80

veh/km (55.6 % and 51.20 % respectively) as compared to 50 ms RRI SPS, which is the best performing fixed RRI scheme.

These results show that the lower RRI chosen is able to help vehicles in both low and high density situations. Observe that even at highly dense situations (80 vehicles/km), Ch-RRI SPS outperforms the 100 ms SPS protocol, although the average RRI chosen for Ch-RRI SPS was 100 ms. It is suspected that a small number of vehicles could be using smaller RRIs during the course of the simulation which helps reduce the number of high risk situations.

Packet Delivery Ratio Analysis. Fig. 5.5 shows that Ch-RRI SPS performs significantly better in terms of PDR when compared to that of SPS with RRIs 20 ms and 50 ms, under all considered vehicle density scenarios. Among the SPS with different RRIs, 100 ms SPS PDR performs the best of all three fixed RRIs. Larger RRIs led to a better PDR, but also yield a large tracking error and collision risk (See Figs 5.4(b) and 5.4(c)). Also notice that other than 100 ms RRI SPS, none of the 20 ms RRI, 50 ms RRI, or Ch-RRI SPS protocols have PDRs near 100%, although at low densities there should be enough subframes for all vehicles. This reduced PDR is likely an effect of the hidden terminal problem, where two transmitters might be out of the sensing range of each other, even if they are both transmitting to the same destination (for example, if both transmitters are far from the destination, in opposite directions). The likelihood of a hidden terminal collision increases with smaller RRIs, as there are fewer subframes that vehicles can use. However, in Ch-RRI SPS the PDR remains the same across vehicular densities, and outperforms the 50 ms fixed RRI PDR at higher densities. This is likely because of the larger RRI chosen by Ch-RRI SPS in the dense scenarios, which likely leads to less congestion and fewer packet collisions.

Discussion. Unlike conventional SPS protocol, the proposed adaptive Ch-RRI SPS is successfully able to adapt to the considered time-varying C-V2X scenarios and exploit the availability of channel resources (or subframes) – which allows each vehicle to dynamically choose the best RRI for the efficient and reliable BSM sharing with neighboring vehicles. This greatly reduces the tracking error between each pair of vehicles, which in turn significantly enhances the road safety of C-V2X networks. Thus, Ch-RRI SPS is a significant step forward for enabling the next-generation of C-V2X Mode-4 based connected vehicles and intelligent transportation systems.

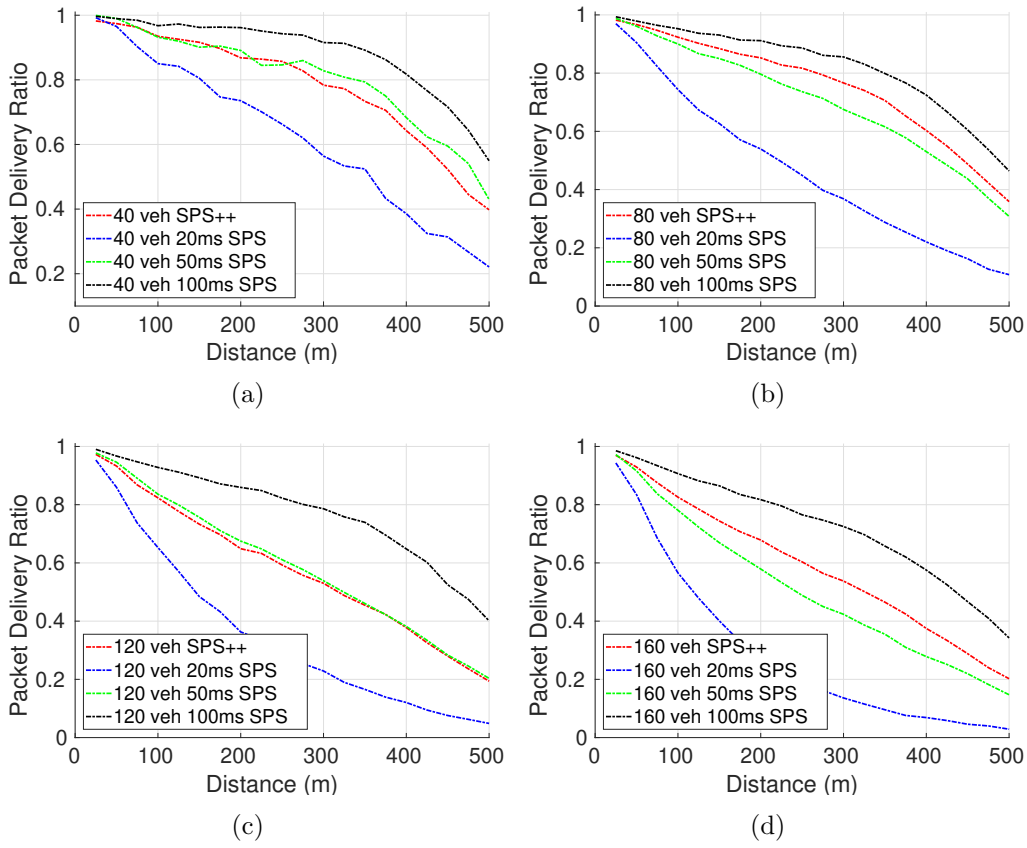

Figure 5.5: (a) PDR for 40 vehicles (b) PDR for 80 vehicles (c) PDR for 120 vehicles and (d) PDR for 160 vehicles.

5.5 Conclusion

In this chapter, we proposed a channel aware RRI selection algorithm for sensing-based semi-persistent scheduling, named Ch-RRI SPS, for the improved on-road safety performance of decentralized V2X networks. Specifically, Ch-RRI SPS, unlike conventional SPS, allows each vehicle to dynamically adjust RRIs based on the availability of channel resources and select suitable transmission opportunities for timely BSM transmissions at adjusted RRIs, while accounting for various vehicle traffic scenarios. Our extensive experiments based on C-V2X Mode-4 standard implemented using an ns-3 simulator demonstrated that the proposed Ch-RRI SPS protocol significantly outperformed conventional SPS in terms of improved on-road safety performance in all considered C-V2X scenarios.

Chapter 6

Adaptive RRI Selection Algorithms for Improved Cooperative Awareness in Decentralized NR-V2X

As discussed in Chapters 2 and 5, decentralized vehicle-to-everything (V2X) networks (i.e., Mode-4 C-V2X and Mode 2a NR-V2X) utilize sensing-based semi-persistent scheduling (SPS) where vehicles sense and reserve suitable radio resources for Basic Safety Message (BSM) transmissions at prespecified periodic intervals termed the *Resource Reservation Interval* (RRI). Vehicles rely on these received periodic BSMs to localize nearby (transmitting) vehicles and infrastructure, referred to as *cooperative awareness*. Cooperative awareness enables line of sight and non-line of sight localization, which can extend a vehicle's sensing and perception range and support future safety and autonomous applications. In this chapter, we show for the NR-V2X Mode-2 standard, that existing SPS scheduling (with prespecified RRIs) suffer from poor cooperative awareness, quantified as *tracking error*. As in Chapter 5, tracking error is defined as the difference between a vehicle's true position and the last location of that vehicle estimated by its neighbors. Although the collision risky models developed in Chapter 5 are useful, in this chapter we primarily focus on tracking error. This is because (1) tracking error has a direct relationship to collision risk, and (2), focusing on reducing tracking error removes assumptions on the behavior of the vehicle, and addresses a larger set of scenarios. To address the issues of static RRI SPS and improve cooperative awareness, we propose and compare two *RRI* selection algorithms – namely, the *Channel-aware RRI* (Ch-RRI) selection algorithm introduced in Chapter 5 and the *Age of Information (AoI)-aware RRI* (AoI-RRI) selection algorithm, discussed in this chapter. Ch-RRI dynamically selects a RRI based on *channel resource availability* depending upon the (sparse or dense) vehicle densities whereas AoI-RRI utilizes a novel information freshness metric, called Age of Information (AoI), to select a suitable RRI. Next, both adaptive RRI algorithms utilize SPS

scheduling for selecting suitable transmission opportunities for timely BSM transmissions at the chosen RRI. System-level simulations show that SPS with adaptive RRI (i.e., Ch-RRI SPS and AoI-RRI SPS) outperform the SPS with fixed RRI in terms of improved cooperative awareness under both low and high vehicle density scenarios. Furthermore, we notice that AoI-RRI SPS outperforms Ch-RRI SPS for larger vehicle density scenarios, whereas for low density scenarios, Ch-RRI SPS does slightly better than AoI-RRI SPS.

6.1 Introduction

The Third Generation Partnership Project (3GPP) Release 16 has introduced a V2X communications technology that uses the 5G New Radio (NR) air interface, referred to as 5G NR-V2X. NR-V2X includes enhancements to the 3GPP's previous cellular V2X communications technology (C-V2X) based on the Long-Term Evolution (LTE) standard. NR-V2X offers two modes of operation, termed Mode-1 and Mode-2, that use sidelink communications, which is direct communication between users or vehicles without data passing through the gNodeB [67]. NR-V2X Mode-1 employs a centralized scheduling approach, where a gNodeB schedules and assigns sidelink radio resources for two or more vehicles to communicate and exchange data directly. NR-V2X Mode-2 assumes communications to occur outside the coverage of a gNodeB; therefore, every vehicle uses a sensing-based semi-persistent scheduling (SPS) protocol to sense and reserve sidelink radio resources. SPS was introduced as part of the Release 14 C-V2X Mode-4 standard, the predecessor to NR-V2X Mode-2 [77]. Since cellular connectivity can not be assumed ubiquitous, NR-V2X Mode-2 is considered as the baseline mode for NR-V2X.

In NR-V2X Mode-2 SPS, vehicles sense radio resources (or channel medium) and select suitable (underutilized) resources for the transmission of packets at prespecified fixed time intervals, termed *Resource Reservation Intervals* (RRI). More formally, RRI is defined as the inter-transmission time interval between two consecutive transmissions. In the Release 14 C-V2X standard, RRIs were restricted to 20 ms, 50 ms, or 100 ms [64]. Release 16 NR-V2X Mode-2 provides more flexibility by allowing any integer RRI between 1 and 99 ms [38].

The primary use case for NR-V2X Mode-2 SPS is the dissemination of basic safety messages (BSMs), which carry time sensitive state information such as transmitting a vehicle's speed, heading, and location [2]. Receiving vehicles can use these BSMs for *cooperative awareness*,

the localization and trajectory prediction of neighboring vehicles and infrastructure. Cooperative awareness can enable safety-critical applications such as forward collision warnings [70], blind spot/lane change warnings [47], and is likely one of the key requirements for autonomous driving [46]. One metric that can quantify cooperative awareness performance is tracking error, the difference between a vehicle's actual and perceived location (via most recent BSM) by its neighboring vehicles. Tracking error, as opposed to conventional communication metrics such as packet delivery ratio (PDR) and throughput, captures the impact of multiple lost or outdated BSMs on a vehicle's awareness.

Since BSMs carry time-sensitive information, outdated BSMs (due to large RRIs) and/or lost BSMs (due to channel congestion) negatively impact the performance of cooperative awareness applications, mainly due to wrong localization of neighboring vehicles. Therefore, it is critical that the state information in each vehicle's transmission be *fresh*, as stale information can compromise the aggregate awareness of the vehicular network. The freshness of information at receiving vehicles can be measured using Age-of-Information (AoI). AoI is the time elapsed since new state information has been generated and is a promising metric to measure the freshness of system state information. Results in [29] have found that AoI has a strong correlation with tracking error in vehicular networks, which motivates further study of AoI.

In this work, we explore the deficiencies of the NR-V2X Mode-2 SPS using static RRIs in terms of tracking error and propose algorithms that choose adaptive RRIs to improve the overall cooperative awareness performance of NR-V2X Mode-2. We show that SPS with static RRIs (e.g. 50 and 100 ms) has cooperative awareness limitations in NR-V2X networks. Consider these scenarios: (i) *high vehicle density scenarios* – the NR-V2X network performance suffers from congestion with a large number of lost packets, leading to an increased tracking error, and (ii) *low vehicle density* – the spectrum resources would be underutilized in time. The tracking error performance in low density scenarios can improve with a smaller RRI, which ensures frequent location updates without fear of channel congestion. We introduce two adaptive RRI algorithms, termed Channel-aware RRI (Ch-RRI) selection and AoI-aware RRI (AoI-RRI) selection. Ch-RRI uses channel occupancy measurements to find the smallest RRI possible without increasing congestion. Motivated by the benefits of reducing AoI, we propose AoI-RRI, an AoI-aware RRI selection algorithm for NR-V2X Mode-2 that uses the average AoI observed by neighboring vehicles to select an optimal RRI.

In this work, we make the following key contributions:

- We show that NR-V2X Mode-2 SPS with static RRIs suffers severely from under- and over-provisioning of radio resources (depending upon the vehicle densities). This in turn negatively impacts the timely successful delivery of BSMs and compromises the cooperative awareness of NR-V2X Mode-2 SPS.
- To address the limitations of SPS with static RRIs, we propose Ch-RRI SPS, which is SPS powered by a *channel aware* RRI selection algorithm. The Ch-RRI algorithm uses channel occupancy measurements and chooses the minimum possible RRI spacing between transmissions without increasing packet loss due to congestion. Ch-RRI SPS uses this RRI spacing to select radio resources for BSM transmissions.
- In a similar vein to Ch-RRI SPS, we develop AoI-RRI SPS, SPS powered by a *AoI aware* RRI selection algorithm. The AoI-RRI algorithm uses neighborhood age and channel resource measurements to choose an age optimal RRI iteratively.
- Experiments developed on our NR-V2X simulator show that when compared to NR-V2X Mode-2 SPS with 20 ms, 50 ms, and 100 ms RRI, the proposed Ch-RRI and AoI-RRI SPS demonstrate a substantial reduction of tracking error. Ch-RRI as compared to AoI-RRI shows a lower AoI and tracking error in low density highway scenarios, and is faster in converging to a local minimum AoI. However, the average AoI and tracking error of AoI-RRI SPS are lower at higher densities.

6.2 State-of-the-art

There has been a surge of research in the area of simulating and enhancing SPS for C-V2X Mode-4 [14, 16, 17, 23, 39, 45, 64, 66, 68] and more recently, for NR-V2X Mode-2 SPS [9, 21]. The research performed in [23] simulated and provided a baseline for semi-persistent scheduling across various densities for highway and urban environments. Research in [66], [14], and [65] varied the probability of reselection, selection window, and RRI in SPS and measured the impact on the packet delivery ratio (PDR). The authors of [45] concluded that using short term sensing before resource selection reduced packet collisions and improved SPS performance. The work in [16] and [57] was amongst the first to adjust the transmission power and RRI accordingly, to improve the overall performance of SPS. To address the scheduling overhead of SPS, [17] has proposed using single shot transmissions as part of SPS for safety critical messages that have an immediate scheduling need. Although much of the

research for semi-persistent scheduling is simulation driven, [39] has provided an analytical model for semi-persistent scheduling in vehicular networks. Recently, the work in [9, 21] has simulated the relatively new NR-V2X Mode-2 SPS, specifically looking at the impact of the flexible numerology on SPS. A potential drawback of these works is the focus on improving the coverage (typically measured through PDR) of C-V2X Mode-4 and NR-V2X Mode-2, and ignoring the cooperative awareness performance of the vehicular network.

AoI has recently emerged as a popular metric for quantifying the performance of scheduling and decentralized radio resource management in vehicular networks. In particular, there has been a lot of research done in optimizing the broadcast rate to reduce the AoI in networks that use Dedicated Short Range Communications (DSRC), a competing V2X technology based on the 802.11p standard. [12, 51, 54, 61, 62, 80, 81]. Although there are notable differences between the two standards, changing the broadcast rate can be seen as the analogous equivalent to using the RRI to minimize the AoI, and merits discussion. The authors in [51] developed a decentralized algorithm that iterated the broadcast rate based on AoI measurements for a DSRC network. The work in [12] proposed a model that uses a vehicular network's connectivity graph to show the relationship between the average system AoI and vehicle density and broadcast intervals. AoI was used to evaluate platooning applications for convoys of vehicles in [80] and [61]. Furthermore, [54] and [62] investigated the effect of the backoff window size in CSMA on the AoI.

Although the SPS protocol in C-V2X Mode-4 and NR-V2X Mode-2 is relatively new, there has been some recent work in applying AoI to SPS. Recently, [68] analyzed the AoI of Release 14 C-V2X Mode-4 and proposed a piggyback collaboration method to help decrease half duplex errors, thereby reducing the AoI. Note that although the Release 14 C-V2X Mode-4 SPS is similar to Release 16 NR-V2X Mode-2 SPS, there are a few key differences between the two standards. Two differences that are particularly relevant to this work are the change in ranking of subframe resources (discussed in Section 5.3) and the inclusion of any integer RRI between 1 and 99 ms[1]. These changes can enable higher transmission rates while preventing collisions from choosing the same subframe resource [9]. While there have been recent works evaluating the overall performance of Release 16 NR-V2X SPS, to the best of our knowledge, this is the first work that evaluates the AoI and cooperative awareness performance for NR-V2X SPS and the first work to directly use AoI measurements

[1]Please refer to [38] for a detailed discussion on the differences between C-V2X Mode-4 and NR-V2X Mode-2.

to optimize the RRI for SPS.

6.3 Cooperative Awareness and NR-V2X Mode-2

In this section, we discuss cooperative awareness, the tracking error metric, and the NR-V2X Mode-2 standard for sidelink communications from the physical layer structure to the semi-persistent scheduling algorithm that vehicles use to find and reserve suitable transmission opportunities.

6.3.1 Cooperative Awareness and Tracking Error

Since cooperative awareness depends on the sharing of time sensitive information with other vehicles via BSMs, conventional communication metrics such as latency, throughput, and packet delivery ratio (PDR) greatly impact a vehicle's awareness. However, these metrics alone cannot capture the impact of multiple lost or outdated BSMs on a vehicle's awareness, as illustrated by the following example. Consider a fast moving vehicle travelling at 140 km/hr (38.89 m/s) while transmitting with a high RRI (100 ms or more). Neighboring vehicles receive location packets reliably, but because there is at least 100 ms between packets, the localization or *tracking* error would be at least 3.89 m. Likewise, a low RRI (50 ms or less) would yield a tracking error of at least 1.94 m, though this tracking error could increase if packets are dropped due to channel congestion. Thus, as the above example shows, a tracking error metric can provide more context to the cooperative awareness performance in vehicular networks.

Illustrated in Fig. 6.1, tracking error (e_{uv}^{track}) in the context of NR-V2X is defined as the difference in the transmitting vehicle's (vehicle u) true location, and u's estimated location by neighboring receiving vehicle v. We assume that the receiving vehicle v is within the transmission range of u and time $t^{'}$ is the generation time of the transmission from u to v. The tracking error is calculated as:

$$e_{uv}^{track} = \sqrt{(x_u^t - \hat{x}_{uv})^2 + (y_u^t - \hat{y}_{uv})^2} \tag{6.1}$$

(x_u^t, y_u^t) is u's true current 2-D location at time t and $(\hat{x}_{uv}, \hat{y}_{uv})$ is u's previous location from

time t' at vehicle v from the last transmission received from u.

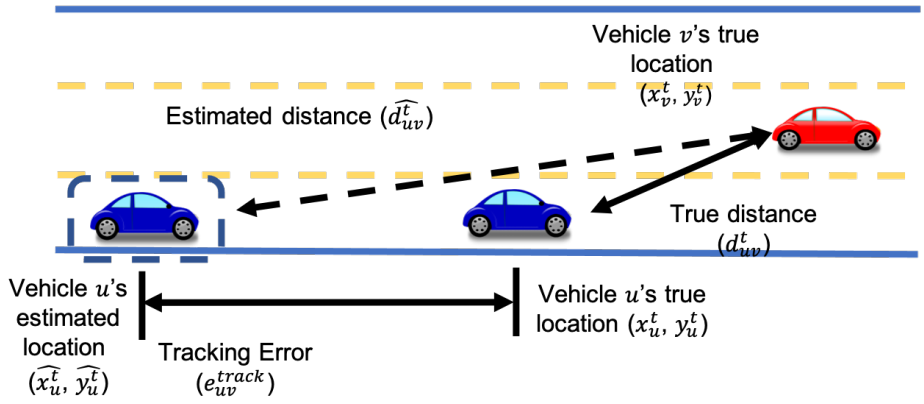

Figure 6.1: Illustration of latency induced tracking error in a vehicular network.

The tracking error has a large impact on the cooperative awareness in vehicular networks because

1. Every transmission has a non-zero propagation delay between transmission and successful reception and the transmitting vehicle would also likely have moved during the transmission and reception times.

2. The RRI (or inter-packet transmission interval) can cause a large tracking error, especially at higher speeds.

3. Channel congestion could lead to several lost and delayed packets, further deteriorating tracking error. In the example of a vehicle traveling at 140 km/hr with a 50 ms RRI in a congested environment, two consecutive missed packets could cause a 5.833 m tracking error.

A lower tracking error at receiving vehicle v implies that v can accurately position (or *localize*) u. Note from the above discussion that a lower RRI can decrease the tracking error but can also increase the number of lost packets due to channel congestion.

6.4 AoI-RRI: Age of Information Aware RRI Selection Algorithm

In this section, we give some intuitions on the potential limitations of Ch-RRI, provide a brief background of Age-of-Information (AoI), and formulate the problem of AoI minimization in vehicular networks as a integer linear programming (ILP) problem. We discuss why the ILP formulation is impossible to solve for a decentralized network and propose AoI-RRI, a decentralized AoI-aware RRI selection algorithm.

6.4.1 Limitations of Ch-RRI on Cooperative Awareness

Though Ch-RRI is a promising RRI adaptation algorithm and promises to improve the cooperative awareness as discussed in Section 5.3, it has certain limitations as presented in this section.

- Ch-RRI SPS is based on the accurate knowledge of channel occupancy at any given time, however, given the dynamics of vehicles and channel usage, obtaining accurate channel availability information at each vehicle is not possible.
- Ch-RRI SPS attempts to enable each vehicle to transmit at the minimum RRI while accounting for 100% channel occupancy. However, the optimal trade-off between channel occupancy and optimal RRI may not be at 100 % channel occupancy.

Motivated by these limitations, we consider optimizing for the novel information freshness metric AoI. Since optimizing for AoI guarantees the best freshness (and thus best tracking error), we can better account for trade-off between the optimal RRI and channel occupancy.

6.4.2 Age of Information (AoI)

Age of Information (AoI), quantifies the *freshness* of information at any receiving node that was originally generated and transmitted by the transmitting node [50]. For the purposes of vehicular networks, AoI is the elapsed time since the last received location packet was generated at the transmitting vehicle. Let t^g denote the time that the most recent location

packet at sender vehicle u was generated. The AoI at receiving vehicle v assuming the current time is t is:

$$AoI_{uv}(t) = t - t^g \tag{6.2}$$

The evolution of the AoI for vehicle v is illustrated in Fig. 6.2. The generation, transmission, and reception times of the i^{th} location packet are denoted by t_i^g, t_i^{tx}, and t_i^r. Therefore, the overall delay for a packet $= (t_i^r - t_i^g)$. Assuming the $(i+1)^{th}$ packet is generated at $t_{(i+1)}^g$, the generation rate is given by $\Delta = (t_{i+1}^g - t_i^g)$. Fig. 6.2 illustrates $\text{AoI}_{uv}(t)$, the AoI at the receiving vehicle v after a sender vehicle u generates and transmits a message, as a function of time .

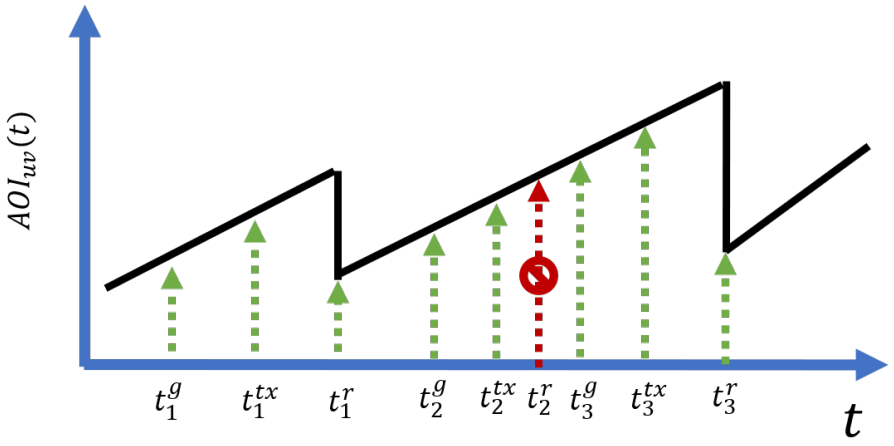

Figure 6.2: AoI_{uv} is the AoI at vehicle v based on the last received transmission from vehicle u.

Equation 6.2 can be used to find the average AoI_{uv} between vehicle v and neighboring vehicle u. The average AoI_{uv} is found by calculating the area under $AoI_{uv}(t)$. The area under $AoI_{uv}(t)$ is normalized by the observation time T_{obs} [50].

$$\text{AoI}_{uv} = \frac{1}{T_{obs}} \int_{T_{obs}} AoI_{uv}(t) \tag{6.3}$$

We represent the set of all vehicles in the environment as $\mathcal{N}$ and the set of all neighboring vehicles of v as $\mathcal{N}_v \subseteq \mathcal{N}$, where $u \in \mathcal{N}_v$. The average AoI at vehicle v is:

$$AoI_v = \frac{1}{|\mathcal{N}_v|} \sum_{u \in \mathcal{N}_v} AoI_{uv} \tag{6.4}$$

The overall system AoI with $|\mathcal{N}|$ vehicles can be computed as:

$$AoI = \frac{1}{|\mathcal{N}||(\mathcal{N}-1)|} \sum_{v \in \mathcal{N}} \sum_{u \in \mathcal{N}_v} AoI_{uv} \tag{6.5}$$

where $|\mathcal{N}||(\mathcal{N}-1)|$ is the number of unique pairs of sender and receiver in the system. Assuming the simple vehicular network in Fig. 6.1 with vehicles u and v, we can assume that inter-packet reception intervals between receiver v and transmitter u are multiples of the RRI. Using these assumptions and the fact that the AoI resets to 0 upon successful reception of location information, the evolution of the AoI at the receiving vehicle can be written as

$$AoI(t + \text{RRI}) = \begin{cases} 0, & \text{if a packet is received} \\ AoI(t) + \text{RRI}, & \text{otherwise} \end{cases} \tag{6.6}$$

Note that Eq. 6.6 implies that minimizing the RRI also minimizes the AoI at the receiving vehicle. However, too many vehicles transmitting with a small RRI can increase the number of lost packets due to congestion, which also increases the AoI. Therefore, as in the case of tracking error, there is a tradeoff between smaller RRIs and improved AoI performance.

6.4.3 AoI ILP Problem Formulation

The objective of AoI-RRI is to minimize the overall system AoI based on what each vehicle observes. As in the Ch-RRI problem formulation, finding an optimal RRI that minimizes the system AoI can be written as a Integer Linear Programming (ILP) problem.

Objective function. Equation 6.7 formally shows the objective function where each vehicle chooses a RRI at each vehicle v (where $v \in \mathcal{N}$) such that the AoI is minimized over the entire time duration T.

$$\sum_{t \in T} \frac{1}{|\mathcal{N}|} \sum_{u,v \in \mathcal{N}} AoI_{uv}(t) \tag{6.7}$$

$$\text{subject to } \text{RRI}_{min} \leq \text{RRI}_v(t) \leq \text{RRI}_{max}, \forall v \in \mathcal{N}, t \in T \tag{6.8}$$

Constraints. Equation 6.8 restricts the RRI for each vehicle to be within the range [RRI_{min},RRI_{max}]. Note that there are no capacity constraints for Eq. 6.7, and the AoI minimization itself decides the optimal tradeoff.

However, as in the case of Eq. 5.9, solving Eq. 6.7 assumes global information at every vehicle and knowledge of each vehicles channel information and mobility even at future time instants, making the ILP formulation impossible to solve. Thus we propose AoI-RRI , an algorithm that attempts to iteratively minimize the NR-V2X system AoI in a decentralized manner, described in Section 6.4.4

6.4.4 AoI-RRI SPS

This section details AoI-RRI SPS, SPS powered by a decentralized AoI-aware RRI selection algorithm. AoI-RRI finds a RRI_v (where $\text{RRI}_v \in [\text{RRI}_{min}\ \text{RRI}_{max}]$) for vehicle v by iterating the previously chosen RRI, denoted RRI^{t-1}, such that the locally measured average AoI is minimized. The algorithm runs in three steps. First, at the RRI selection time, v uses the sensing window history to measure the channel congestion in the network. Second, v calculates the time since the last received packet from every vehicle in the vicinity to estimate the local average AoI, and adjusts its RRI according to minimize this last measured AoI. Finally, v uses the NR-V2X semi-persistent scheduling procedure presented in Fig. 2.2 and selects subframe resources using the latest selected RRI. The algorithm details are as follows:

Step 1: Sensing and Channel Congestion Detection. In line 1 of Algorithm 1, AoI-RRI uses a channel congestion detection algorithm, further detailed in Algorithm 2, to measure and detect whether or not significant channel congestion has occurred. The channel congestion algorithm returns **true** if there is significant congestion detected and like Ch-RRI SPS, uses the previously chosen RRI^{t-1} and the RSRP sensing measurements for the last N_{sensing} subframes, i.e. the sensing window, as inputs. In line 2 of Algorithm 2, v calculates the size of the set S_{total}, which is the set of all possible subframe resources using RRI^{t-1}. Lines 3-5 of Algorithm 2 populate set S_{avail} with those subframes with linear average RSRP measurements higher than P_{th}^{t-1}. If the number of subframes in S_{avail} is less than 20% of total available subframes, that means that network congestion has increased since the previous resource reservation, and RRI^{t-1} or P_{th}^{t-1} must be increased. Using RSRP measurements can give a robust estimate of the channel congestion without adding any sensing overhead since the sensing window measurements and RSRP threshold are taken as part of the SPS

procedure. If the channel congestion has increased, lines 2-3 of Algorithm 1 automatically increase the RRI to avoid congesting the channel further.

Step 2: AoI estimation and RRI adjustment. If the channel has not become significantly congested, vehicle v uses Eqs. 6.2 and 6.4 and calculates its local AoI by calculating and averaging the time since the last received packet from each neighboring vehicle. The AoI-RRI algorithm iterates upon the last chosen RRI to minimize the most recent average AoI at each vehicle v. AoI-RRI uses one of the following three actions– (1) **DECR** - decrease RRI, (2) **INCR** - increase RRI, and (3) **SAME** - maintain the same RRI [2]. Algorithm 1 presents the pseudocode for this step.

Lines 4-9 form the core of AoI-RRI where AoI_{avg} for the current and previous T_{obs} are compared. In lines 4-6 AoI-RRI checks if the local AoI has increased by a factor of more than σ_t, in which case the AoI has significantly worsened and AoI-RRI reverses the previous selected action. If in lines 7-9 v sees that if the local AoI has decreased by a factor of more than σ_t, the previous action selected by the algorithm is repeated, i.e. the RRI continues to increase or decrease. If there is no significant change in AoI, AoI-RRI chooses the same RRI as before. Finally, in 10-20 the new RRI is calculated based on the action selected in lines 2-9. The new RRI returned is maintained until the end of the current T_{obs}. β decides the magnitude by which the RRI changes if the chosen action was **INCR** or **DECR**.

Step 3: Semi-persistent Scheduling. Finally, v uses the RRI selected from Algorithm 1 to choose a subframe for transmission using the SPS procedure presented in Fig. 2.2. Note that the P_{th} value that is used to select the subframes is stored as part of the procedure, and again the next time resources are selected.

6.5 Simulation Overview and Results

In this section we cover the simulation settings, performance metrics, and evaluates the proposed Ch-RRI SPS and AoI-RRI SPS against conventional SPS.

[2]The concept of utilizing these actions for adjusting the RRI is inspired by the algorithm presented in [50]

Algorithm 3 AoI-RRI algorithm at vehicle v

Input: RSRP of N_{sensing} subframes across J subchannels in sensing history, $sf_{\text{total}} = [sf_1^j, \cdots, sf_{N_{\text{sensing}}}^j]$, Minimum Power threshold (P_{min}), Maximum Power threshold (P_{max}), RRI chosen during the previous T_{obs}, RRI^{t-1}, local average AoI of the previous T_{obs}, AoI_{avg}^{t-1}, Action chosen during the previous T_{obs}, α^{t-1}), Power threshold chosen during the previous T_{obs}, (P_{th}^{t-1})

Output: New RRI^t, subframe sf_v for node v, and number of retransmissions N_{resel}

$[\text{channel}_{\text{flag}}] = \text{channel}_{\text{cong}}(\text{RRI}^{t-1}, sf_{\text{total}}, P_{th}^{t-1})$ ▷ Checks to see if channel is congested
if $\text{channel}_{\text{flag}}$ ==true **then**
    $\boldsymbol{\alpha^t}$ =INCR
if $AoI_{avg}^t > AoI_{avg}^{t-1} + \sigma_t$ **then**
    $\boldsymbol{\alpha^t} = \text{inverse}(\alpha^{t-1})$ ▷ Previous action caused AoI to worsen significantly, so inverse action
else if $AoI_{avg}^t < AoI_{avg}^{t-1} - \sigma_t$ **then**
    $\boldsymbol{\alpha^t} = (\alpha^{t-1})$ ▷ Previous action caused AoI to get better so continue action
else
    $\boldsymbol{\alpha^t}$ =SAME ▷ AoI has not significantly changed from previous value, so maintain same RRI
if $\boldsymbol{\alpha^t}$ == INCR **then**
    if $\text{RRI}^{t-1} \geq \text{RRI}_{max}$ **then**
        $\text{RRI}^t = \text{RRI}^{t-1}$ ▷ AoI has improved but RRI has hit maximum
    else
        $\text{RRI}^t = \beta\ \text{RRI}^{t-1}$
else if $\boldsymbol{\alpha^t}$ == DECR **then**
    if $\text{RRI}^{t-1} \leq \text{RRI}_{min}$ **then**
        $\text{RRI}^t = \text{RRI}^{t-1}$ ▷ AoI has improve but RRI has hit minimum
    else
        $\text{RRI}^t = \frac{1}{\beta}\ \text{RRI}^{t-1}$
else if $\boldsymbol{\alpha^t}$ == SAME **then**
    $\text{RRI}^t = \text{RRI}^{t-1}$
return P_{th}, RRI^t

6.5.1 Simulation Setting

We modified and enhanced a system-level simulator originally designed to model C-V2X Mode-4 [22] to model and compare AoI-RRI SPS, Ch-RRI SPS, and NR-V2X Mode-2 SPS with three different static RRIs. We use the 3GPP highway mobility models [38] to validate our simulation results.

In the highway mobility model, vehicles move along a six lane highway, with three lanes dedicated to each direction. The highway models assumes the velocity of vehicles moving in the positive direction (lanes 1, 2 and 3) and negative direction (lanes 4, 5, and 6) are drawn from truncated Gaussian distributions with means of v_{avg} and $-v_{avg}$, respectively.

Algorithm 4 Channel Congestion

Input: All subframes in sensing history, $sf_{total}(1 : N_{\text{sensing}})$, Power threshold selected from previous subframe selection (P_{th}^{t-1}), RRI selected from previous AoI scheduling instance, RRI^{t-1}

Output: Returns true if the channel is congested as compared to the previous RRI, and false otherwise

procedure $\text{channel}_{\text{cong}}(sf_{total}(1 : N_{\text{sensing}}), P_{th}^{t-1}, \text{RRI}^{t-1})$
    $N_{\text{RRI}} = \text{floor}(\frac{N_{\text{sensing}}}{\text{RRI}^{t-1}} - 1)$
    $S_i^j = \frac{1}{N_{\text{RRI}}} \sum_{k=0}^{N_{RRI}} sf^j_{1+i+k\cdot\text{RRI}^{t-1}}$
    $S_{\text{total}} = [S_0^j, S_1^j, \ldots, S^j_{\text{RRI}^{t-1}}]$
    if $S_i^j < P_{th}^{t-1}$ **then**
        $S_{\text{avail}} \leftarrow S_i^j$
    if $\frac{|S_{\text{avail}}|}{|S_{\text{total}}|} < 0.2$ **then**
        return **true** ▷ The value of P_{th} has not changed as compared to the previous subframe selection, so the channel is not congested
    else
        return **false** ▷ The value of P_{th} needs to increase by 3 dB as compared to the previous subframe selection, so the channel is congested

The Gaussian distribution mean and variance values are 19.44 m/s (70 km/hr) and 3.0 m/s, respectively. As each vehicle in each lane approaches the length of the highway, the warp used in the model places the vehicle at the opposite end of the highway. All vehicles remain in the same lane for the duration of the simulation. Each vehicle's initial location along the highway followed a Poisson distribution.

For extensive analysis, we compare the performance of Ch-RRI SPS and AoI-RRI SPS against conventional NR-V2X Mode-2 SPS with three different static RRIs: 20 ms RRI, 50 ms RRI, and 100 ms RRI. The vehicle densities in the simulation ranged from 20 to 160 veh/km, and initial positions and velocities did not change across AoI-RRI SPS, Ch-RRI SPS, and NR-V2X SPS. All simulations used a 10 MHz system bandwidth, 25 second simulation time, and results were averaged over 10 trials. Table 6.1 shows the critical simulation values for AoI-RRI SPS, Ch-RRI SPS, and NR-V2X SPS with static RRIs.

6.5.2 Performance Metrics

This work uses the following three metrics to compare AoI-RRI SPS, Ch-RRI SPS, and static RRI SPS.

Table 6.1: AoI-RRI and Ch-RRI simulation comparison parameters

Parameter	Value
Vehicle density	{20-160} veh/km
Road Length/Number of lanes/Lane width	2000 m/ 6 lanes/ 4 m
β	1.1
Reselection time	0.5 -1.5 s
Simulation time	25 seconds
Transmission Power	23 dBm
Transmission and Sensing Range	300 meters
Distribution of vehicle speeds	N(19.44 m/s, 3 m/s)
AoI-RRI/Ch-RRI RRI_{max}	100 ms
AoI-RRI/Ch-RRI RRI_{min}	20 ms
Packet Size	190 B
MCS Index	7
Number of trials	10
Initial RSRP threshold, P_{th}	-90 dBm

- **Tracking error (e_{track})**- e_{track} is calculated as the difference in the transmitting vehicle u's actual location and estimated location from u's last received transmission at receiver vehicle v. (see Section 5.2.1). Note that e_{track} is computed in a slightly different manner as compared to Chapter 5. The estimated location of u incorporates the generation time for the i^{th} packet, as opposed to only the transmission and reception time as in Chapter 5. Furthermore the tracking error is computed over the x and y coordinates. These changes are intended to better measure the overall cooperative awareness, and realistically model what would be observed in actual vehicular networks.

- **Age of Information (AoI)** - The difference in the reception time at receiver vehicle v of vehicle u's last location and the generation time of u's last location (see Section 6.4.2).

- **Packet Delivery Ratio (PDR)** - The likelihood that all neighbors inside the transmission range of a vehicle successfully receive the sent packet. Formally, the PDR is computed as $\text{PDR}_u = \frac{PR_i}{PD_i}$. PD_i is the number of packets sent by vehicle i and PR_i is the number of packets received by neighboring vehicles originally transmitted by vehicle i.

6.5.3 Experimental Results

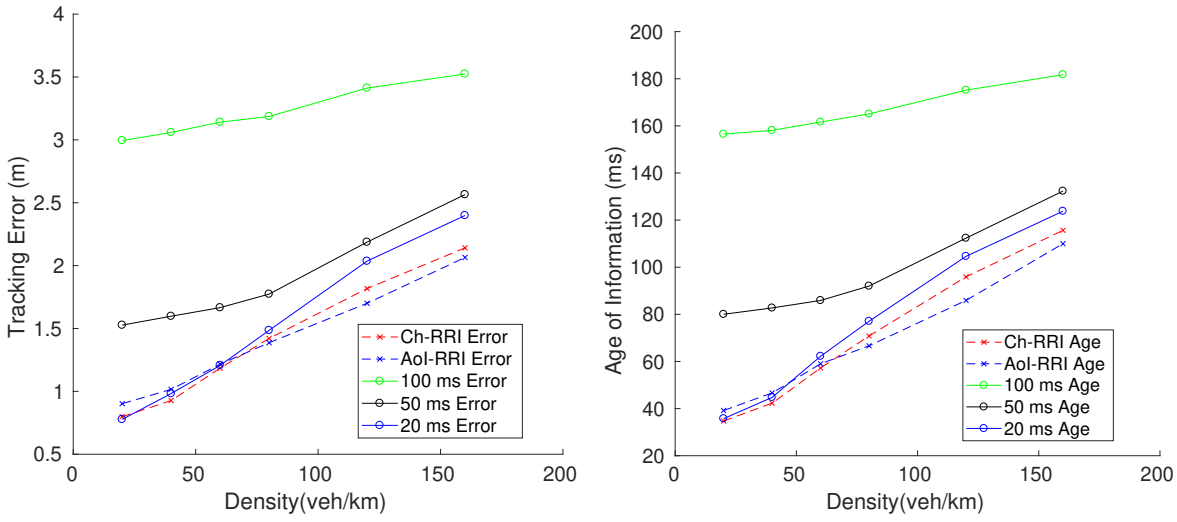

(a) (b)

Figure 6.3: (a) Average Tracking Error and (b) Average System Age of Information.

We compare AoI-RRI, Ch-RRI, and static RRI SPS using the previously discussed tracking error, AoI, and PDR performance metrics. In addition to these metrics, we also look at the final RRI distributions and average AoI over time to better understand the operation of AoI-RRI and Ch-RRI.

Average Tracking Error and System *AoI* Analysis. Figs. 6.3(a) and 6.3(b) compare the system tracking error and AoI, respectively, of AoI-RRI SPS and Ch-RRI SPS to 20 ms, 50 ms, and 100 ms static RRI SPS. Fig. 6.3(a) demonstrates that tracking error worsens with increasing density, with the 20 ms RRI SPS tracking error giving the best static RRI SPS performance. Both tracking error and AoI increase drastically at higher densities (larger than 100 veh/km). Since there are insufficient subframe resources to support a 20 ms RRI without two vehicles in the same vicinity choosing the same subframe resource, there are increased packet losses, leading to worse performance at high densities. The tracking error for AoI-RRI is smaller than the tracking error of Ch-RRI and all three static RRIs across large vehicle densities. AoI-RRI outperforms 20 ms RRI NR-V2X (the best performing fixed RRI) in terms of AoI by almost 19% and 16% respectively at 120 and 160 veh/km. This indicates that AoI-RRI finds for each vehicle a RRI that minimizes packet losses and enables timely cooperative awareness in the network. The AoI improvements found with AoI-RRI extend to the tracking error. AoI-RRI was also found to have an advantage over Ch-RRI in

high density scenarios as well outperforming Ch-RRI at 120 and 160 veh/km by 9.16% and 10.81%, respectively. The tracking error results show that lower average RRIs aid vehicles in high and low density situations. Even in high density scenarios, (160 vehicles/km), both AoI-RRI and Ch-RRI outperform the 20 and 50 ms RRI.

RRI Distribution Analysis. Figs. 6.4(a)-6.4(f) show the average RRI distributions for AoI-RRI and Ch-RRI for selected densities over the last five seconds of the simulation [3]. Across densities, AoI-RRI shows a larger RRI variance as compared to the Ch-RRI. This large variance in the AoI-RRI RRI distribution can be attributed to varying traffic densities and noisy estimates of the measured AoI leading vehicles to choose different RRIs depending on the AoI observed. Although there is a large variance in the RRI distribution of the AoI-RRI, the AoI-RRI tracking error performance approaches Ch-RRI and 20 ms SPS for low densities, and outperforms all methods in high density scenarios. In Ch-RRI, the RRI distribution is comparatively narrow, and the average chosen RRI is similarly small for low densities (20 and 40 veh/km). This means that there are enough channel resources to support small RRIs for both Ch-RRI and AoI-RRI. In Fig. 6.4(f), we see that while the AoI-RRI RRI distribution skews towards RRI_{max}, many vehicles use lower RRIs, which likely contributes to the improved AoI performance.

[3]We use the last five seconds because by then, every vehicle has had sufficient time to choose a acceptable RRI and we can analyze steady state behavior.

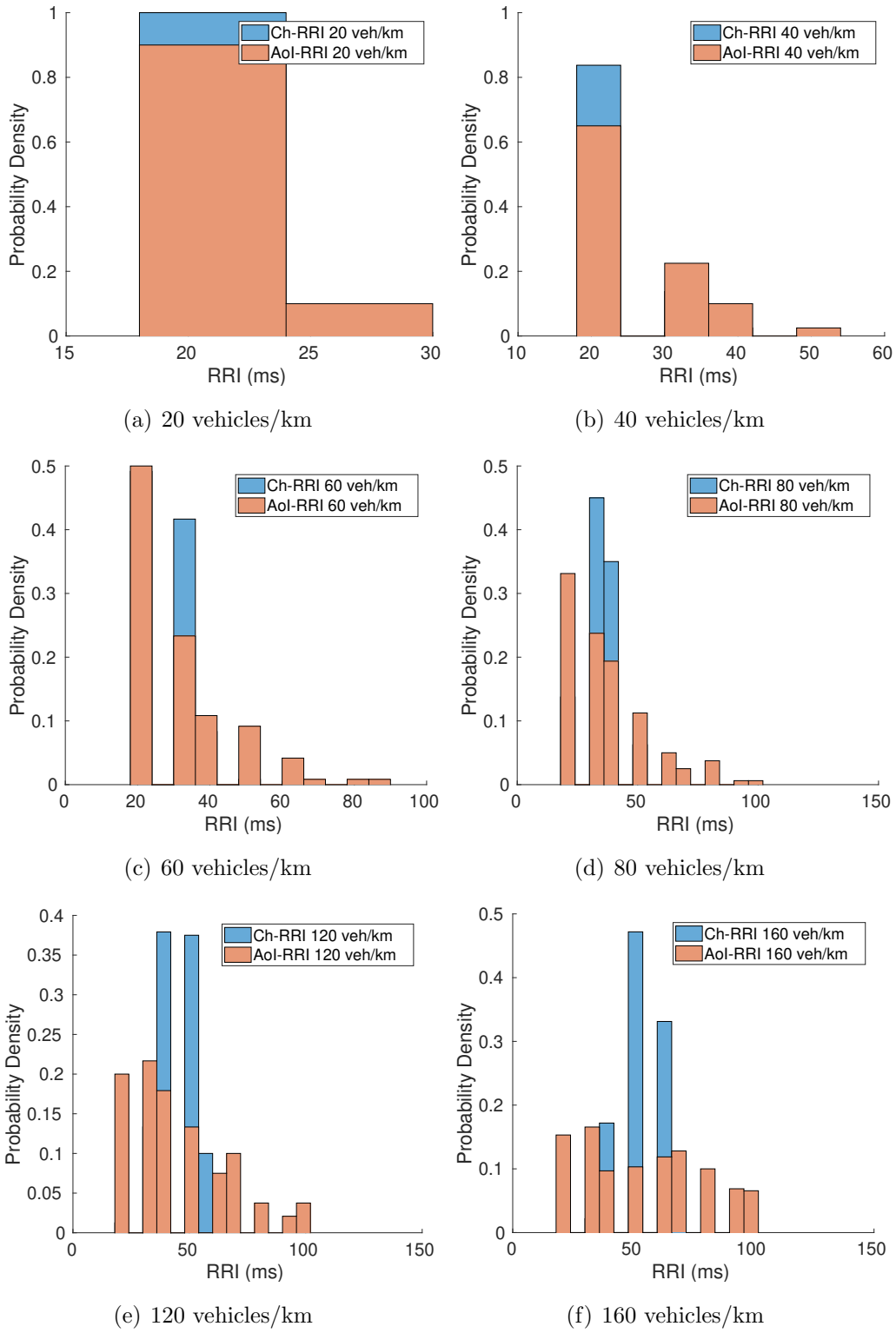

(a) 20 vehicles/km

(b) 40 vehicles/km

(c) 60 vehicles/km

(d) 80 vehicles/km

(e) 120 vehicles/km

(f) 160 vehicles/km

Figure 6.4: RRI distribution during the last 5 simulated seconds across vehicle densities for Ch-RRI and AoI-RRI.

Average *AoI* vs time analysis. Figs. 6.5(a)-6.5(f) show the average AoI over simulation time of AoI-RRI SPS and Ch-RRI SPS. Both AoI-RRI and Ch-RRI algorithms start with an initial RRI of 50 ms, and only allow for adaptive RRIs to be chosen after 5 sec. This gives enough time for each algorithm to (i) allow all vehicles to transmit at least once and (ii) allow each algorithm to gather channel and AoI measurements. Notice that both AoI-RRI and Ch-RRI start with an initial value of 120 ms. This is because both algorithms start with observing the channel for 100 ms (following the NR-V2X Mode-2 SPS standard) before selecting an initial subframe. Once both algorithms start transmitting, the AoI drops to 70 ms, which is expected for a RRI of 50 ms. In the low density cases (20 and 40 veh/km), both algorithms drop to average AoI of 40-50 ms. Note that Ch-RRI slightly outperforms AoI-RRI in lower densities. This is because Ch-RRI detects a empty channel and automatically transmits at the lowest possible RRI. Ch-RRI is also able to converge to a steady state value faster than AoI-RRI, likely because of the noisy nature of the AoI estimates. When the density increases, AoI-RRI is able to perform better, and is able to take actions to lead to a lower average AoI.

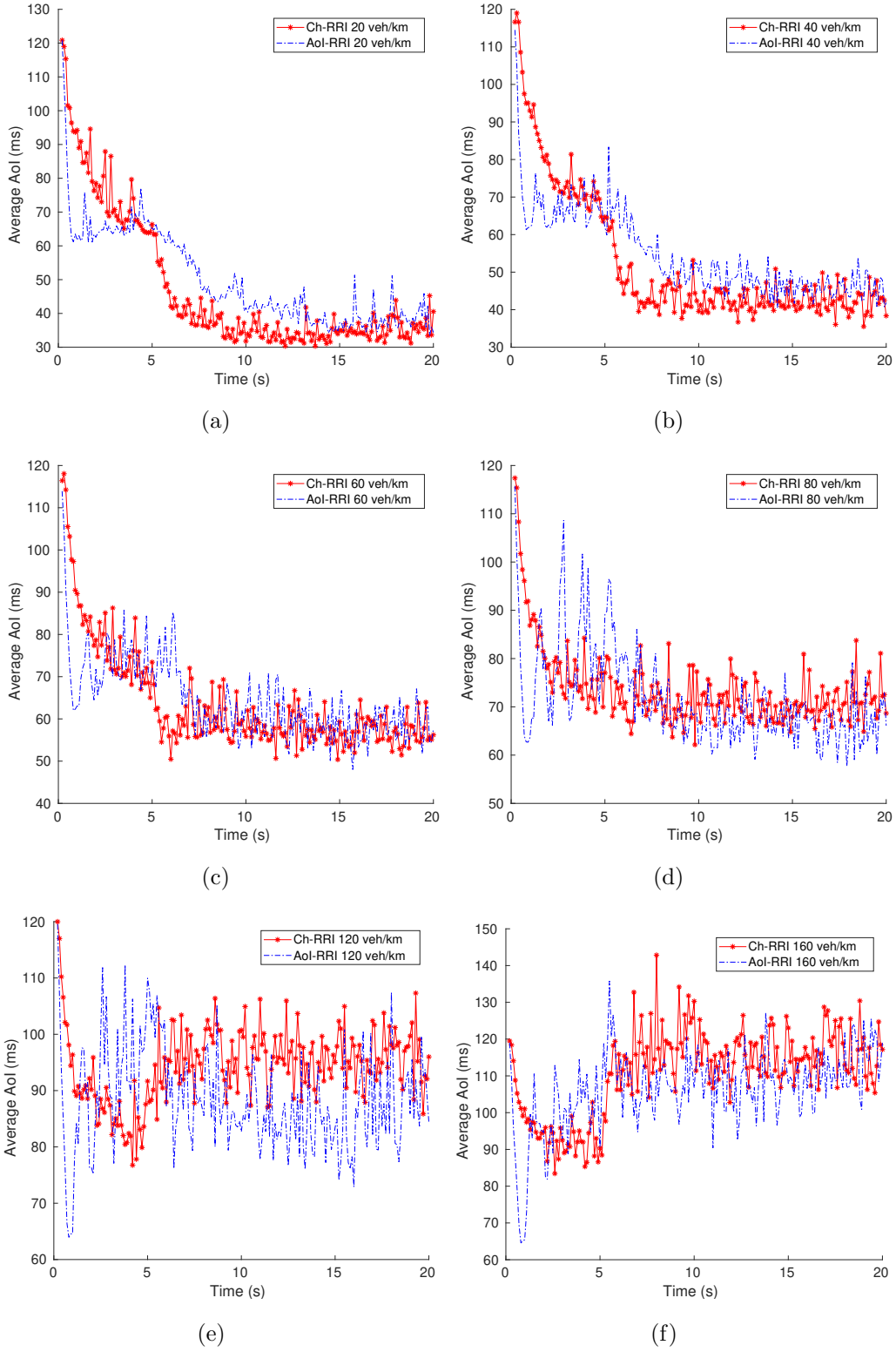

Figure 6.5: (a) Average AoI vs time for 20 vehicles (b) Average AoI vs time for 40 vehicles (c) Average AoI vs time for 60 vehicles and (d) Average AoI vs time for 80 vehicles (e) Average AoI vs time for 120 vehicles (f) Average AoI vs time for 160 veh/km.

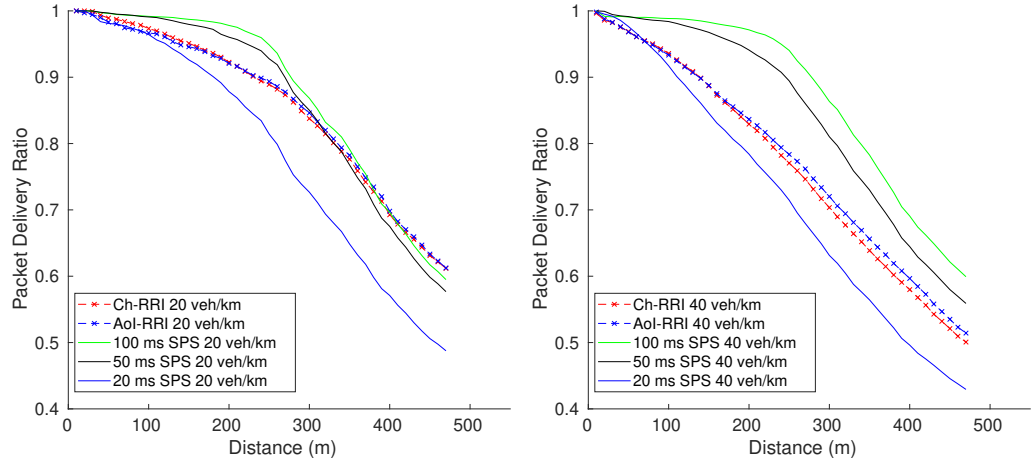

(a)

(b)

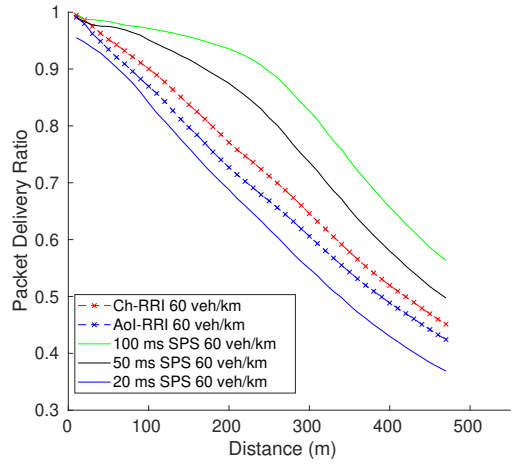

(c)

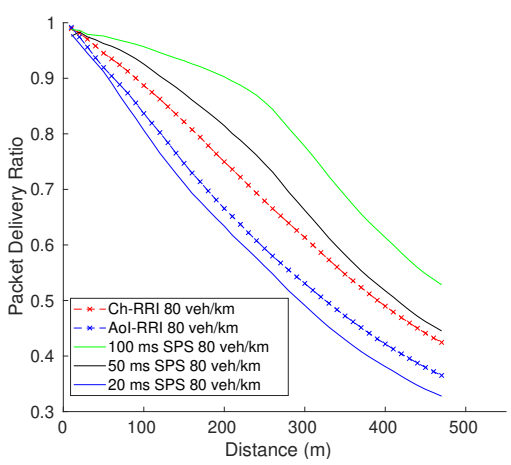

(d)

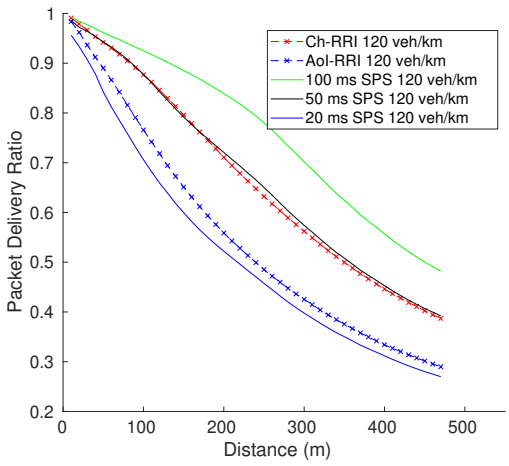

(e)

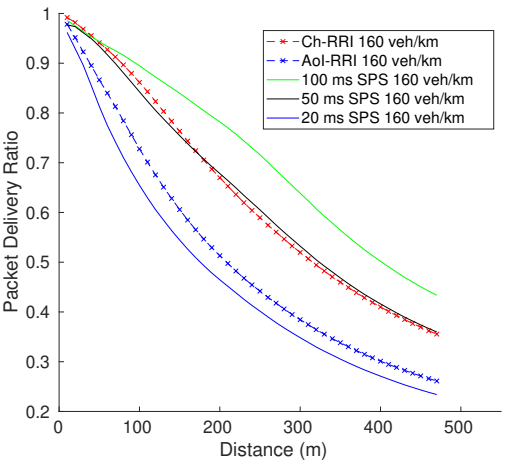

(f)

Figure 6.6: (a) PDR for 20 veh/km (b) PDR for 40 veh/km (c) PDR for 60 veh/km (d) PDR for 80 veh/km (e) PDR for 120 veh/km and (f) PDR for 160 veh/km.

Packet Delivery Ratio Analysis. Fig. 6.6 compares the AoI-RRI, Ch-RRI, and NR-V2X Mode-2 SPS PDRs across vehicle densities. Among the fixed RRI results, the 100 ms RRI performs the best, but correspondingly yielded a large tracking error and AoI. Similarly, 100 ms RRI NR-V2X gives the worst PDR performance, but gave the best tracking error and AoI performance, meaning there is a tradeoff between PDR and RRI, that affects AoI performance. Both AoI-RRI and Ch-RRI attempt to find the best RRI to optimize the tracking error and AoI.

Notice that at low densities (20 and 60 veh/km), the PDR of AoI-RRI and Ch-RRI are similar, as is the the average AoI and tracking error. Both AoI-RRI and Ch-RRI choose similar RRIs and are able to achieve the best tracking error performance. As the densities increase the RRI distribution of AoI-RRI tends towards lower RRIs, and the PDR performance is worse than that of Ch-RRI, which chooses a larger average RRI. This indicates that the AoI-RRI finds that choosing a slightly lower RRI distribution can minimize the AoI, as the average age of AoI-RRI is lower than Ch-RRI. However, AoI-RRI does not select a 20 ms RRI for all vehicles since the AoI results show there are diminishing returns for selecting a low RRI, and eventually the increased congestion and packet collisions will lead to a larger AoI and tracking error.

Discussion. The proposed AoI aware SPS is able to successfully learn the system AoI and adapt each vehicle's RRI across time-varying NR-V2X scenarios. As a result of choosing a optimal RRI, it is shown that the average tracking error of every vehicle pair is also reduced. This is expected to significantly improve the cooperative awareness of vehicular networks. Notice from Figs. 6.5(a)-6.5(f) the large variance of the AoI estimates. This large variance comes from a combination of the dynamic nature of the vehicular environment, multiple vehicles choosing the same subframe (i.e. the hidden terminal effect), and the AoI estimation process. Despite the noisy nature of the average AoI, AoI-RRI is able to choose a optimal RRI for each vehicle. As a result of choosing an optimal RRI, it is shown that the average tracking error of every vehicle pair is also reduced. This significantly improves the cooperative awareness of vehicular networks.

Chapter 7

Conclusions and Future Work

In this dissertation, we have made four practical contributions in the area of decentralized vehicular communications. In our first contribution, we have developed a transmission rate protocol for vehicles using Dedicated Short Range Communications (DSRC) that is intended to improve communications in safety critical situations. We use the distance and relative velocity between vehicles to estimate likelihoods of collisions, and adjust the transmission rate accordingly. For our second contribution, we develop a framework using tools from stochastic geometry to analyze the coverage probability and the rate coverage for vehicular networks under different scenarios. We analyze the expected interference of two transmission policies, one where as the vehicles grow closer together, they *listen more*, and one where they *transmit more*. We derive and show the coverage probability across various densities of these two schemes with the locations of the vehicles modeled as a 1D Poisson point process. In our third and fourth contributions, we suggest and implement improvements for C-V2X systems. We first propose *Ch-RRI* SPS, a RRI selection algorithm for semi-persistent scheduling that allows each vehicle to adjust the resource reservation interval in real time. We also introduce tracking error and an improved collision risk model. ns-3 simulations show that *Ch-RRI* SPS outperforms SPS in reducing collision risky scenarios, and improves tracking error and PDR across various densities. Finally, we propose *AoI-RRI* SPS, a RRI selection algorithm for semi-persistent scheduling that allows each vehicle to adjust the resource reservation interval based on the last measured AoI.

In Chapter 3, we proposed using time-to-collision (TTC) as a metric for determining the rate at which safety messages are transmitted for vehicles using DSRC to communicate with other vehicles. Chapter 3 introduced the concept of risk as a part of beacon rate selection in vehicular networks. Changing the beacon rate based on the risk each vehicle sees led to significant improvements in PDR and network performance, while also improving the safety for each vehicle. Based on the results of this work, it can be suggested that such a beacon rate algorithm be included into future standard to help improve the performance of areas

with a large number of vehicles, particularly those environments with greater than 80 nodes in a 1 km region.

Continued research in this area would include exploring an optimization based approach on deciding the upper limits of the beacon rate algorithms. Further work can also be done to investigate how the distribution of vehicle velocities can affect the performance of the adaptive beacon rate protocol. Additionally, this algorithm could be tested on actual vehicular traces to observe the benefits of the adaptive beacon rate selection.

In Chapter 4, we use a Poisson point process to analyze the performance of a risk based transmission scheme inspired by the work in Chapter 3. The success probability of a typical link was derived assuming the beacon rate of each vehicle is adjusted based on the spacing between adjacent nodes.

The next line of work is incorporating relative velocities into the two transmission policies. Currently, each transmission policy only considers the distance between adjacent nodes. Modeling the velocities as a random variable would be a useful addition to the analysis and help in evaluating the performance of the network. Another addition for future work is analyzing vehicular nodes in two dimensions. This would likely be done by using a Cox process, where a 1D PPP would be used to model the locations on nodes along a highway, and the spatial layout of the roads would be modeled by a Poisson Line process.

In Chapter 5, we investigated possible improvements to C-V2X networks. Specifically, we proposed an improved adaptive semi-persistent scheduling, termed *Ch-RRI* SPS that allowed each vehicle to dynamically adjust in real-time the BSM rate (or Resource Reservation Interval, RRI). Adjusting the RRI in real time allowed each vehicle to utilize the available channel resources under the considered C-V2X environment (e.g., sparse or dense density scenarios). ns-3 simulations showed that Ch-RRI SPS outperformed SPS in terms of both on-road safety performance, measured as collision risk and network performance.

Finally, in Chapter 6 we investigated RRI selection algorithms for the improved cooperative awareness performance of decentralized V2X networks. In addition to Ch-RRI, we proposed an AoI-aware RRI selection algorithm, termed *AoI-RRI*, which chose RRIs based on the last measured AoI. AoI-RRI SPS and Ch-RRI SPS then choose suitable BSM transmission opportunities (using the SPS procedure) with those chosen RRIs. Our extensive experiments based on NR-V2X Mode-2 standard demonstrated that SPS powered by either algorithm significantly outperforms conventional SPS in terms of improved cooperative awareness per-

formance in all considered NR-V2X scenarios. In the future, we will explore using nonlinear age functions and designing reinforcement learning (RL) based scheduling protocols that can learn vehicle priorities and other contextual factors over time.

Bibliography

[1] ETSI EN 302 637-2 V1.3.2 (2014-11) Intelligent Transport Systems (ITS); Vehicular Communications; Basic Set of Applications; Part 2: Specification of Cooperative Awareness Basic Service.

[2] ETSI EN 302 637-2 V1.3.2 (2014-11) Intelligent Transport Systems (ITS); Vehicular Communications; Basic Set of Applications; Part 2: Specification of Cooperative Awareness Basic Service.

[3] On-board system requirements for v2v safety communications. In *Soc. Autom. Eng.* SAE International, 2016.

[4] 3GPP. Study on lte-based v2x services. Technical Report (TR) 36.885, 3rd Generation Partnership Project (3GPP), 06 2011. Version 14.0.0.

[5] 3GPP. Evolved universal terrestrial radio access (e- utra); physical channels and modulation (v14.3.0, release 14). Technical Report (TR) TS 36.211, 3rd Generation Partnership Project (3GPP), 06 2017. Version 14.3.0.

[6] 3GPP. Evolved Universal Terrestrial Radio Access (E-UTRA); Radio Resource Control (RRC); Protocol specification. Technical Specification (TS) 36.331, 3rd Generation Partnership Project (3GPP), 04 2017. Version 14.2.2.

[7] 3GPP. Study on evaluation methodology of new Vehicle-to- Everything (V2X) use cases for LTE and NR. Technical Report (TR) 37.885, 3rd Generation Partnership Project (3GPP), 06 2019. Version 15.3.0.

[8] S. A. Ahmad, A. Hajisami, H. Krishnan, F. Ahmed-Zaid, and E. Moradi-Pari. V2v system congestion control validation and performance. *IEEE Transactions on Vehicular Technology*, 68(3):2102–2110, 2019.

[9] Zoraze Ali, Sandra Lagén, Lorenza Giupponi, and Richard Rouil. 3GPP NR V2X Mode 2: Overview, Models and System-Level Evaluation. *IEEE Access*, 9:89554–89579, 2021.

[10] J. Aznar-Poveda, E. Egea-Lopez, A. Garcia-Sanchez, and P. Pavon-Mariáo. Time-to-Collision-Based Awareness and Congestion Control for Vehicular Communications. *IEEE Access*, 7:154192–154208, 2019.

[11] Juan Aznar-Poveda, Esteban Egea-Lopez, Antonio-Javier Garcia-Sanchez, and Pablo Pavon-Mariao. Time-to-Collision-Based Awareness and Congestion Control for Vehicular Communications. *IEEE Access*, 7:154192–154208, 2019.

[12] Andrea Baiocchi and Ion Turcanu. Age of information of one-hop broadcast communications in a csma network. *IEEE Commun. Letters*, 25(1):294–298, 2020.

[13] G. Bansal, J. B. Kenney, and C. E. Rohrs. Limeric: A linear adaptive message rate algorithm for dsrc congestion control. *IEEE Trans. Veh. Technol.*, 62(9):4182–4197, 2013.

[14] A. Bazzi, G. Cecchini, A. Zanella, and B. M. Masini. Study of the Impact of PHY and MAC Parameters in 3GPP C-V2V Mode 4. *IEEE Access*, 6:71685–71698, 2018.

[15] A. Bazzi, B. M. Masini, A. Zanella, and I. Thibault. On the Performance of IEEE 802.11p and LTE-V2V for the Cooperative Awareness of Connected Vehicles. *IEEE Transactions on Vehicular Technology*, 66(11):10419–10432, 2017.

[16] Alessandro Bazzi. Congestion control mechanisms in IEEE 802.11 p and sidelink C-V2X. In *Proc., IEEE Asilomar*, pages 1125–1130, 2019.

[17] Maria Bezmenov, Zoran Utkovski, Klaus Sambale, and Slawomir Stanczak. Semi-Persistent Scheduling with Single Shot Transmissions for Aperiodic Traffic. In *2021 IEEE 93rd Vehicular Technology Conference (VTC2021-Spring)*, pages 1–7, 2021.

[18] B. Blaszczyszyn, P. Mühlethaler, and Y. Toor. Maximizing throughput of linear vehicular ad-hoc networks (vanets) — a stochastic approach. In *2009 European Wireless Conference*, pages 32–36.

[19] S. Busanelli, G. Ferrari, and R. Gruppini. Performance analysis of broadcast protocols in VANETs with Poisson vehicle distribution. In *2011 11th International Conference on ITS Telecommunications*, pages 133–138.

[20] Tracy Camp, Jeff Boleng, and Vanessa Davies. A survey of mobility models for ad hoc network research. *Wireless Communications and Mobile Computing*, 2(5):483–502, 2002.

BIBLIOGRAPHY

[21] Claudia Campolo, Antonella Molinaro, Francesco Romeo, Alessandro Bazzi, and Antoine O Berthet. 5G NR V2X: On the impact of a flexible numerology on the autonomous sidelink mode. In *Proc. of IEEE 2nd 5G World Forum (5GWF)*, pages 102–107. IEEE, 2019.

[22] Giammarco Cecchini, Alessandro Bazzi, Barbara M. Masini, and Alberto Zanella. LTEV2Vsim: An LTE-V2V simulator for the investigation of resource allocation for cooperative awareness. In *2017 5th IEEE International Conference on Models and Technologies for Intelligent Transportation Systems (MT-ITS)*, pages 80–85, 2017.

[23] S. Chen, J. Hu, Y. Shi, and L. Zhao. LTE-V: A TD-LTE-Based V2X Solution for Future Vehicular Network. *IEEE Internet of Things Journal*, 3(6):997–1005, 2016.

[24] Shanzhi Chen, Jinling Hu, Yan Shi, Ying Peng, Jiayi Fang, Rui Zhao, and Li Zhao. Vehicle-to-everything (v2x) services supported by lte-based systems and 5g. *IEEE Communications Standards Magazine*, 1(2):70–76, 2017.

[25] V. V. Chetlur and H. S. Dhillon. Coverage analysis of a vehicular network modeled as cox process driven by poisson line process. 17(7):4401–4416.

[26] V. V. Chetlur and H. S. Dhillon. Success probability and area spectral efficiency of a vanet modeled as a cox process. 7(5):856–859.

[27] Vishnu Vardhan Chetlur and Harpreet S Dhillon. Downlink coverage analysis for a finite 3-D wireless network of unmanned aerial vehicles. *IEEE Trans. on Comm,*, 65(10):4543–4558, 2017.

[28] B. Choudhury, V. K. Shah, A. Dayal, and J. H. Reed. Experimental Analysis of Safety Application Reliability in V2V Networks. In *2020 IEEE 91st Vehicular Technology Conference (VTC2020-Spring)*, pages 1–5, 2020.

[29] Biplav Choudhury, Vijay K Shah, Avik Dayal, and Jeffrey H. Reed. Experimental Analysis of Safety Application Reliability in V2V Networks. In *2020 IEEE 91st Vehicular Technology Conference (VTC2020-Spring)*, pages 1–5, 2020.

[30] Biplav Choudhury, Vijay K Shah, Avik Dayal, and Jeffrey H Reed. Joint age of information and self risk assessment for safer 802.11 p based V2V networks. In *IEEE INFOCOM 2021-IEEE Conference on Computer Communications*, pages 1–10. IEEE, 2021.

[31] A. Dayal, E. Colbert, V. Marojevic, and J. Reed. Risk Controlled Beacon Transmission in V2V Communications. In *2019 IEEE 89th Vehicular Technology Conference (VTC2019-Spring)*, pages 1–6, 2019.

[32] A. Dayal, V. K. Shah, H. Dhillon, and J. Reed. Adaptive RRI Selection Algorithms for Improved Cooperative Awareness in Decentralized NR-V2X. *Submitted to IEEE Transactions on Intelligent Transportation Systems (Under Review)*, pages 1–12.

[33] A. Dayal, A. Tbaileh, Y. Deng, and S. Shukla. Distributed VSCADA: An integrated heterogeneous framework for power system utility security modeling and simulation. In *2015 Workshop on Modeling and Simulation of Cyber-Physical Energy Systems (MSCPES)*, pages 1–6.

[34] A. Dayal, Yi Deng, A. Tbaileh, and S. Shukla. VSCADA: A reconfigurable virtual SCADA test-bed for simulating power utility control center operations. In *2015 IEEE Power Energy Society General Meeting*, pages 1–5.

[35] Avik Dayal, Vijay K. Shah, Biplav Choudhury, Vuk Marojevic, Carl Dietrich, and Jeffrey H. Reed. Adaptive Semi-Persistent Scheduling for Enhanced On-road Safety in Decentralized V2X Networks. In *2021 IFIP Networking Conference (IFIP Networking)*, pages 1–9, 2021.

[36] Salman Durrani, Xiangyun Zhou, and Abhas Chandra. Effect of vehicle mobility on connectivity of vehicular ad hoc networks. In *2010 IEEE 72nd Vehicular Technology Conference-Fall*, pages 1–5. IEEE, 2010.

[37] M. J. Farooq, H. ElSawy, and M. Alouini. A stochastic geometry model for multi-hop highway vehicular communication. 15(3):2276–2291.

[38] M. H. C. Garcia, A. Molina-Galan, M. Boban, J. Gozalvez, B. Coll-Perales, T. Şahin, and A. Kousaridas. A Tutorial on 5G NR V2X Communications. *IEEE Communications Surveys Tutorials*, pages 1–1, 2021.

[39] M. Gonzalez-Martín, M. Sepulcre, R. Molina-Masegosa, and J. Gozalvez. Analytical Models of the Performance of C-V2X Mode 4 Vehicular Communications. *IEEE Transactions on Vehicular Technology*, 68(2):1155–1166, 2019.

[40] Marc Green. "how long does it take to stop?" methodological analysis of driver perception-brake times. *Transportation Human Factors*, 2(3):195–216, 2000.

[41] Maurizio Guida, Maurizio Longo, Fabio Postiglione, Kishor S Trivedi, and Xiaoyan Yin. Semi-markov models for performance evaluation of failure-prone ip multimedia subsystem core networks. *Proceedings of the Institution of Mechanical Engineers, Part O: Journal of Risk and Reliability*, 227(3):290–301, 2013.

[42] Amir Haider and Seung-Hoon Hwang. Adaptive Transmit Power Control Algorithm for Sensing-Based Semi-Persistent Scheduling in C-V2X Mode 4 Communication. *Electronics*, 8(8), 2019.

[43] Zeeshan Hameed Mir and Fethi Filali. LTE and IEEE 802.11p for vehicular networking: a performance evaluation. 2014(1-89).

[44] Hannes Hartenstein and LP Laberteaux. A tutorial survey on vehicular ad hoc networks. *IEEE Communications magazine*, 46(6):164–171, 2008.

[45] X. He, J. Lv, J. Zhao, X. Hou, and T. Luo. Design and Analysis of a Short Term Sensing Based Resource Selection Scheme for C-V2X Networks. *IEEE Internet of Things Journal*, pages 1–1, 2020.

[46] Laurens Hobert, Andreas Festag, Ignacio Llatser, Luciano Altomare, Filippo Visintainer, and Andras Kovacs. Enhancements of V2X communication in support of cooperative autonomous driving. *IEEE Communications Magazine*, 53(12):64–70, 2015.

[47] C. Huang, Y. P. Fallah, R. Sengupta, and H. Krishnan. Adaptive intervehicle communication control for cooperative safety systems. *IEEE Network*, 24(1):6–13, 2010.

[48] Daniel Jiang, Vikas Taliwal, Andreas Meier, Wieland Holfelder, and Ralf Herrtwich. Design of 5.9 ghz DSRC-based Vehicular Safety Communication. *IEEE Wireless Communications*, 13(5):36–43, 2006.

[49] Sanjit Kaul, Marco Gruteser, Vinuth Rai, and John Kenney. Minimizing age of information in vehicular networks. In *2011 8th Annual IEEE Communications Society Conference on Sensor, Mesh and Ad Hoc Communications and Networks*, pages 350–358. IEEE, 2011.

[50] Sanjit Kaul, Marco Gruteser, Vinuth Rai, and John Kenney. Minimizing age of information in vehicular networks. In *2011 8th Annual IEEE Communications Society Conference on Sensor, Mesh and Ad Hoc Communications and Networks*, pages 350–358. IEEE, 2011.

[51] Sanjit Kaul, Roy Yates, and Marco Gruteser. Real-time status: How often should one update? In *2012 Proceedings IEEE INFOCOM*, pages 2731–2735. IEEE, 2012.

[52] John B. Kenney. Dedicated Short-Range Communications (DSRC) Standards in the United States. 99(7):1162–1182.

[53] John B. Kenney. Dedicated Short-Range Communications (DSRC) Standards in the United States. *Proceedings of the IEEE*, 99(7):1162–1182, 2011.

[54] Antzela Kosta, Nikolaos Pappas, Anthony Ephremides, and Vangelis Angelakis. Age of information performance of multiaccess strategies with packet management. *Journal of Communications and Networks*, 21(3):244–255, 2019.

[55] Jim Lansford, John B. Kenney, and Peter Ecclesine. Coexistence of unlicensed devices with dsrc systems in the 5.9 ghz its band. In *2013 IEEE Vehicular Networking Conference*, pages 9–16.

[56] Jim Lansford, John B. Kenney, and Peter Ecclesine. Coexistence of unlicensed devices with DSRC systems in the 5.9 GHz ITS band. In *2013 IEEE Vehicular Networking Conference*, pages 9–16, 2013.

[57] Tsern-Huei Lee and Chieh-Fu Lin. Reducing Collision Probability in Sensing-Based SPS Algorithm for V2X Sidelink Communications. In *2020 IEEE REGION 10 CONFERENCE (TENCON)*, pages 303–308, 2020.

[58] Xingqin Lin, Jeffrey G Andrews, Amitabha Ghosh, and Rapeepat Ratasuk. An overview of 3GPP device-to-device proximity services. *IEEE Communications Magazine*, 52(4):40–48, 2014.

[59] H. P. Luong, M. Panda, H. L. Vu, and B. Q. Vo. Beacon rate optimization for vehicular safety applications in highway scenarios. *IEEE Trans. Veh. Technol.*, 67(1):524–536, 2018.

[60] H. P. Luong, M. Panda, H. L. Vu, and B. Q. Vo. Beacon Rate Optimization for Vehicular Safety Applications in Highway Scenarios. *IEEE Trans. on Vehicular Technology*, 67(1):524–536, 2018.

[61] N. Lyamin, B. Bellalta, and A. Vinel. Age-of-Information-Aware Decentralized Congestion Control in VANETs. *IEEE Networking Letters*, 2(1):33–37, 2020.

BIBLIOGRAPHY

[62] Ali Maatouk, Mohamad Assaad, and Anthony Ephremides. On the Age of Information in a CSMA Environment. *IEEE/ACM Transactions on Networking*, 28(2):818–831, 2020.

[63] A. Mansouri, V. Martinez, and J. Härri. A First Investigation of Congestion Control for LTE-V2X Mode 4. In *2019 15th Annual Conference on Wireless On-demand Network Systems and Services (WONS)*, pages 56–63, 2019.

[64] R. Molina-Masegosa and J. Gozalvez. LTE-V for Sidelink 5G V2X Vehicular Communications: A New 5G Technology for Short-Range Vehicle-to-Everything Communications. *IEEE Vehicular Technology Magazine*, 12(4):30–39, 2017.

[65] Rafael Molina-Masegosa, Javier Gozalvez, and Miguel Sepulcre. Comparison of IEEE 802.11 p and LTE-V2X: An evaluation with periodic and aperiodic messages of constant and variable size. *IEEE Access*, 8:121526–121548, 2020.

[66] A. Nabil, K. Kaur, C. Dietrich, and V. Marojevic. Performance Analysis of Sensing-Based Semi-Persistent Scheduling in C-V2X Networks. In *2018 IEEE 88th Vehicular Technology Conference (VTC-Fall)*, pages 1–5, 2018.

[67] G. Naik, B. Choudhury, and J. Park. IEEE 802.11bd and 5G NR V2X: Evolution of Radio Access Technologies for V2X Communications. *IEEE Access*, 7:70169–70184, 2019.

[68] F. Peng, Z. Jiang, S. Zhang, and S. Xu. Age of Information Optimized MAC in V2X Sidelink via Piggyback-Based Collaboration. *IEEE Transactions on Wireless Communications*, 20(1):607–622, 2021.

[69] Richard Rouil, Fernando J Cintrón, Aziza Ben Mosbah, and Samantha Gamboa. Implementation and Validation of an LTE D2D Model for ns-3. In *Proceedings of the Workshop on ns-3*, pages 55–62, 2017.

[70] Raja Sengupta, Shahram Rezaei, Steven E Shladover, Delphine Cody, Susan Dickey, and Hariharan Krishnan. Cooperative collision warning systems: Concept definition and experimental implementation. *Journal of Intelligent Transportation Systems*, 11(3):143–155, 2007.

[71] Steven E Shladover and Swe-Kuang Tan. Analysis of vehicle positioning accuracy requirements for communication-based cooperative collision warning. *Journal of Intelligent Transportation Systems*, 10(3):131–140, 2006.

[72] Ralph Tanbourgi, Harpreet S Dhillon, Jeffrey G Andrews, and Friedrich K Jondral. Dual-branch mrc receivers under spatial interference correlation and nakagami fading. *IEEE transactions on communications*, 62(6):1830–1844, 2014.

[73] Gokulnath Thandavarayan, Miguel Sepulcre, and Javier Gozalvez. Analysis of Message Generation Rules for Collective Perception in Connected and Automated Driving. In *2019 IEEE Intelligent Vehicles Symposium (IV)*, pages 134–139, 2019.

[74] J. Thota, N. F. Abdullah, A. Doufexi, and S. Armour. V2V for Vehicular Safety Applications. 21(6):2571–2585.

[75] T. Tielert, D. Jiang, Q. Chen, L. Delgrossi, and H. Hartenstein. Design methodology and evaluation of rate adaptation based congestion control for vehicle safety communications. In *2011 IEEE Vehicular Networking Conference (VNC)*, pages 116–123, 2011.

[76] Tessa Tielert, Daniel Jiang, Hannes Hartenstein, and Luca Delgrossi. Joint power/rate congestion control optimizing packet reception in vehicle safety communications. In *Proceeding of the Tenth ACM International Workshop on Vehicular Inter-Networking, Systems, and Applications*, VANET '13, page 51–60, New York, NY, USA, 2013. Association for Computing Machinery.

[77] B. Toghi, M. Saifuddin, H. N. Mahjoub, M. O. Mughal, Y. P. Fallah, J. Rao, and S. Das. Multiple Access in Cellular V2X: Performance Analysis in Highly Congested Vehicular Networks. In *2018 IEEE Vehicular Networking Conference (VNC)*, pages 1–8, 2018.

[78] Zhen Tong, Hongsheng Lu, Martin Haenggi, and Christian Poellabauer. A stochastic geometry approach to the modeling of dsrc for vehicular safety communication. 17(5):1448–1458.

[79] Roberto A Uzcátegui, Antonio Jose De Sucre, and Guillermo Acosta-Marum. WAVE: A tutorial. *IEEE Communications magazine*, 47(5):126–133, 2009.

[80] Alexey Vinel, Lin Lan, and Nikita Lyamin. Vehicle-to-vehicle communication in C-ACC/platooning scenarios. *IEEE Commun. Mag.*, 53(8):192–197, 2015.

BIBLIOGRAPHY

[81] Roy D Yates and Sanjit K Kaul. The age of information: Real-time status updating by multiple sources. *IEEE Trans. on Info. Theory*, 65(3):1807–1827, 2018.

[82] Junwei Zang, Vahid Towhidlou, and Mohammad-Reza Shikh-Bahaei. A Priority-Based Cross-Layer Design for Future VANETs Through Full-Duplex Technology. *IEEE Trans. Veh. Technol.*, 69(7):7531–7544, 2020.

[83] Kayhan Zrar Ghafoor, Linghe Kong, Sherali Zeadally, Ali Safaa Sadiq, Gregory Epiphaniou, Mohammad Hammoudeh, Ali Kashif Bashir, and Shahid Mumtaz. Millimeter-Wave Communication for Internet of Vehicles Status, Challenges, and Perspectives. *IEEE Internet of Things Journal*, 7(9):8525–8546, 2020.